PROBING DYNAMIC CELLULAR PROPERTIES USING GENOME EDITING AND SYSTEMS BIOLOGY

by

Chance Michael Nowak

APPROVED BY SUPERVISORY COMMITTEE:

Leonidas Bleris, Chair

Kelli Palmer

Tae Hoon Kim

Zachary Campbell

Dedicated to my friends and family.

PROBING DYNAMIC CELLULAR PROPERTIES USING GENOME EDITING AND SYSTEMS BIOLOGY

by

CHANCE MICHAEL NOWAK, BS, MS

DISSERTATION

Presented to the Faculty of

The University of Texas at Dallas

in Partial Fulfillment

of the Requirements

for the Degree of

DOCTOR OF PHILOSOPHY IN

MOLECULAR AND CELL BIOLOGY

THE UNIVERSITY OF TEXAS AT DALLAS

December 2021

ACKNOWLEDGMENTS

I would first like to thank my parents, Tim and Teri, for their continued love, support, and encouragement. I am grateful for the opportunities you have granted me to pursue my doctoral degree. It has been a long road, and you were there every step of the way to push me when it was most crucial. I would also like to thank my fiancée, Apoorva, for her support, love, and affection, especially in the most trying times throughout this journey. Your persistent encouragement has been a cornerstone to my perseverance, and I could not be more grateful. I would like to thank my supervisor, Leo. You have afforded me opportunities that would otherwise have been unattainable, and you have instilled in me an appreciation for utilizing engineering practices for addressing biological problems. Thank you for the privilege of working in your lab, and for allowing me to work with so many outstanding scientists. I would like to thank my lab members for their support and collaborations throughout my doctoral degree, especially Yi who has helped guide me through my experiments to make me a better scientist. Lastly, I would like to thank my dear friends Jude, Eric, John Henry, Luke, Michael, and Taek. I could not have done this without your friendship, which has been invaluable.

November 2021

PROBING DYNAMIC CELLULAR PROPERTIES USING GENOME EDITING AND SYSTEMS BIOLOGY

Chance Michael Nowak, PhD
The University of Texas at Dallas, 2021

Supervising Professor: Leonidas Bleris

Genome editing has revolutionized not only the future of biological research, but also holds the promise of being a powerful therapeutic for genetic diseases. When considering the multitude of genetic regulations that contribute to various biological processes and their individual contributions that permit diseased cellular states, especially in instances where more than a single genetic aberration is attributed to the diseased phenotype, it is crucial to consider the interconnectivities of gene regulators and their individual contributions to cell health. Biological network maps that reveal the relation of gene products to one another can provide insight into the biological properties they govern. A biological network map consists of nodes (gene products) connected by edges that are dictated by the nature of the interaction between the two nodes. Nodal ablation (i.e., knocking out a gene to render it non-functional) has been crucial in understanding diseased states. However, this type of mutational analysis essentially disregards the impact that individual edges have on the network as a whole. The goal of my dissertation work was to utilize the genome editing tool Cas9 to disrupt the p53-miR-34a network in an edge-specific manner in order to demonstrate not only the complexity of these networks, but to also

underscore the importance that individual edges have on the tumor suppressor phenotype. To this end, I, along with a team of researchers, developed a genetic screen using Cas9-bearing lentiviral vectors to disrupt 93 miR-34a binding sites within the 3' untranslated region (UTR) of 71 genes impactful to cell survival under apoptotic conditions. I quantified the degree of apoptosis in two colorectal cancer cell lines that differ in functional p53 status, and that each harbored miR-34a binding site mutations within the pro-survival gene Bcl-2 3'UTR, demonstrating the importance of the miR-34a-Bcl-2 edge on apoptotic progression. Concurrently, I investigated the phenomenon of cell cycle desynchronization by tracking the DNA distribution of a population of cells starting from a synchronized state until asynchrony with flow cytometry analysis. In doing so, I utilized statistical tools to quantify the degree of desynchronization that does not rely on individual cell cycle phase labeling. Additionally, with the help of my peers, tested and validated a mathematical model the capitulates experimental observations. I explored the sensitivity of the model to changes in its parameters to reveal that cell cycle variability within the population is a main contributor to cell cycle desynchronization. Furthermore, I tested this model prediction by treating cells with lipopolysaccharide to enhance cellular noise, resulting in a greater variability of cell cycle duration, which was also shown to increase the rate of cell cycle desynchronization. Taken together, my research provides insight into the importance individual edges have to biological networks and their resulting phenotypes, as well as the underlying sources of cell population heterogeneity and its contribution to cell cycle variability.

TABLE OF CONTENTS

LIST OF FIGURES

LIST OF TABLES

LIST OF ABBREVIATIONS

ASF	auto-similarity function
BrdU	bromodeoxyuridine
Cas	CRISPR associated protein
CDF	cumulative distribution function
CDK	cyclin dependent kinases
CPM	counts per million
CRISPR	Clustered Regularly Interspaced Short Palindromic Repeats
crRNA	CRISPR RNA
EIV	error-in-variables
GC	growth control
HR	homologous recombination
lncRNA	long non-coding RNA
LPS	lipopolysaccharide
miRNA	microRNA
MOI	multiplicity of infection
mRNA	messenger RNA
NGS	next generation sequencing
NHEJ	non-homologous end-joining
NUC	nuclease lobe
ORF	open reading frame
PAM	protospacer adjacent motif
PCR	polymerase chain reaction
PI	PAM-interacting domain
PI	propidium iodide
PS	phosphatidylserine
qRT-PCR	quantitative reverse transcription PCR
REC	recognition lobe
RISC	RNA induced silencing complex
RNAP	RNA polymerase
RNP	ribonucleoprotein
R-point	restriction point
sgRNA	single guide RNA
SpCas9	Streptococcus pyogenes Cas9
TP	transition probability
tracrRNA	transactivating CRISPR RNA
UTR	untranslated region

CHAPTER 1

INTRODUCTION

1.1 Author contributions

Chance M. Nowak prepared this chapter. A section of this chapter is reused from the original manuscript "Guide RNA engineering for versatile Cas9 functionality". The open-access article distributed under the terms of the Creative Commons Attribution License allows the reuse of portions of the full article as a part of the author's dissertation. Oxford University Press, *Nucleic Acids Research,* Volume 44, Issue 20, 16 November 2016, Pages 9555–9564, DOI: 10.1093/nar/gkw908

1.2 Biological networks: nodes vs edges

The complex, overlapping macromolecular interactions, whether it be physical or biochemical, dictate all aspects of biological processes and can be depicted as an interaction network map. Biological network maps consist of nodes and edges, in which nodes are the gene product and their functional relation to other nodes is described by the nature of the edge (**Figure 1.1a**). Networks can depict multiple cellular processes from protein-protein, protein-DNA, RNA-RNA, or amalgamation of all the aforementioned interactions. The interconnectivity of nodes via edges can reveal molecular interactions that govern specific molecular processes that manifest as observable phenotypes. Highly connected nodes (a node with many edges) are generally referred

to as hubs and are typically genes or gene products that are essential to a particular biological process.

Mutations that completely inactivate a gene or render the gene product nonfunctional can be viewed as a nodal ablation, and loss of highly connected hubs can reveal the biological processes the given node governs. Analogously, the classic mutational analysis approach typically seeks to inactivate genes, which has been pivotal in elucidating the biological function of genes, particularly in instances of monogenic diseases in which the functional loss of a given gene removes all of the interconnected edges and the network essentially collapses and the loss of the biological process is detected as a clear observable phenotype (**Figure 1.1b**). However, this type of network analysis does not capture the full range of potential biological malignancies. Indeed, there are multiple instances in which edge perturbations can "rewire" biological networks resulting in phenotypic changes (Sahni et al. 2013).

For example, genetic mutations that exhibit gain-of-function traits are essentially gene products that have gained new edges distinct from the their unperturbed interactome counterpart (**Figure 1.1c**). The tumor suppressor transcription factor p53 can mutate such that it in contrast to its usual transcriptional activation of genes involved in DNA damage response, cell cycle arrest, and programmed cell death (apoptosis) can, through altered binding specificity, upregulate pro-survival and proliferation-enhancing gene products that significantly alter the canonical p53 interactome (C. Zhang et al. 2020). Missense mutations within the DNA-binding domain of p53 can lead to alternative binding that results in upregulation of cell cycle progression genes in

response to DNA damage (Di Agostino et al. 2006), thus propagating mutations that can lead to genomic instability.

Similarly, edges can be lost through missense mutations that have significant impact on disease phenotypes (Zhong et al. 2009) (**Figure 1.1d**). For example, a missense mutation in the p53-inhibitor, Mdm2, can result in the inability to bind to ribosomal proteins associated with ribosomal stress, which ordinarily would lead to p53 activation (Macias et al. 2010). Interestingly, Mdm2 can still regulate p53, under DNA damaging conditions for instance, but loses the ability to regulate it under ribosomal stress in particular. This results in a failure of p53 to become active under ribosomal stress, leading to sustained c-myc (proto-oncogene)-mediated upregulation of proteins involved in ribosome biogenesis contributing to tumorigenesis (Macias et al. 2010). It is therefore pivotal to not just understand the interconnectivity of nodes, but to consider the nature of the "edgetic" interactions in order to build complete mechanistic details that govern specific biological processes, especially those integral to diseased states (Zhong et al. 2009).

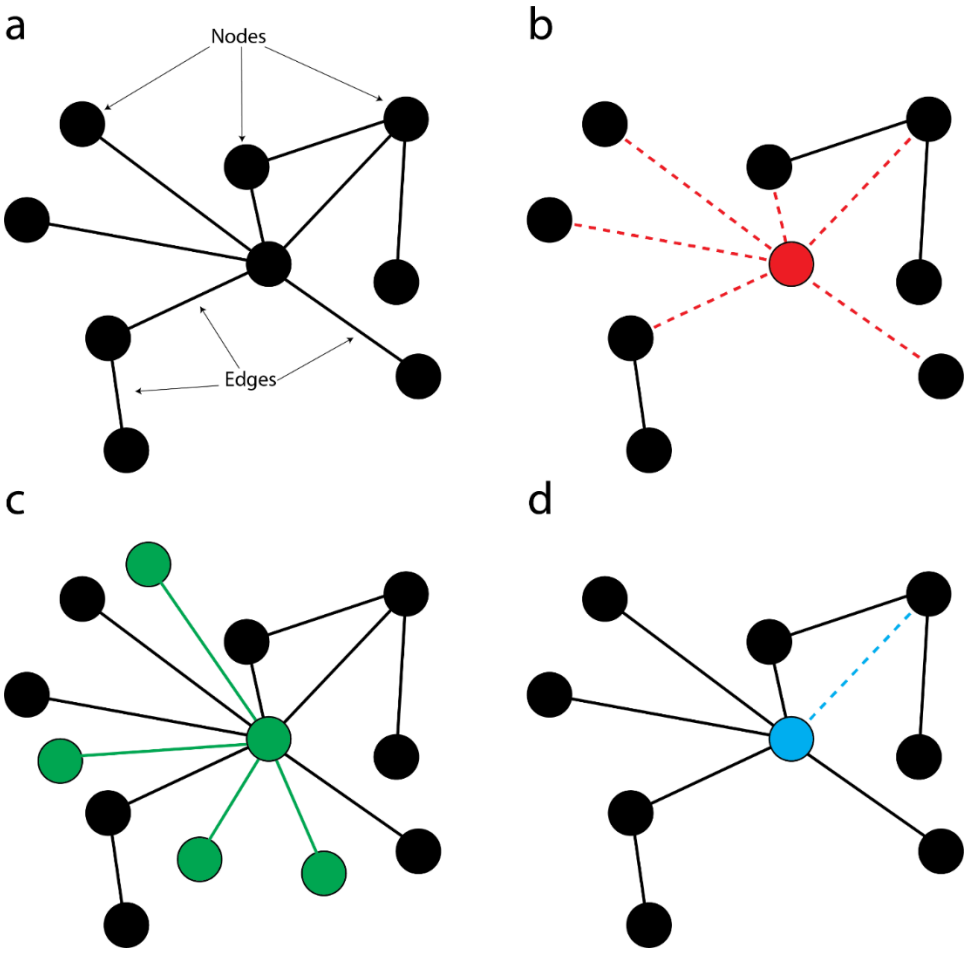

Figure 1.1: Biological network map demonstrating node- and edge-specific mutations. a) intact wildtype network consisting of nodes (i.e., gene and gene products) and edges (i.e., regulatory interaction) with a central hub (highly connected node) that functional regulates multiple nodes. b) mutation of hub that renders the gene completely nonfunctional removes all edge interactions, collapsing the entire network. c) mutation of hub that results in gaining new edges (e.g., mutated transcription factor that binds alternative DNA sequences, resulting in transactivation of new genes. d) mutation of hub that results in loss of edge (e.g., mutated sensory response protein, resulting in compromised network regulation)

Perturbing networks by augmenting edgetic interactions holds great promise for understanding the properties of the network as a whole. When considering mutational perturbations for edge function and relation, it is crucial to preserve the overall function of the nodes connected to the given edge. Gene structures contain regions that are not involved in the protein functions itself,

but do contain regulatory motifs that are directly responsible for the degree of expression, particularly in instances of responding to environmental cues. Thus, there is a unique opportunity to investigate these regulatory interactions without compromising protein function, while understanding what conditions are edges crucial to cell state and environmental responses. An attractive network for edge investigations would be a network that contains hubs with high connectivity that respond to changes in cellular state in highly phenotypic manner. One such network paradigm are microRNA networks, as not only can some miRNA networks be highly connected (hundreds of interactions) but can respond to cellular states. In the next section, a prominent miRNA network will be discussed with the emphasis on the method of regulation miRNAs confer as well as the states under which they are induced (e.g., cellular stress) with robust phenotypic reactions.

1.3 p53 and miR-34a

microRNAs (miRNAs) are a class of small non-coding RNAs ~22 nucleotides (nt) in length that post-transcriptionally regulate gene expression through translational repression. miRNAs must go through extensive processing before becoming functionally mature and are processed in a step-wise and compartmentalized fashion with biogenesis beginning in the nucleus as long hairpin structures that are extensively processed (trimmed to shorter hairpin structures) before being exported to the cytoplasm for further processing in and trimming and strand separation (removing the hairpin structure) (Bohnsack, Czaplinski, and Gorlich 2004). Ultimately, the miRNA is trimmed down to a mature 22 nt double-stranded RNA in the cytoplasm, which then associates with a member of the Argonaute protein family, namely Ago1-4 with Ago2 being

functionally distinct by its endonuclease activity (Höck and Meister 2008; Ruda et al. 2014). Of the two strands, one acts as a guide strand and the other a passenger strand, with the latter being degraded while the guide strand tightly associates to the Ago protein to form the RNA induced silencing complex (RISC) (Marzi et al. 2016). The guide strand dictates which mRNA substrates the RISC binds, and is largely dependent on partial complementary base pairing with a small ~7 nt "seed" sequence typically found in the mRNA's 3' untranslated region (UTR) (Brennecke et al. 2005), although non-canonical (i.e. seed-independent) binding interactions have been shown to occur (Seok et al. 2016; Clark et al. 2015). In canonical mRNA-RISC interactions, this seed region has been shown to be a crucial determinant of which mRNAs to target, and such a relatively small determinant enables some miRNAs to have a multitude of targets, with some miRNAs predicted to have hundreds (Lim et al. 2005; David P Bartel 2009).

Some miRNAs are basally expressed in the cells to constrictively curb gene expression of some gene products. Other miRNAs are highly inducible depending on the cellular state. For example, DNA damage can result in the acquisition of multiple mutations, and while there are sophisticated DNA repair pathways to ameliorate this cellular stress, under extreme conditions, however, the cell may not be able to repair the damage abruptly, thus necessitating a halt on cell cycle progression, or in some cases the damage may be so severe that the cell self-destructs in order to prevent the propagation of these mutations to daughter cells. One highly connected node that serves as a hub for this response process is the p53 protein that actively upregulates the transcription of miRNAs to downregulate a host of genes.

p53 is a transcription factor that is crucial in maintaining genome integrity, and has earned the title as guardian of the genome (Lane 1992). In response to cellular stress such as DNA damage, p53 activation induces cell cycle arrest allowing the cell to repair the damage before any mutations can be propagated; if the damage is beyond repair, p53 will initiate programmed cell death (apoptosis) to prevent the propagation of a compromised genome. These anti-proliferative functions of p53 are well documented (Muller and Vousden 2013; Bieging, Mello, and Attardi 2014), and accordingly, most human cancers have been found to acquire a mutated or dysfunctional p53 (Hainaut and Hollstein 1999). Furthermore, the importance of p53 in tumor suppression is underscored by the activation of target genes that suppress cell proliferation and promote apoptosis. p53 can exert cell cycle arrest by transactivating the expression of potent cyclin-dependent kinases (CDKs) inhibitors such as p21, p27, and p16 (Polager and Ginsberg 2009; G. He et al. 2005) that regulate of the transition of G_1 to S phase. Not only can p53 regulate cell fate by transactivating inhibitors of key cell cycle regulatory proteins, but also can transactivate the expression of miRNAs that directly repress genes involved in cell cycle progression, proliferation, and pro-survival, such as miRNA-34a.

RISC-mediated silencing has been implicated in most, if not all, cellular processes from mammalian development to disease (Kloosterman and Plasterk 2006). In relation to disease, specifically cancer, some miRNAs can be classified as oncogenic or anti-oncogenic (B. Zhang et al. 2007). One prominent miRNA that exhibits tumor suppressive functions is miR-34a (Rokavec et al. 2014; Bader 2012; Hermeking 2010). miR-34a expression is strongly associated with cell cycle arrest and apoptosis. A subset of miRNA-34a targets are those involved in the cell cycle

progression at the G_1-S phase transition, of which include proto-oncogenes such as c-myc (Christoffersen et al. 2010; Sotillo et al. 2011; Yamamura et al. 2012), CDK4 (Hargraves, He, and Firestone 2016; Tianyou Wang 2014; Guo et al. 2015) and CDK6 (Navarro et al. 2009; Yunqing Li et al. 2009; Sun et al. 2008), and cyclins E2 (Lin He et al. 2007; Sun et al. 2008) and D1 (Sun et al. 2008; Hermeking 2010). Unsurprisingly, miR-34a-mediated regulation of the G_1/S phase transition can be induced by the tumor suppressor protein p53, due to the presence of the p53 response element located near the miR-34a transcriptional start site (Chang et al. 2007; Concepcion et al. 2012). miR-34a is also involved in repressing the expression of proliferation promoting genes such as SIRT1 (Yamakuchi, Ferlito, and Lowenstein 2008), which can inactivate the p53 protein via deacetylation, and pro-survival genes such as BCL-2 (Lin et al. 2014), which inhibit proteins that initiate apoptosis. Interestingly, while miR-34a is transactivated by p53 resulting in repression of cell cycle regulators of the G_1/S transition in a redundant fashion to p53 upregulation of CDK inhibitors, miR-34a can also exhibit antiproliferative functions independent of p53 functional status (i.e., wildtype p53).

Importantly, given the prevalence of p53 inactivation as well as gain of function mutations in multiple cancer types it is worth considering modes of treatment that allow p53-independent functional interactions as potential therapeutics. While miR-34a is highly connected to p53 activity, it is worth noting that there are reported incidents of miR-34a tumor suppressor activity independent of p53 status, that is miR-34a has shown to be activated without functional p53 status (Zhao et al. 2013; Christoffersen et al. 2010; Tazawa et al. 2007).

Thus, the p53-miR-34a network seems to be an ideal candidate for edgetic interventions given its robust phenotypes, namely cell cycle arrest as well as promoting cell death, as well as its response to cellular states, such as cell stress, and lastly the highly interconnected edges that make up this network. The question then becomes, how can we perturb these regulatory interactions in a precise manner? One such manner is genomic intervention via genome editing such as the programmable nuclease Cas9 to independently and systematically remove these edges in a way that does not compromise the function of the individual nodes that describe these relations. Interestingly, however, while the tumor suppressor p53 is constitutively expressed, the protein is rapidly degraded due to the p53 inhibitor E3 ubiquitin ligase Mdm2 (Kubbutat, Jones, and Vousden 1997; Haupt et al. 1997), and despite studies that have demonstrated post-transcriptional regulation motifs within the p53 3'UTR via reporter assays (Haronikova et al. 2019), genomic deletion of the endogenous p53 3'UTR was shown to have no impact on p53 translation under normal conditions or following DNA damage (Mitschka and Mayr 2021). Thus, highlighting the importance of genomic perturbations in native gene contexts for elucidating the impact of regulatory elements over synthetic gene reporter constructs (such as luciferase or fluorescent proteins). In **Chapter 2**, genomic editing of edge-specific interactions within the p53-miR34a are explored further.

1.4 SpCas9 as genome editing tool

1.4.1 SpCas9 endogenous system

The Clustered Regularly Interspaced Short Palindromic Repeats (CRISPR) system allows a single guide RNA (sgRNA) to direct a protein with combined helicase and nuclease activity to the DNA. *Streptococcus pyogenes* Cas9 (SpCas9), a CRISPR-associated protein, has revolutionized our ability to probe and edit the human genome in vitro and in vivo. CRISPR loci are present in prokaryotes, including both bacteria and archaea (Horvath and Barrangou 2010; Garneau et al. 2010), and are primarily characterized by direct repeat sequences interspaced by similarly sized variable sequences (Sorek, Kunin, and Hugenholtz 2008; Brouns et al. 2008; Barrangou et al. 2007; Jansen et al. 2002). Early investigations into the nature of the repeat and variable sequences revealed that CRISPR and the CRISPR-associated proteins (Cas) work in tandem to recognize and cleave invading foreign DNA (Barrangou et al. 2007; Lander 2016; Brouns et al. 2008; Jansen et al. 2002; Sorek, Kunin, and Hugenholtz 2008; Deveau et al. 2008; Garneau et al. 2010; Horvath and Barrangou 2010). The characterization of CRISPR-Cas as a type of prokaryotic immune system laid the groundwork for what has now become a powerful tool for various applications well outside the original biological context (Mali et al. 2013b; Le Cong et al. 2013; Niu et al. 2014; Hai et al. 2014; Richard Moore et al. 2015; Yi Li et al. 2016; Hilton et al. 2015; Jinek et al. 2013).

In prokaryotes, the CRISPR-Cas system functions as a microbial analog to the acquired (adaptive) immune system present in higher organisms (Barrangou et al. 2007; Bolotin et al. 2005; Makarova et al. 2006). The variable sequences of the CRISPR array, known as spacers, are

relics of previous infectious events whereby fragments of invading DNA, or protospacers, have been captured and integrated into the host genome at the CRISPR locus to serve as an immunological memory (Deveau et al. 2008). Once a new protospacer has been integrated into the CRISPR array, the entire array can be transcribed into pre-crRNA and processed into mature crRNA.

The processing of pre-crRNA into mature crRNA is distinct in type II CRISPR systems in that it relies on the presence of trans-activating crRNAs (tracrRNAs) that hybridize with the pre-crRNA through complementary base pairing to the repeat regions (Deltcheva et al. 2011; Gasiunas et al. 2012; Jinek et al. 2012). RNase III, a dimeric endoribonuclease that cleaves double-stranded RNA, then recognizes the pre-crRNA:tracrRNA hybrid and cleaves individual crRNA:tracrRNA hybrids from the primary CRISPR array transcript (Deltcheva et al. 2011). Ultimately the crRNA-tracrRNA hybrid spacer sequence (**Figure 1a)** is trimmed down to 20 nucleotides (Deltcheva et al. 2011) before tightly associating with the SpCas9 nuclease and forming the catalytically active ribonucleoprotein (RNP) complex used for targeted DNA cleavage (Bolotin et al. 2005; Makarova et al. 2006).

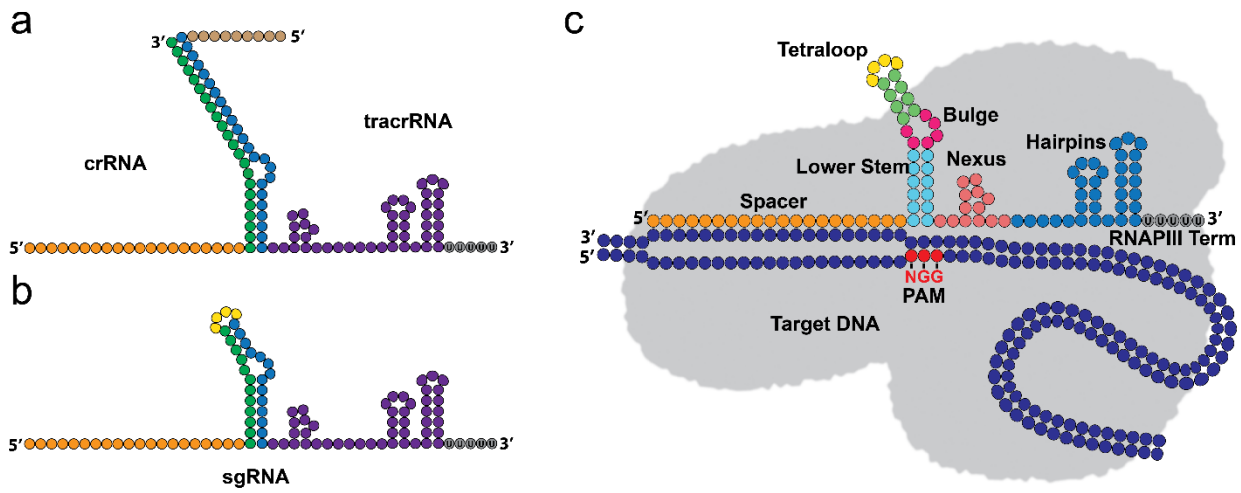

Figure 1.2: S. pyogenes CRISPR-SpCas9 guide RNA anatomy. (a) Endogenous CRISPR RNA (crRNA) and transacting crRNA (tracrRNA). The spacer sequence (orange) is 20 nucleotides in length and the repeat sequence (green) is 22 nucleotides that basepairs with tracrRNA complementary region (blue). The 3' handle region (purple) has functional significance for structure-dependent recognition by SpCas9. (b) The synthetic sgRNA retains dual-tracrRNA:crRNA secondary structure via a fusion of the 3' end of the crRNA to the 5' end of the tracrRNA with an engineered tetraloop. (c) Individual functional modules of the sgRNA (sgRNA structure adopted from Briner et al., 2014). The 5' spacer sequence dictates SpCas9 localization within the genome. The lower stem is formed by the duplex between the CRISPR repeat sequence from the crRNA and the region of complementarity in the tracrRNA. SpCas9 interacts with the upper and lower stems in a sequence-independent manner, whereas the bulge interactions with SpCas9 appear to be sequence-dependent. The nexus contains both sequence and structural features necessary for DNA cleavage and lies at the center of the sgRNA:SpCas9 interactions. The nexus also forms a junction between the sgRNA and both SpCas9 and the target DNA. The terminal hairpins assist in stabilizing the sgRNA and supports stable complex formation with SpCas9.

An indispensable aspect of any immune system is the ability to distinguish self from non-self; in other words, the components of the immune system must be able to recognize molecules that do not originate from the host. The SpCas9 CRISPR system achieves this distinction through the recognition of a protospacer adjacent motif (PAM), which is a short G-rich oligonucleotide sequence downstream of the target DNA (Deveau et al. 2008; Marraffini and Sontheimer 2010). This feature is crucial for targeted DNA cleavage, as the corresponding spacer in the CRISPR

array is identical to the target DNA, and would otherwise be cleaved. It is not until after SpCas9 scans invading foreign DNA for the PAM sequence 5'NGG that complementary base pairing between the target DNA and crRNA can occur and trigger targeted DNA cleavage (Mojica et al. 2009; Sternberg et al. 2014).

The high-resolution crystal structure of SpCas9 in complex with a sgRNA, and its cognate target DNA obtained by Nishimasu et *al.* identified key functional interactions that govern the molecular mechanism of SpCas9-mediated DNA cleavage. The crystal structure revealed that SpCas9 has a bilobed architecture composed of a Recognition lobe (REC) and a Nuclease lobe (NUC), and the site of heteroduplex formation between the sgRNA and its cognate target DNA is a positively charged cleft at the interface between the two lobes (Nishimasu et al. 2014; Jinek et al. 2014). The REC lobe is comprised of an α-helical region termed the bridge helix domain that recognizes the "seed" region (the 10-12 PAM-proximal nucleotides of the guide region) of the sgRNA through salt bridges with sgRNA backbone, a REC1 domain that recognizes repeat:anti-repeat duplex of the sgRNA, and the REC2 domain that does not interact with the guide:target heteroduplex. The NUC lobe is comprised of a RuvC catalytic nuclease domain that cleaves the non-complementary strand of the target DNA, a HNH catalytic nuclease domain that cleaves the complementary strand of the target DNA, and a PAM-interacting (PI) domain that recognizes the 5'NGG PAM on the non-complementary strand (Jinek et al. 2012; Nishimasu et al. 2014; Jinek et al. 2014; Gasiunas et al. 2012).

SpCas9 interacts with the sgRNA in both sequence-dependent and independent manners—the guide region is recognized in a sequence-independent mechanism, whereas SpCas9 recognition of the sgRNA repeat:anti-repeat duplex involves sequence-dependent interactions (Nishimasu et al. 2014). Additional information on the base pair interactions and details regarding conformational changes due to sgRNA and target DNA/PAM recognition can be found in recent literature (Nishimasu et al. 2014; Jinek et al. 2014; Sternberg et al. 2015; Anders et al. 2014).

1.4.2 SpCas9 genome editing in mammalian cells

Endogenous Type II CRISPR RNA components require extensive processing before becoming functional (Jinek et al. 2012; Gasiunas et al. 2012). The first effort to recapitulate the bacterial CRISPR system in mammalian cells involved the delivery of SpCas9, SpRNase III, the tracrRNA, and the pre-crRNA array, which contained the spacer sequence flanked by direct repeats (Le Cong et al. 2013). Interestingly, the inclusion of SpRNase III was found to be unnecessary for cleavage of the target DNA sequence in mammalian cells (Le Cong et al. 2013).

A key advance in CRISPR programmability came with the engineering of the chimeric single guide RNA (sgRNA) (Jinek et al. 2012). The chimeric sgRNA (**Figure 1b)** is a single transcript that retains the dual-tracrRNA:crRNA secondary structure via a fusion of the 3' end of the crRNA to the 5' end of the tracrRNA with an engineered tetraloop (Jinek et al. 2012). The most common approach to produce sgRNAs in human cells is using the human U6 RNA polymerase III (RNAP III) promoter (Mali et al. 2013b; Le Cong et al. 2013; Jinek et al. 2013). This constitutive RNAP III promoter allows the sgRNA transcript to escape post-transcriptional

modifications that are coupled to RNAP II transcription (such as 5' methyl capping and polyadenylation), which would otherwise result in its export out of the nucleus (Hamm and Mattaj 1990; McCracken et al. 1997).

The use of Cas9 and engineered sgRNA has served as a molecular toolkit that provided a foundation from which an innumerable number of applications have spurred. Applications using the wildtype SpCas9 include: gene knockout via targeting genes in their open reading frame (ORF) and subsequent error-prone DNA repair via the non-homologous end-joining (NHEJ) (L Cong et al. 2013; Mali et al. 2013a), regulatory motif ablation through NHEJ by targeting noncoding genetic regions (Yi Li et al. 2018; Hsieh et al. 2019), and gene knock-in with DNA fragments that contain regions of homology for targeted genomic integration via homologous recombination (HR) DNA repair(L Cong et al. 2013; Mali et al. 2013a). Additionally, Cas9 can be mutated to have nickase activity at the RuvC domain (D10A) or the HNH domain (H840A) resulting in single strand cleavage of the target strand or non-target stand, respectively (Jinek et al. 2012). Single strand nicking has recently been used in conjunction with deaminase fusions for single nucleotide base editing (Komor et al. 2016; Gaudelli et al. 2017) as well as fused to reverse transcription and elongated 3' gRNA for templated DNA repair (i.e., prime editing) (Anzalone et al. 2019). If both mutations are installed, Cas9 becomes nuclease deficient (dCas9) (Qi et al. 2013) and can be used as programmable DNA binding domain in which various functional proteins (or protein domains) can be fused to dCas9 for localized functional activity including: transcriptional activation (L. A. A. Gilbert et al. 2013), transcriptional repression (L.

A. A. Gilbert et al. 2013), epigenetic alterations (Hilton et al. 2015), fluorescent imaging of DNA (B. Chen et al. 2013).

While Cas9 has shown to be an indispensable tool for biological research into the function of genes, one promise intrinsic to the ability to alter genetic sequences with such precision is the use of genome editing intervention is use as a therapeutic to change genetic abnormalities. However, genetic alterations with genome editing tools ought to be used with consideration to p53 status (Haapaniemi et al. 2018). For example, one approach to utilizing genome editing tools such as Cas9 is to integrate Cas9 expressing constructs into the genome, which often harbor genetic antibiotic selection cassettes. Cells selected with the antibiotic in the presence of Cas9, which due to its nuclease activity, is considered cytotoxic, not only due to its on-target DNA cleavage, but additional off-targeted DNA cleavage can result in the inadvertent selection of nonfunctional p53 (Enache et al. 2020). As described previously, the p53 protein is a crucial regulator of DNA damage response, and can lead to cell cycle arrest in order to prevent the propagation of mutations from the subsequent daughter cells. Therefore, the artificial selection of the antibiotic resistance gene used to sustain Cas9 expression, which may persistently induce DNA damage, selects for p53 deficient cells, which may lead to further oncogenic activation (Conti and Di Micco 2018).

1.5 Cell cycle variability

While much attention has been focused on elucidating the cellular interactions that govern cell cycle regulation, one interesting phenomenon is the overall variability of cell cycle duration

within a population. Indeed, a great deal in effort has been investigating the source of heterogeneity within cellular populations to account for cell cycle variation (Robert F. Brooks 2021; D. A. Gilbert 1982; Perez-Carrasco, Beentjes, and Grima 2020; Alberghina, Mariani, and Martegani 1985; Koch 1980), and additionally, developing models that accurately describe cell population behavior, particularly the variability of the cell cycle. The cell cycle is a tightly regulated process that is mediated by multiple feedback networks (Pomerening, Kim, and Ferrell 2005; Gérard, Gonze, and Goldbeter 2012; Pomerening 2009; Ferrell and Jr. 2013) that enable oscillatory timing of events that result in the duplication of DNA and cellular division. Particular consideration has been focused on the genetic mechanisms regulating this process, especially the G_1/S transition, which is a critical point (termed the restriction point, or R-point) in the cell cycle in which the cell either commits to DNA synthesis, enters quiescence, or initiates apoptosis.

There are multiple factors that can contribute to the cellular fate of the cell, such as environmental cues, resource availability, and cell type. Interestingly, despite the highly regulated mechanisms that compute this decision, there exists noticeable variations in the timing of these events within a cellular population. Indeed, identical daughter cells that enter the cell cycle at the same time can have vastly different cell cycle durations. These overall variations in periodicity have been largely been attributed to the variable timing a given cell spends in the G_1 phase (especially in cell types that can exit G_1 and enter quiescence). Critically, cancer cells that have can highly dysregulated cell cycle regulatory mechanisms (Otto and Sicinski 2017; Leal-Esteban and Fajas 2020) can also demonstrate variability in the cell cycle duration. One realm of investigation to this phenomenon is to consider cellular noise in gene expression.

Gene expression noise can be divided into two sources: extrinsic and intrinsic. Extrinsic noise can arise from variations in cellular constituents such as transcriptional processivity or ribosome availability. Intrinsic noise arises from the inherent stochasticity of biomolecular interactions. Interestingly, multiple modes of thought have sought to provide an explanation for sources of cell cycle variability that also take into account cellular noise (Swain, Elowitz, and Siggia 2002; Zopf et al. 2013; Soltani et al. 2016; Gonze et al. 2018). Additionally, one of the crucial regulatory motifs of the G_1/S transition are bistable switches that are ultrasensitive to stochastic fluctuations (Yao et al. 2008b; T. J. Lee et al. 2010) that can commit a cell to engage in DNA synthesis. The variations in cell cycle periodicity are frequently analyzed through mathematical modeling, with an emphasis on incorporating sources of stochasticity to accurately capture cell cycle dynamics.

One of the earliest models proposed was the transition probability (TP) model (Smith and Martin 1973) used to describe entry into S phase from G_1 thus initiating DNA synthesis. This model postulates that the cell cycle is both probabilistic and deterministic. Specifically, the cell cycle was divided into and A state and a B phase. The B phase consisted of S, G_2, and M which are deterministic in that once DNA synthesis starts in S phase it is committed to reaching G_2 (and ultimately mitosis if conditions are permissive). Thus, its duration is determinate. Whereas in the A-state, cells are not directed towards DNA synthesis and subsequent division, and as such can spend an indeterminate time within this state where the probability of leaving the A state at any time is constant. Therefore, the entry into S phase is dictated by a stochastic process, similar to the random radioactive decay of an atomic nucleus. However, this model had difficulties in

rectifying cells that enter quiescence (G_0) or from cells that are arrested at the R-point, and the model used a general strategy to describe these instances as just high or low probabilities of transition (Shields and Smith 1977). Later the model was updated to include an additional transition probability to account for quiescence cells, but is amenable to environmental factors such as serum deprivation and replenishment, which has shown to cause quiescent cells to reenter the cell cycle (R. F. Brooks, Bennett, and Smith 1980). Later, a second model was developed that posited that the duration of the entire cell cycle is largely dictated by the G_1 phase, and should be modeled separately from the rest of the cell cycle, i.e. the G_1-rate model (Castor 1980) (later referred to as growth control model, GC). The model removes the unpredictable aspect of the transition model and instead attributes variability in S-phase reentry timing to differences in cell metabolism. The authors support this claim with the additional observation that the amount of RNA in a cell correlates with the rate of progression through initiation and completion of DNA synthesis, and the variability in G_1 arises from the capacity at which a cell can synthesize the proteins necessary for DNA replication. This thresholding description implicit in the GC model was later re-interpreted as an alternative description of the R-point (Cooper 2003). Interestingly, these two phenomenological models (TP and GC) largely escape the need for any mechanistic details, while still maintaining accurate descriptions of cell cycle control.

However, it was eventually shown that R-point is actually governed by bistable switch within the Rb-E2F pathway (Yao et al. 2008a), in which E2F (a master cell cycle transcription factor, and Rb its transcriptional repressor) is involved in two positive feedback motifs that put E2F in either

an ON or OFF state depending on nutritional availability (e.g. serum concentration). Later the activation of these ON or OFF states was shown to be stochastic, arising from intercell variability of gene expression such as intrinsic noise (e.g. stochastic nature of biochemical interactions within a cell) and extrinsic noise (e.g. heterogeneity in cellular components affected by environmental factors or cell age) (T. J. Lee et al. 2010; M. Elowitz et al. 2002). Importantly, the sensitivity to stochastic fluctuations could account for the inherent variability in cell cycle duration. This stochastic activation of the bistable switch controlling the R-point seems to reconcile differing aspects of the TP and GC models by extracting parameters from both models. Namely, the transition rate and time delay from the TP model, and mean growth rate and its variance from the GC model. Critically, simulated nodal perturbations of the Rb-E2F pathway led to changes in these parameters both predicted by their respective model.

These models have provided useful insight into the nature of cell population dynamics; moreover, the nature of the cell cycle heterogeneity gained further insight from the ability to synchronize cells to the same cell cycle phase and monitor cell cycle progression following synchronization. Indeed, investigations into cell cycle progression and regulation has often started with the need to synchronize all cells within a population to the same cell cycle phase. For example, the experiments in these early investigations described previously largely relied in serum deprivation for cell cycle synchronization. Another common approach to cell synchronization is the double thymidine block that interferes with nucleotide metabolism resulting in an inability of the cells to synthesize DNA causing a cell cycle arrest at the G_1/S boundary (Bjursell and Reichard 1973; G. Chen and Deng 2018).

One interesting observation discovered from observing the behavior of synchronized cell populations is that they desynchronize, and quickly reach a state of "asynchronicity," whereby the individual cell cycle phases stabilize into fixed percentages. This phenomena has also been studied in cultured cells that were pulse labeled with bromodeoxyuridine (BrdU), thus creating a semi-synchronous cell population where only cells that are actively progressing through S-phase incorporate the thymidine analog BrdU into their genome, and thus can be tracked overtime by using a fluorescently conjugated BrdU antibody (Chiorino et al. 2001). These investigations hinted at the possibility of cell cycle variance (potentially manifesting from inherent cellular noise) as a contributor to desynchronization rates. Therefore, it is crucial to utilize mathematical models to capture cell cycle behavior at the population level to gain insight into the nature of cell cycle progression and regulation. In **Chapter 3**, the role of cell cycle variability with respect to the rate of cell cycle desynchronization is explored further.

1.6 Summary

Understanding the extent of cellular behavior in response to various conditions does not only lay the groundwork for understanding basic biological functions, but also provides insight in to how diseased cell states are acquired. Furthermore, the ability to describe these phenomena by representing biological pathways and processes via network analysis or mathematical modeling can lead to a greater appreciation of the highly organized and complex interactions and reactions that govern cell fate in a more holistic and approachable fashion. In this work, I present experimental results that support the contributions edges have to shaping overall networks through genome editing of miRNA target sites within the 3'UTR of genes involved in the p53-

miR-34a network. Additionally, I present experimental results coupled with in silico mathematical modeling to describe cell cycle desynchronization, and demonstrate that a main contributor of this process is cell cycle variability between cells, which may arise from stochastic sources of cellular noise.

CHAPTER 2

CRISPR-BASED EDITING REVEALS EDGE-SPECIFIC EFFECTS IN BIOLOGICAL NETWORKS

2.1 Author Contributions

The original manuscript was published along with Yi Li (YL), Daniel Withers (DW), Alexander Pertsemlidis (AP), and Leonidas Bleris (LB). YL and LB designed the experiments. YL, Chance Nowak (CN), and DW performed the experiments. YL, CN, AP, and LB analyzed the data. YL, CN, AP, and LB wrote the manuscript. LB supervised the project. Permission from YL was obtained for use of this manuscript in this dissertation in conjunction with © Mary Ann Liebert, Inc., *The CRISPR Journal*, Volume 1, Number 4, 4 November 2018, Pages 286-293, DOI: 10.1089/crispr.2018.0018.

2.2 Abstract

Unraveling the properties of biological networks is central to understanding both normal and disease cellular phenotypes. Networks consist of functional elements (nodes) that form a variety of diverse connections (edges) with each node being a hub for multiple edges. Herein, in contrast to node-centric network perturbation and analysis approaches, we present a high-throughput CRISPR-based methodology for delineating the role of network edges. Ablation of network edges using a library targeting 93 miRNA target sites in 71 genes reveals numerous edges that control, with variable importance, cellular growth and survival under stress. To compare the impact of removing nodes versus edges in a biological network, we dissect a specific p53-

microRNA pathway. We show that removal of the miR-34a target site from the anti-apoptotic gene BCL2 desensitizes the cell to ectopic delivery of miR-34a in a p53-dependent manner. In summary, we demonstrate that network edges are critical to the function and stability of biological networks. Our results introduce a novel genetic screening opportunity via edge ablation and highlight a new dimension in biological network analysis.

2.3 Introduction

We focus on the network formed by p53 and its upstream and downstream regulators, which is critical to cell health, yet incompletely understood. Since its discovery in 1979 (DeLeo et al. 1979), p53 has been shown to play a crucial role in maintaining genomic stability (Vousden and Prives 2009), with more than 50% of human cancers harboring mutant or deleted p53 (Levine 1997). Under normal conditions, the p53 protein exists in a latent form and at low concentration, but in response to various cellular stress signals such as DNA damage, hypoxia, and oncogene expression, post-translational modification of p53 results in its stabilization and accumulation (Batchelor, Loewer, and Lahav 2009). As most human malignancies shut down the p53 tumor-suppressing responses, p53 is one of the critical targets for drug interventions in cancer therapy (Parrales and Iwakuma 2015; Hong et al. 2014) .

A class of post-transcriptional regulators, called microRNAs (miRNAs), is directly associated with p53, either regulating the mRNA responsible for p53 production or being regulated by p53 and its partners (L He et al. 2007; Tarasov et al. 2007). miRNAs, in their mature forms, are small non-coding RNAs approximately 22 nucleotides in length that act as major regulators of gene

expression. Since miRNAs are involved in critical cellular and physiological processes such as growth, differentiation, apoptosis and metastasis, the gain or loss of critical miRNAs in a given cell type can have significant implications for cell fate (D P Bartel 2009; Filipowicz, Bhattacharyya, and Sonenberg 2008; Richard; Moore et al. 2015; J. Lee et al. 2014). Studies have revealed extensive crosstalk between the p53 network and miRNAs, but the specifics of how miRNAs participate in the regulation of p53 signaling and what they contribute to the role of p53 as a tumor suppressor remain largely elusive.

In miRNA-based networks, the edges are regulatory interactions between miRNAs and target mRNAs. These interactions are mediated by sequence complementarity and therefore are susceptible to genetic variation in either the miRNA or the target site – the seed sequence of the miRNA and the complementary region in the target site are considered the largest determinants of the interaction. Variation in miRNA binding sites has been associated with numerous diseases, including Tourette Syndrome (Abelson et al. 2005), rheumatoid arthritis (Chatzikyriakidou et al. 2010), lupus (Consiglio et al. 2011), psoriasis (Wu et al. 2011), Crohn's disease (Brest et al. 2011; Kulkarni et al. 2013), Parkinson's disease (G. Wang et al. 2008), hypertension (Sethupathy et al. 2007; Hanin et al. 2014), diabetes and obesity (Lv et al. 2008; Richardson et al. 2011), and multiple cancers (Ryan et al. 2015; Chin et al. 2008; Zu et al. 2013; Xiong et al. 2011; Pu et al. 2013). In the context of p53 signaling (Okada et al. 2014), miR-34a regulates HDM4, a strong repressor of p53, creating a positive feedback loop in which high levels of miR-34a de-repress p53, which in turn transcriptionally up-regulates the expression of miR-34a.

Network edges (e.g., miRNA-gene target interactions) are central to the function and stability of biological pathways. Today, we have the unprecedented opportunity to dissect individual cells and pathways with single-nucleotide specificity using genome editing. The most widely adopted editing methodology to date is the bacterial type II clustered regularly interspaced short palindromic repeats (CRISPR) system consisting of the CRISPR-associated protein Cas9 derived from *Streptococcus pyogenes* (SpCas9), a DNA endonuclease, and a guide RNA, which directs the binding of Cas9 to a DNA target upstream of a protospacer adjacent motif (PAM). The CRISPR technology has revolutionized our ability to probe and edit the human genome *in vitro* and *in vivo*, through targeted gene disruption, insertion, deletion, single-nucleotide mutation, and chromosomal rearrangement (Mali et al. 2013; Rong et al. 2014; J.-F. Li et al. 2013). Furthermore, pooled sgRNA libraries can be used for versatile *in vitro* screening to investigate phenotypes of interest. Recent examples include screens identifying genes conferring drug resistance (Tim Wang et al. 2014), genes involved in metastasis (S. Chen et al. 2015), and long non-coding RNAs (lncRNAs) regulating human cancer cell growth (Zhu et al. 2016). Thus far, pooled sgRNA libraries have been applied to transcribed loci, which correspond to network *nodes*. Here, we selectively remove *edges* in the miRNA-p53 network, using a first-of-a-kind CRISPR-based screen. We demonstrate that removing edges sheds new light on pathways, in ways not achievable through node-based approaches, which may lead to novel and non-obvious therapeutic opportunities.

2.4 Materials and Methods

2.4.1 Preparation of the CRISPR plasmid library

The CRISPR plasmid library was prepared by following the lentiCRISPRv2 cloning protocol provided by Dr. Feng Zhang (Department of Biology, MIT). Briefly, for each identified sgRNA target (20 nt), two oligos were synthesized. The first oligo was designed as 5'-CACCG-(20 nt sgRNA target sequence)-3'. The second oligo was designed as 5'-AAAC-(20 nt reverse complement of the sgRNA target sequence)-C-3'. All 93 pairs of oligonucleotides were synthesized by Sigma-Aldrich using its customized 96-well plate format (**Table A.9**). Each well contained the pair of oligos for a specific sgRNA target (100 nmol for each). The oligo pairs were reconstituted using 100 µL of dH_2O. For annealing the oligo pairs, 2 µL of each of the reconstituted oligo solutions was mixed with 2 µL of 10X T4 DNA Ligase Buffer (New England Biolabs, catalog number: B0202S) and 16 µL dH_2O. The mixtures were heated at 95°C for 4 minutes, then left at room temperature for 60 minutes. 1 µg of the lentiCRISPRv2 plasmid (Addgene, catalog number: 52961) was digested with 1 µL Esp3I (ThermoFisher Scientific, catalog number: ER0451) at 37°C for 1 hour and run out on an 1% agarose gel. The 12 kb band was extracted using the QIAquick Gel Extraction Kit (Qiagen, catalog number: 28704). 1 µL of each of the annealed oligo pairs was mixed with 9,904 µL dH_2O. Subsequently, 1 µL of the oligo mixture was ligated with Esp3I-digested lentiCRISPRv2 using T4 DNA Ligase (New England Biolabs, catalog number: M0202S). To prepare the library, XL10-Gold Ultracompetent cells (Agilent, catalog number: 200314) were transformed and more than 300 individual clones were pooled. To confirm complexity, the library was subjected to Sanger sequencing (Genewiz) using primer P1 and analyzed using FinchTV (Geospiza).

2.4.2 General cloning protocols

Q5 High-Fidelity 2X Master Mix (New England Biolabs, catalog number: M0492) was used for all polymerase chain reactions (PCR) according to the manufacturer's protocol. All oligonucleotides were ordered from Sigma-Aldrich and are listed in **Table A.9**. Plasmids were constructed using PCR amplification, restriction digest (all restriction enzymes were ordered from New England Biolabs), and ligation with T4 DNA ligase (New England Biolabs, catalog number: M0202S). Gel purification and PCR purification were performed with QIAquick Gel Extraction (catalog number: 28704) and PCR Purification kits (catalog number: 28104) (Qiagen). Transformations were performed using NEB 5-alpha electrocompetent *Escherichia coli* (New England Biolabs, catalog number: C2987P). Minipreps were performed using QIAprep Spin Miniprep kit (Qiagen, catalog number: 27104). The final plasmids were confirmed by both restriction enzyme digestion and direct Sanger sequencing. To generate the Bcl-2 sgRNA a pair of oligonucleotides (Forward: 5'-CACCGAATCAGCTATTTACTGCCAA-3', Reverse: 5'-AAACTTGGCAGTAAATAGCTGATTC-3') was annealed and cloned into the Esp3I-treated lentiCRISPRv2 plasmid following the same procedure for the lentiviral library construction The zeocin resistance gene/sgRNA1 and zeocin resistance gene/sgRNA2 sequences were prepared from two rounds of PCR. First, the fragments were PCR amplified from U6-BCL2/sgRNA-PEF1 using primers P12 and P13 or P14. Second, the final fragments were PCR amplified from the first round PCR products using primers P12 and P15. Subsequently, the PCR products were cloned into the U6-BCL2/sgRNA-PEF1 plasmid using KpnI and EcoRI sites.

2.4.3 Cell culture

HEK293 cells were acquired from American Type Culture Collection (ATCC, catalog number: CRL-1573). HCT116 wild-type and HCT 116 $p53^{-/-}$ cells were gifts from Dr. Michael A. White (University of Texas Southwestern Medical Center). Flp-In-293 cells were purchased from ThermoFisher Scientific (catalog number: R75007). All cell lines were maintained at 37°C, 100% humidity and 5% CO_2. Cells were grown in Dulbecco's modified Eagle's medium (DMEM, Invitrogen, catalog number: 11965–1181) supplemented with 10% fetal bovine serum (FBS, Invitrogen, catalog number: 26140), 0.1 mM MEM non-essential amino acids (Invitrogen, catalog number: 11140–050), and 0.045 units/mL of penicillin and 0.045 units/mL of streptomycin (Invitrogen, catalog number: 15140). In addition, 100 µg/mL zeocin (ThermoFisher Scientific, catalog number: R25001) was used for maintaining the Flp-In-293 cells. To pass the cells, adherent cultures were first washed with Dulbecco's phosphate-buffered saline (PBS, Mediatech, catalog number: 21-030-CM), then trypsinized with Trypsin-EDTA (0.25% Trypsin with EDTAX4Na, Invitrogen, catalog number: 25200) and finally diluted in fresh medium.

2.4.4 Transient transfection

For transient transfection of miRNA mimics, 200 µL of DMEM was mixed with 25 nM (final concentration) of miR-34a mimic (Qiagen, catalog number: MSY0000255) or miR-cel-67 mimic (Dharmacon, catalog number: CN-001000-01), in addition to 2 µL of RNAiMAX (Invitrogen, catalog number: 13778030). The mixture was added to each well of 12-well culture treated plastic plates (Greiner Bio-One, catalog number: 665180) and incubated at room temperature for 20

minutes. Adherent cell cultures were washed with PBS, then trypsinized with Trypsin-EDTA and finally diluted in fresh medium to the cell density of 200,000 cells/800 µL medium. 800 µL of the diluted cell suspension was then added to the well containing the miRNA-RNAiMAX complex.

2.4.5 Generation of the CRISPR lentiviral screen library

To generate the lentiviral vectors, HEK293T cells were grown to 50–70% confluence and then transfected with 3.3 µg of the CRISPR plasmid library, 3.3 µg of the pMD2-VSVG plasmid, and 3.3 µg of the psPAX2 plasmid using 20 mL of JetPRIME (Polyplus, catalog number: 114-01). 24 h later, the medium was removed and replenished with 5 mL of complete growth medium. In the next 3 days, the growth medium containing lentiviral vectors was harvested, and 5 mL of fresh complete growth medium was replenished. The final pooled 15 mL growth medium was centrifuged at 3,000 rpm for 15 min at 4°C to remove cell debris. The supernatant was filtered through a 0.45 µm filter, dispensed into 1–2 mL aliquots and stored at -80°C. Viral titers were determined using qPCR Lentivirus Titration Kit (ABMGood, catalog number: LV900) following manufacturer's instructions. Briefly, 2 µL of viral stock was mixed with 18 µL of Virus Lysis Buffer and incubated at room temperature for 3 minutes. This viral lysate, together with positive control (STD1), positive control (STD2), and negative control (NTC), were subjected to qRT-PCR. Finally, the titer of the viral stock was calculated based on the formula provided by the manufacturer and determined to be 2.07×10^7 IU/mL. To generate the LIB-WT and LIB-$p53^{-/-}$ stable cells, ~10 million cells were seeded onto a 10 cm petri dish. 16 hours later, cells were transduced using the lentiviral vectors at a multiplicity of infection (MOI) of 0.3. 48 hours post-transduction, cells were treated with 0.5 µg/mL of puromycin (ThermoFisher Scientific, catalog

number: A1113802). Polyclonal stable cell line libraries were established after ~2 weeks of drug selection.

2.4.6 Sanger amplicon sequencing

To confirm the complexity of the LIB-WT and LIB-p53$^{-/-}$ cell line libraries, total genomic DNA was isolated from LIB-WT and LIB-p53$^{-/-}$ cells using the DNeasy Blood & Tissue Kit (Qiagen, catalog number: 69504). The cDNA fragments harboring the sgRNA target sequences were PCR amplified by using ~100 ng of the genomic DNA and primers P2 and P3. PCR conditions were one cycle of 30 seconds at 98°C, 40 cycles of 10 seconds at 98°C, 30 seconds at 60°C, and 30 seconds at 72°C. The 181 bp product was then subjected to direct Sanger sequencing using primer P2 and analyzed using FinchTV (Geospiza). To determine editing efficiency, total genomic DNA was isolated from BCL2tgt-WT and BCL2tgt-p53$^{-/-}$ cells using the DNeasy Blood & Tissue Kit (Qiagen, catalog number: 69504). cDNA fragments harboring the miR-34a target site within the 3'UTR of BCL2 were PCR amplified by using ~100 ng of genomic DNA and primers P8 and P9. The 191 bp product was then subjected to direct Sanger sequencing using primer P9 and analyzed using FinchTV (Geospiza).

2.4.7 Next generation sequencing

To determine the relative abundance of the 93 sgRNA target sequences before and after the CRISPR screen, total genomic DNA was isolated from miR-34a-treated LIB-WT and LIB-p53$^{-/-}$ cells at days 0 and 6 using the DNeasy Blood & Tissue Kit (Qiagen, catalog number: 69504).

cDNA fragments harboring the sgRNA target sequences were PCR amplified by using ~100 ng of the genomic DNA and primers P10 and P11, which added the 5'-overhang adapter sequence (5'-TCGTCGGCAGCGTCAGATGTGTATAAGAGACAG-3') and the 3'-overhang adapter sequence (5'-GTCTCGTGGGCTCGGAGATGTGTATAAGAGACAG-3') for subsequent Illumina NGS amplicon sequencing, which was performed at the Genome Sequencing Facility (GSF) at The University of Texas Health Science Center at San Antonio (UTHSCSA). To determine the editing efficacies of the BCL2 targets in the BCL2tgt-WT and BCL2tgt-p53$^{-/-}$ cells, total genomic DNA was isolated using the DNeasy Blood & Tissue Kit. cDNA fragments harboring the miR-34a target site within the 3'-UTR of BCL2 gene were PCR amplified by using ~100 ng of the genomic DNA and primers P16 and P17, and subsequently subjected to Illumina NGS amplicon sequencing, with ~2 million reads generated for each sample. The relative abundances of all 93 sgRNA target sequences were calculated and represented as counts per million reads (CPM). Log-transformed values were used for presentation.

2.4.8 Next generation sequencing data analysis

Four genomic DNA samples (LIB-WT-D0, LIB-WT-D6, LIB-p53$^{-/-}$-D0, LIB-p53$^{-/-}$-D6) were subjected to the NGS amplicon sequencing. ~2 million individual reads were generated for each sample. Next, the 20-nt sgRNA sequences were extracted and matched to the 93 designed sgRNA sequences (valid reads) using the script NGS_processing.py. For all 4 samples, the valid reads account for more than 90% of the total reads. Next, the relative abundances of the 93 sgRNA targets were calculated by dividing the number of the reads matching a specific sgRNA target by the number of the total valid reads (**Table A.6**). Subsequently, for each sgRNA target

sequence, the normalized $\log_2$(transformed counts per million reads) were calculated by evaluating $\log_2$(relative abundance of a specific sgRNA target sequence * 1,000,000 + 1), which was shown in **Table A.7**. Finally, the cell line samples without miR-34a treatment (LIB-WT-D0 and LIB-p53$^{-/-}$-D0) were used as normalization controls and the normalized fold change for a specific sgRNA between day 6 (D6) and day 0 (D0) was calculated by evaluating 2^(normalized $\log_2$(transformed counts per million reads of day 6) – normalized $\log_2$(transformed counts per million reads of day 0)), which was shown in **Table A.8**. To examine the indels generated within the 3'-UTR of the BCL2 gene in BCL2tgt-WT and BCL2tgt-p53$^{-/-}$ cells, the top 10 most frequently detected sequences were extracted and aligned (**Figure A.7**).

2.4.9 Apoptosis assay

To determine the non-apoptotic cell population 72 hours post-transfection with 25nM of miR-34a mimic, 1 mL of the original cell growth medium was transferred into a 15 mL conical tube. Cells were washed with 1 mL of PBS solution, which was also collected. Cells were trypsinized using 150 µL of trypsin-EDTA for 5 minutes at 37°C. Subsequently, the trypsin-EDTA was neutralized using 2 mL of the original cell growth medium/PBS washing solution mixture. The cells were harvested by centrifugation at 1,000 rpm for 5 minutes. The cell pellet was then re-suspended in 1 mL PBS solution, then subjected to centrifugation at 1,000 rpm for 5 minutes. Apoptosis was quantified using the Dead Cell Apoptosis Kit with Annexin V Alexa Fluor™ 488 & Propidium Iodide (PI) (Invitrogen, catalog # V13241), following manufacturer's instructions. Briefly, the harvested cell pellets were re-suspended in 100 µL of 1X annexin-binding buffer before being stained with 1 µL propidium iodide (100 µg/µL) and 5 µL of stock annexin V,

Alexa Fluor™ 488 conjugate for 15 minutes in the dark. Stained cells were then diluted with 400 µL of 1X annexin-binding buffer before subjected to flow cytometry. Excitation/emission wavelengths for the annexin V, Alexa Fluor™ 488 conjugate are 495/519 nm; for propidium iodide they are 533/617 nm.

2.4.10 Cell viability assay

Approximately 150,000 of the HEK293, Flp-In-293, FLP-EDIT1 and FLP-EDIT2 cells were seeded into 6-well plates in 2 mL of complete medium. FLP-EDIT1 and FLP-EDIT2 cells were maintained with 0.5 µg/mL puromycin. All cells were treated with 100 µg/mL zeocin. For each cell type, 6 wells were included so that one of the wells could be harvested and counted on each day (from day 1 to day 6 after seeding). Three independent experiments were performed. For live cell counting, the cell suspension was mixed with 0.4% Trypan Blue solution (Invitrogen, catalog number: 15250) at a 1:1 ratio (volume:volume). Unstained, live cells were then counted using a hemocytometer (Hausser Scientific, catalog number: UX-79001-00) under a light microscope.

2.4.11 Quantitative reverse transcription-PCR (qRT-PCR)

For measurement of BCL2 mRNA levels, total RNA was extracted using the RNeasy Mini Kit (Qiagen, #74104) 48 hours post-transfection. First strand synthesis was performed using the QuantiTect Reverse Transcription Kit (Qiagen, #205311). Quantitative PCR was performed using the KAPA SYBR FAST Universal qPCR Kit (KAPABiosystems, #KK4601), with

GAPDH levels used for normalization. Quantitative analysis was performed using the $2^{-\Delta\Delta Ct}$ method. Fold-change values are reported as mean with standard deviation. Primers used for BCL2 were (P4) 5'-CATGCTGGGGCCGTACAG-3' and (P5) 5'-GAACCGGCACCTGCACAC-3'. Primers used for GAPDH were (P6) 5'-AATCCCATCACCATCTTCCA-3' and (P7) 5'-TGGACTCCACGACGTACTCA-3'.

2.5 Results

2.5.1 CRISPR-based screen for microRNA target editing

We focus on five miRNAs – miR-34a, miR-145, miR-192, miR-194 and miR-215 – which are known to be directly or indirectly regulated by p53, and play elaborate roles in the p53 pathway (Navarro and Lieberman 2015; Sundaram et al. 2011; Feng et al. 2011). The target genes for each miRNA were compiled from miRTarBase (Chou et al. 2016). We selected targets that have been experimentally validated by multiple methods, including luciferase reporter assay, western blot, and quantitative RT-PCR (qRT-PCR) (**Tables A1-A5**). For each of the target genes, the miRNA target sites within its 3'UTR were determined using TargetScan (Agarwal et al. 2015). In total, 93 miRNA target sites were identified across the 71 target genes. The miRNAs and the 71 target genes are the nodes of the derived network, while the experimentally verified and high-confidence predicted interactions between the nodes, including interactions between miRNAs and target genes and between target genes themselves, are the network edges (**Figure 2.1a**). To selectively edit these edges, we employed SpCas9-mediated NHEJ, which typically introduces short insertions or deletions (indels) near its cutting site, and designed sgRNAs in which a PAM

is adjacent to the miRNA target seed sequence(s) in the 3'UTR (David P Bartel 2009) (**Tables A1-A5**).

Next, we constructed a pooled CRISPR sgRNA library, containing both SpCas9 and sgRNA expression cassettes (Sanjana, Shalem, and Zhang 2014). Equimolar amounts of the 93 pairs of oligonucleotides were mixed and cloned into a lentiviral vector (lentiCRISPRv2). To confirm library complexity, we sequenced the resulting plasmid library. The resulting reads displayed consistent flanks with a 20-bp "noisy" sgRNA target sequence, matching the expected pattern from the sgRNA mixture (**Figure A.1**). Subsequently, the lentiviral library was used to infect HCT116 wild-type (WT) and HCT116 $p53^{-/-}$ cells at a multiplicity of infection (MOI) of 0.3, which has been shown (Shalem et al. 2014) to yield at most one integration of the sgRNA cassette in the majority of cells (**Figure 2.1b**). To verify the complexity of our resulting libraries in cells (named LIB-WT and LIB-$p53^{-/-}$) was maintained, the sgRNA locations were amplified from genomic DNA and subjected to Sanger sequencing, which again displayed the expected pattern (**Figure A.2**).

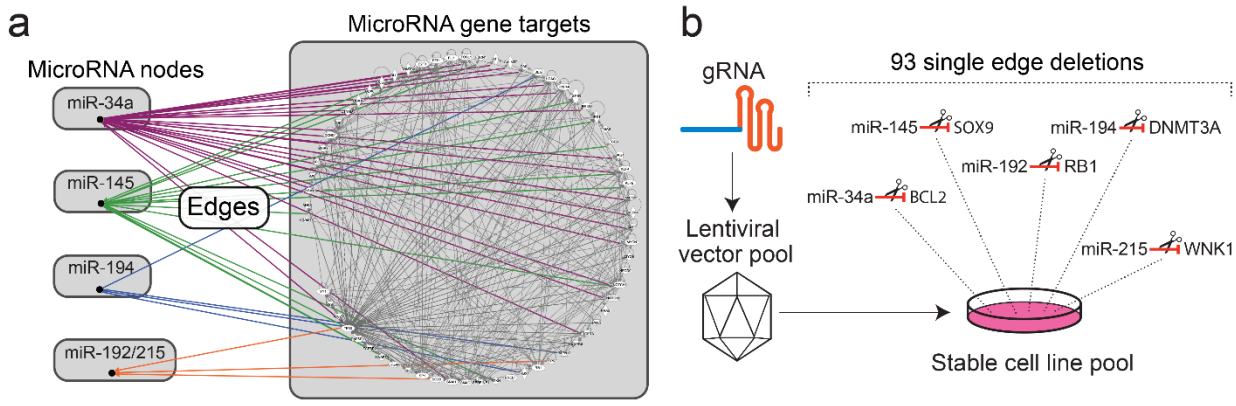

Figure 2.1: p53-miRNA network and CRISPR-based edge screens. (a) Complexity of the p53-miRNA network with nodes comprising the indicated miRNAs and their 71 target genes (detailed list provided in Table A.1-A.5) and edges based on experimentally verified and high-confidence predicted direct interactions, derived using Qiagen Ingenuity Pathway Analysis. (b) CRISPR-based lentiviral libraries were prepared using the lentiCRISPRv2 system. The stably integrated CRISPR sgRNA constructs were recovered by PCR and the sgRNA targets were identified using NGS.

In parallel, to test the efficacy of the viral system, we prepared two CRISPR lentiviral vectors that target the open reading frame (ORF) of the zeocin resistance gene (target 1: 5'-TCGCCGGAGCGGTCGAGTTC-TGG; target 2: 5'-CTCACCGCGCGCGACGTCGC-CGG; PAM underlined), and stably integrated them into cell line Flp-In-293 (ThemoFisher Scientific) which harbors the zeocin resistance gene. As shown in **Figure A.3**, disruption of the zeocin resistance gene abolished resistance to zeocin (100 µg/mL) in the two resulting cell lines (FLP-EDIT1 and FLP-EDIT2), compared to the parental Flp-In-293 cells.

Using the established cell lines (LIB-WT and LIB-p53$^{-/-}$), we focused on the role of miR-34a in the overall p53-miRNA network (**Figure 2.1a**). miR-34a is transcriptionally activated by p53 and induces an anti-proliferative phenotype including senescence, cell cycle arrest at the G_1 phase, and apoptosis (Chang et al. 2007; Bader 2012). In turn, over-expression of miR-34a

increases p53 protein level and stability (Navarro and Lieberman 2015). Importantly, our established cell lines (LIB-WT and LIB-p53$^{-/-}$) do not produce miR-34a (**Figure A.4**), and can therefore be considered to lack the miR-34a node. The miR-34a targets and target sites are still present, however, and therefore the addition of miR-34a to these cells re-establishes the miR-34a network. Compared to baseline miR-34a expression there is a 71-fold increase in mature miR-34a levels 48 hours post-transfection.

We adopted a growth competition assay mediated by ectopic exposure to miR-34a mimics. miRNA mimics are chemically synthesized double-stranded RNA molecules that when transfected into a cell behave similar to a mature endogenous miRNA, regulating the same mRNA (and non-mRNA) targets through the same interactions as the endogenous miRNAs. We treated both cell lines (LIB-WT and LIB-p53$^{-/-}$) to 25 nM of miR-34a mimic for 6 days. Cells were harvested at day 0 (before miRNA mimic transfection) and at day 6. For each sample, sgRNA constructs were amplified from genomic DNA and subjected to NGS amplicon sequencing to assess the relative abundance for each of the 93 sgRNA target sequences (**Tables A.6-A.7**). The most enriched or depleted sgRNA targets, defined by fold-changes between day 6 and day 0 larger than 10, were identified for both LIB-WT and LIB-p53$^{-/-}$ cells (**Figure 2.2, Table A.8**).

Intriguingly, RBX1 (RING-box protein 1), a RING subunit of SCF (Skp1, Cullins, F-box) E3 ubiquitin ligases, was highly enriched in both cell lines. Although not a direct target of miR-34a, over-expression of RBX1 has been demonstrated to increase cancer cell survival (Jia and Sun

2009), and thus could serve as a general response mechanism to cellular stress induced by ectopic miR-34a. Additionally, for a subset of gene targets, we observed differential response to miR-34a mimic between the LIB-WT and LIB-p53$^{-/-}$ cells (**Table A.8**). For example, the sgRNA targeting the anti-apoptotic gene BCL2 was enriched in the LIB-p53$^{-/-}$ cells after miR-34a mimic transfection while no enrichment was observed in the LIB-WT cells (**Table A.9**).

2.5.2 Node perturbations versus edge edits in biological networks

Our edge editing approach revealed (**Figure 2.2a**) several clones that are enriched or depleted after prolonged exposure to ectopic miR-34a. To assess the impact of edge removal (through ablation of miRNA:target interactions) we focused on BCL2, a gene that shows differential expression in response to miR-34a treatment between the two cell lines (**Figure 2.2b**) and is known to be involved in cell survival (Cory and Adams 2002).

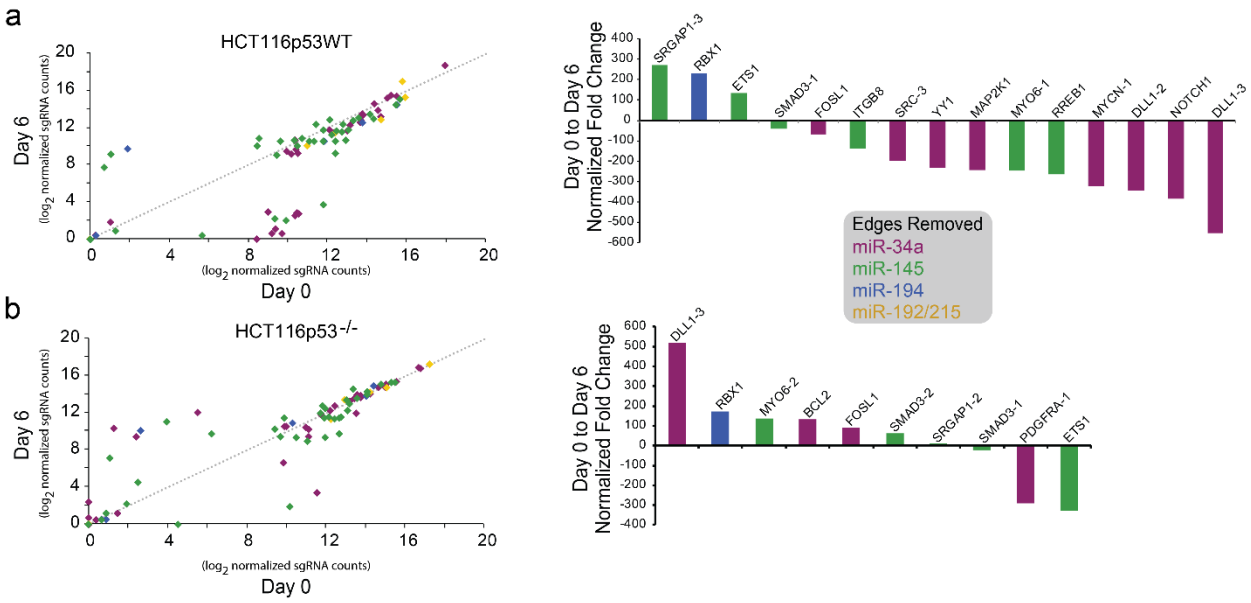

Figure 2.2: High-throughput editing of edges with CRISPR libraries in (a) HCT116p53WT (LIB-WT) and (b) HCT116p53-/- (LIB-p53-/-) cells. The sgRNA targets showing the highest fold changes (> 10) after 6 days treatment of 25nM with miR-34a mimic are shown, with values indicating enrichment and negative values indicating depletion.

Returning to the HCT116 wild-type (WT) and HCT116 $p53^{-/-}$ cells, we removed the miR-34a target site from the BCL2 locus. We prepared a single sgRNA construct designed against the BCL2 3'UTR and established stable cell lines (BCL2tgt-WT and BCL2tgt-$p53^{-/-}$) using the same viral delivery system. Sanger and NGS sequencings of PCR products spanning the sgRNA target site showed that edits (indels) occurred immediately upstream of the PAM (**Figure A.6-A.7**) in both cell lines. Additionally, we compared the sgRNA sequence targeting BCL2 (5'-AATCAGCTATTTACTGCCAAAGG-3', **Table A.1**) against the human genome, confirming BCL2 as the unique target and indicating that non-specific targeting by this sgRNA should be minimal.

Treating delivery of ectopic miR-34a mimic as perturbation of a network node and removal of the miR-34a/BCL2 interaction as perturbation of a network edge (**Figure 2.3a**), there are four possible combinations (node and edge present/absent). When miR-34a levels are low (i.e., the node is absent) the presence or absence of the edge does not impact survival (**Figure A.8)** of either cell line.

In the context of node perturbation, the introduction of ectopic miR-34a in wild-type cells induces apoptosis (**Figure 2.3b right panel** and **Figure A.9**; cell viability is 87.6% without the miR-34a node, and 71.6% with the miR-34a node; $p = 0.006$). Similar changes were observed in $p53^{-/-}$ cells (**Figure 2.3b left panel** and **Figure A.9**; cell viability is 86.1% without the miR-34a node, and 80.0% with the miR-34a node; $p = 0.002$). In this case, perturbing the miR-34a node results in the same behavior for both p53 wild-type and $p53^{-/-}$ cells.

In the context of edge perturbation, the response of the cell lines to ectopic miR-34a is sensitive to the presence of the miR-34a/BCL2 edge. Specifically, removing the ability of miR-34a to regulate BCL2 in the $p53^{-/-}$ cells induces apoptosis (**Figure 2.3b left panel** and **Figure A.9**; cell viability is 84.8% without the miR-34a/BCL2 edge, and 80.0% with the miR-34a/BCL2 edge; $p = 0.015$), while no such phenotypic changes are observed in p53 WT cells (**Figure 2.3b right panel** and **Figure A.9**; cell viability is 72.0% without the miR-34a/BCL2 edge, and 71.6% with the miR-34a/BCL2 edge; $p = 0.900$). We note that the same conclusions can be drawn when quantifying the early- or late-apoptotic cells (**Figure A.10**).

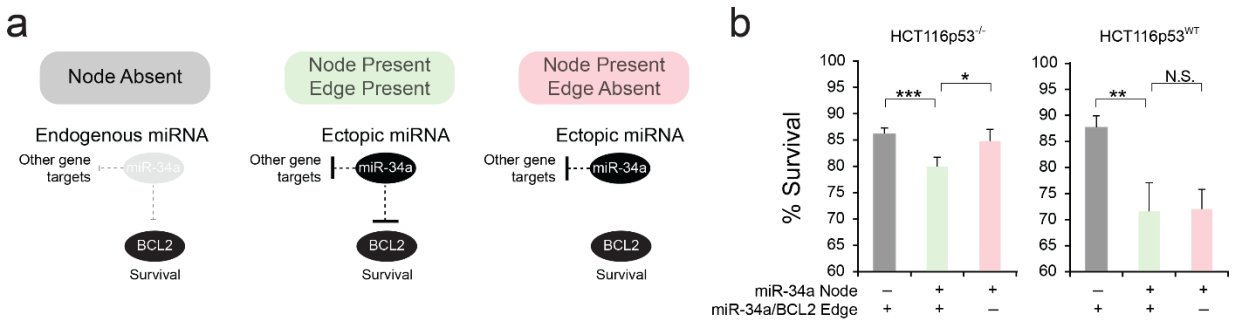

Figure 2.3: Growth competition analysis after ectopic miR-34a delivery using node vs. edge approaches**.** (a) Schematic illustration of node vs. edge analysis. Ectopic miR-34a represents a network node and the miR-34a/BCL2 interaction represents a network edge. (b) The node-based approach shows that addition of the miR-34a node induces apoptosis in both p53 WT and deficient cells. In contrast, the edge-based approach reveals that introduction of the miR-34a/BCL2 edge induces apoptosis only in the p53-deficient cells and not in p53-WT cells.

To further explore the response to miR-34a in BCL2tgt-WT cells, we quantified expression of the BCL2 mRNA in response to miR-34a mimics using qRT-PCR. As expected, miR-34a suppresses the expression of BCL2 mRNA in the WT and $p53^{-/-}$ cells by 55% and 40%, respectively (**Figure A.11**). In the BCL2tgt-$p53^{-/-}$ cells, ectopic miR-34a has a minimal effect on BCL2 mRNA level (95% compared to the control-treated sample; $p = 0.71$). In the BCL2tgt-WT cells, ectopic miR-34a results in a significant down-regulation of BCL2 expression (62% compared to the control-treated sample; $p = 0.028$), possibly due to additional p53-miR-34a regulatory mechanisms.

2.6 Discussion

Biological networks consist of nodes and the interactions between them (edges). Conventional screening methods remove one node at a time, disrupting all edges connected to that node, and therefore producing a relatively blunt effect. An inhibitor that perturbs or removes a single

node yields diverse and systemic changes in the whole network through both direct and indirect connections (Kang et al. 2015), which may explain the heterogeneity observed with single-molecule associated therapeutics.

Our approach reveals edge-specific effects related to the pro-apoptotic p53 and anti-apoptotic Bcl-2 proteins, focal nodes of apoptotic signaling. Normally, p53-dependent inhibition of Bcl-2 and induction of BAX, PUMA and NOXA overcome the anti-apoptotic threshold set by Bcl-2 family members. Conceivably, the difference in apoptosis observed between the BCL2tgt-WT and BCL2tgt-p53$^{-/-}$ cells treated with miR-34a mimics (**Figure 2.3b**) may be explained by the presence of wild type p53-dependent upregulation of PUMA or NOXA in p53 WT cells and not in p53$^{-/-}$ cells. Additionally, p53 could disrupt the binding of POU4F1 (POU Class 4 Homeobox 1) to the promoter of BCL2 and thus indirectly down-regulate BCL2 expression (**Figure A.11**).

2.7 Acknowledgements

This work was funded by the US National Science Foundation (NSF) CAREER grant 1351354, NSF 1361355, and the University of Texas at Dallas. We thank Seth Lawson for technical support.

CHAPTER 3

IMPACT OF VARIABILITY IN CELL CYCLE PERIODICITY ON CELL POPULATION DYNAMICS

3.1 Author contributions

This work was completed alongside Tyler Quarton (TQ) and Leonidas Bleris (LB). Chance Nowak (CN) performed the experiments. CN, TQ, and LB analyzed the data and developed the models. CN, TQ, and LB wrote the manuscript. LB supervised the project.

3.2 Abstract

The cell cycle consists of a series of orchestrated events controlled by molecular sensing and feedback networks that ultimately drive the duplication of total DNA and the subsequent division of a single parent cell into two daughter cells. The ability to block the cell cycle and synchronize cells within the same phase has helped understand factors that control cell cycle and the properties of each individual phase. Intriguingly, when cells are released from a synchronized state, they do not maintain synchronized cell division and rapidly become asynchronous. The rate and factors that control cellular desynchronization remain largely unknown. In this study, using a combination of experiments and simulations, we investigate the desynchronization properties in cervical cancer cells (HeLa) starting from the G_1/S boundary following double-thymidine block. Propidium iodide (PI) DNA staining was used to perform flow cytometry cell cycle analysis at regular intervals of 8 hours, and a custom auto-similarity function to assess the desynchronization and quantify the convergence to asynchronous state. In parallel, we developed

a single-cell phenomenological model the returns the DNA concentration across the cell cycle stages and fitted the parameters using experimental data. Simulations of population of cells reveal that the cell cycle desynchronization rate is primarily sensitive to the variability of cell cycle duration within a population. To validate the model prediction, we introduced lipopolysaccharide (LPS) to increase cell cycle noise. Indeed, we observed an increase in cell cycle variability under LPS stimulation in HeLa cells, accompanied with an enhanced rate of cell cycle desynchronization. Our results show that the desynchronization rate of artificially synchronized in-phase cell populations can be used a proxy of the degree of variance in cell cycle periodicity, an underexplored axis in cell cycle research.

3.3 Introduction

Cell division is traditionally described as a general process divided into two phases, the interphase and mitosis (cell division). Interphase is further divided into three subphases; Gap 1 phase (G_1) in which the cell has a DNA content of 2N, synthesis phase (S) in which the cell's DNA content is greater than 2N but less than 4N, and Gap 2 phase (G_2) in which the cell's DNA content is 4N upon completion of synthesis. Early observations into cell cycle progression showed that the timing of G_1 phase is highly variable not just between cell types but also between cells within a monoclonal population, and that this variable length directly impacts the heterogeneity observed in clonal populations for cell cycle periodicity (Smith and Martin 1973; Prescott 1968). Additionally, a critical point in the cell cycle was discovered (Temin 1971), in which cells were found to be committed to DNA synthesis independent of environmental factors. Moreover, it was later demonstrated that under various suboptimal nutritional conditions, cell

cycle progression could be arrested at the G_1/S boundary, and escapement into S-phase could only occur once suitable nutritional needs were restored (Pardee 1974). The boundary was termed the restriction point (R-point), whereby cells could enter a lower metabolic rate (a quiescent state) to remain viable until adequate nutrition is restored allowing the necessary constituents to be present in suitable amount to enable DNA synthesis (Pardee 1974). Ultimately, it was shown that the high variability of G_1 phase duration can be attributed to a cell's ability to overcome the restriction point (Zetterberg and Larsson 1985).

Investigations into cell cycle progression and regulation often start with the need to synchronize cells within a population to the same cell cycle phase (Schorl and Sedivy 2007; PK, A, and SF 2001). One common approach to cell cycle synchronization is the double-thymidine block that interferes with nucleotide metabolism resulting in an inability of the cells to synthesize DNA causing a cell cycle arrest at the G_1/S boundary (Bjursell and Reichard 1973; G. Chen and Deng 2018). Interestingly, when synchronized cell populations are released from cell cycle arrest, they quickly desynchronize, and reach a state of "asynchronicity," whereby the individual cell cycle phases stabilize into fixed percentages within the overall population. Indeed, simply sampling cells from an asynchronously growing *in vitro* cell culture will reveal (**Figure 3.1a**) the fixed percentages for the three phases of interphase (G_1, S, and G_2). Additionally, cells can be pulse-labeled with bromodeoxyuridine (BrdU) to create a semi-synchronous cell population in which only cells in actively progressing through S-phase incorporate the thymidine analog BrdU into their genome, and thus the original pulse-labeled population can be tracked overtime by using a fluorescently conjugated BrdU antibody (Chiorino et al. 2001). These observations again showed

that the initially pulse-labeled cells progressed synchronously through the cell cycle for some time before quickly desynchronizing and resorting back to an asynchronous DNA distribution profile.

The inherent variability of cell cycle duration between identical cells may be accounted for by considering sources of cellular noise. In other words, the variability between cellular constituents such as signaling and transcriptional factors, along with the biochemical stochasticity of molecular interactions do likely propagate to the phenotypic level and may be responsible for varying timing events that dictate cell cycle progression. For example, signalling factors in a tumor microenvironment that confer a higher degree of intercell variability contribute to tumor cell heterogeneity and pathology (Nguyen et al. 2016; O'Duibhir et al. 2014). Therefore, it is important to examine the implications of cellular noise to cell cycle periodicity.

In this report, we investigated the rate of cell cycle desynchronization by measuring the change in the DNA distribution of a population of cells over time. To this end, we measured the single-cell DNA concentration of a population of cells as they transition from an initial state of cell cycle synchrony, where cells are experimentally locked into the G_1/S boundary, to a state of asynchrony. We used statistical tools to quantify the dynamic change in the DNA probability density function over time from an initial synchronized cell population. Subsequently, we developed a mathematical model to simulate at single-cell level the DNA concentration as the cell transitions through cell cycle states, and finally, experimentally validated our model prediction. More specifically, our model revealed that cell cycle desynchronization rates were

particularly sensitive to the variability of cell cycle duration within a population. With this insight, to validate the results we introduced external noise in synchronized cells using lipopolysaccharide and, indeed, confirmed an increase in cell cycle desynchronization. Considering the ubiquitous role of the cell cycle properties to cell health, the implications of our work extend to numerous fronts.

3.4 Materials and Methods

3.4.1 Cell culturing and synchronization

HeLa cells were grown in Gibco DMEM supplemented with 10%FBS, 1X PenStrep, 2mM glutamine, and 1X Gibco NEAA and grown at 37°C with 5% CO_2. 50,000 cells were seeded per well in 6 well plates. 24 hours post-seeding cells were treated with 2mM of thymidine for 19 hours after which the cells were washed with 1X PBS and given fresh complete media to release from the first thymidine block. The cells then incubated for 9 hours before receiving a second dose of 2mM of thymidine for 15 hours. Cells were washed with 1X PBS to remove thymidine before given fresh media to continue to grow unimpeded. Cells harvested at t=0 were collected immediately following the second PBS wash. Additional wells were harvested every 8 hours for 88 hours. Asynchronous cells were harvested at same time as synchronized cells for each time point. Cells were harvested by washing with PBS, detached from the well with trypsin-EDTA (0.25%) for 3 min at 37°C then quenched with fresh complete media. Harvested cells were pelleted at 1000rpms for 5 min at room temperature. The supernatant was removed and the cell pellet was resuspended in 1X PBS, then pelleted again at 1000rpms for 5 min at room

temperature. The supernatant was removed and the cell pellet was resuspended in 1 mL of 70% ethanol and stored at 4°C for a minimum of 24 hours to fix the cells. LPS derived from *E. coli* 0E111 was reconstituted in PBS without Mg^{2+} or Ca^{2+} at a concentration of 1mg/mL. LPS solution was added directly to the cell culture media after replacing with fresh media initiating the release from the double thymidine arrested state.

3.4.2 Propidium iodide staining

After fixation, cells were pelleted by centrifuged at 1000 rpms for 5 minutes at room temperature. The fixing solution was aspirated off the cell pellet, and resuspended in 1X PBS. Cells were counted for each sample, and then normalized to the lowest cell count for uniform propidium iodide (PI) staining across samples. The PI staining procedure was done according to manufacturer's directions (Propidium Iodide Flow Cytometry Kit, cat# ab139418).

3.4.3 Cell cycle phase analysis

Stained cells were subjected flow cytometry using a BD LSRFortessa™ flow cytometer. PI fluorescence was excited with a 561nm laser and emission was detected using a 610/20 nm band-pass filter. Assignment of cell cycle phases were performed using the univariate modeling via the Dean-Jett-Fox algorithm with FlowJo 10.7.1.

3.4.4 Lentiviral HeLa transduction for H2B-FT expression

The fluorescent tracker sequence was obtained from addgene (#157671) and cloned using primers P1: gaagagttcttgcagctcggtgac and P2: cagtagggtaccccggaattagatcgatctctcgacatcc. The amplicon was digested with restriction enzymes BsiWI and KpnI and inserted into the LentiCRISPRv2 (addgene #52961) backbone. The resulting plasmid was transfected into HEK293T cells along with pMD-VSVG and psPAX2 plasmids to generate viral particles that are released into the media. The media was aspirated two days post-transfection, and replenished with 5 mL of fresh media every day for three days. The 15 mL of harvested viral-containing media was passed through a 0.45 μm filter and dispensed into 1 mL aliquots. 250 μl was used to transduce HeLa cells, and 0.5μg/mL of Puromycin was used to select for integrated clones for 7 days.

3.4.5 Time-lapse microscopy

Images were collected every 20 min for 72 hours using Hamamatsu camera attached to the Olympus IX81 microscope at 10x magnification. Cells were maintained at 37°C and 5% CO_2. The exposure time was 250 ms for Brightfield and 100ms for TexasRed using Chroma filter ET560/40x (excitation) and ET630/75m (emission).

3.4.6 Modeling and simulations

All models and simulations were developed and tested in Mathematica.

3.5 Results

3.5.1 Thymidine-based arrest and desynchronization

The exogenous introduction of excessive thymidine into cells interrupts DNA synthesis, arresting the population of cells in the G_1/S-phase transition. Upon release, the population of cells are permitted to reenter their respective cell cycles. Ultimately, the population of cells will become asynchronous with respect to their cell cycles, yielding a PI fluorescent profile. The PI distributions dynamically change as the population desynchronizes.

After cells were synchronized via double-thymidine block, timepoints were collected every 8 hours for a total of 88 hours. Both asynchronous (untreated) cells (**Figure 3.1b**) and synchronized (**Figure 3.1c**) were subjected propidium iodide staining and flow cytometry analysis. Notably, we observed near full synchronization of cells as judge by the first few timepoints (**Figure 3.1c**) in the synchronous population. While inhibition of DNA synthesis can cause replicative errors due to stalled replication forks, resulting in quiescence or cell death, we did not observe neither an increase in cell death nor any quiescent populations, which would manifest as a sub-G_1/G_1 population at timepoint 8. Each PI histogram was subjected to cell cycle phase classifier (Watson, Chambers, and Smith 1987; Fox 1980; Dean and Jett 1974) with the cell cycle phase distribution displayed as percentages of the total population. As we observe in **Figure 3.1d**, the synchronized population eventually reaches an asynchronous distribution. The residual plots of the DNA distribution of the synchronous population against the asynchronous population ultimately converges to within 8.4%, 1.5%, and 6.1% of G_1, S, and G_2, respectively (**Figure B.1**).

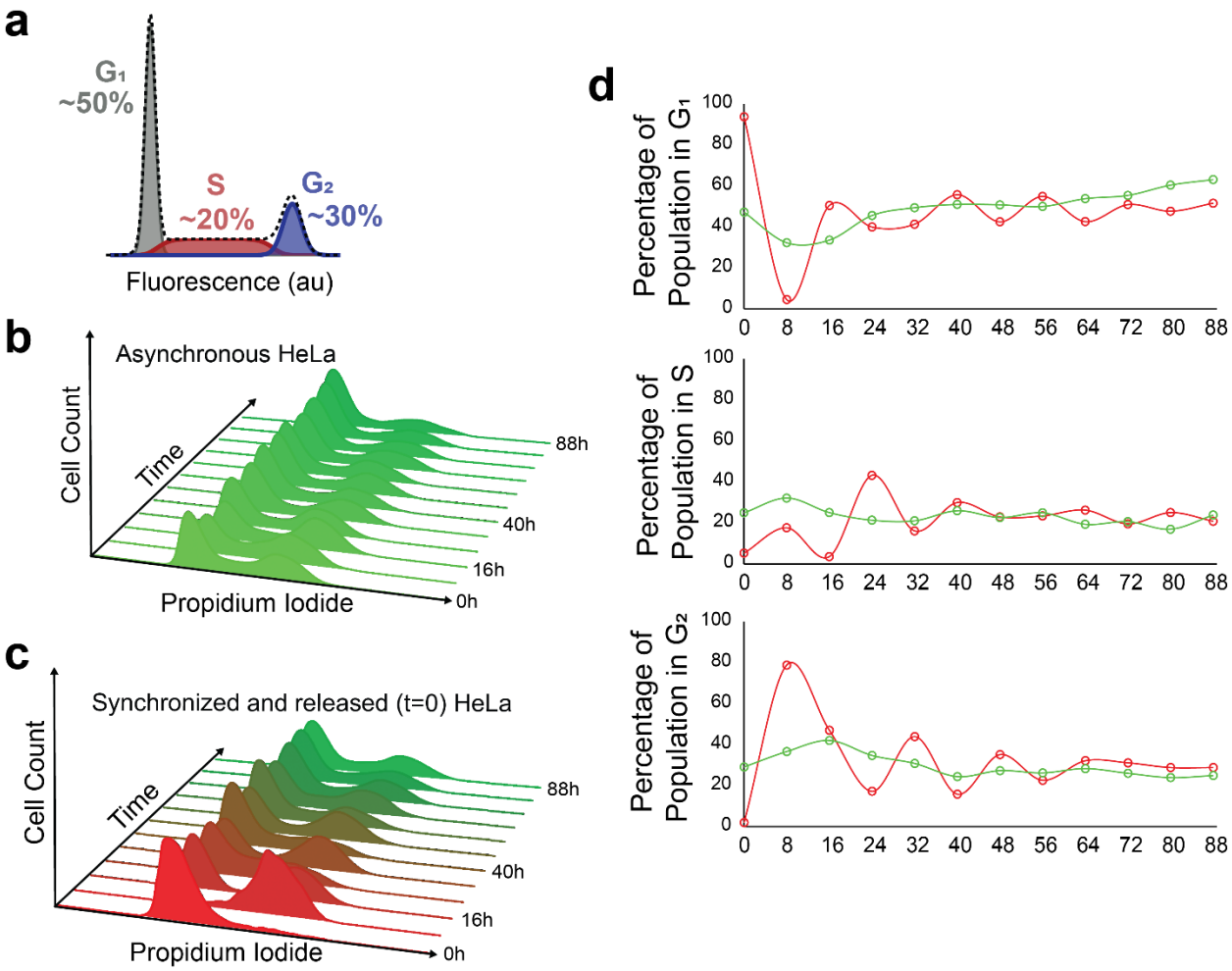

Figure 3.1: Cell cycle desynchronization via double thymidine block and release. a) Cell cycle phases as indicated by cell DNA content and approximate phase distribution in an asynchronous population. b) Fluorescent profile of propidium iodide (PI) stained cells during asynchronous growth from t=0 to t=88. c) Fluorescent profile of PI-stained cells following G_1/S synchronization by double thymidine block from t=0 to t=88. d) Percentages of cells in a given cell cycle phase at a given time point; asynchronous cell growth in green and desynchronous cell growth in red. The cell cycle phase percentages for each time point were determined via the Dean-Jett-Fox model.

3.5.2 Quantifying cell synchronicity

The DNA dynamics during interphase of a population of cells is defined by the population's collective distribution of its DNA at a given time. If all the cells within a population are undergoing interphase synchronously, time separated measurements of the population's DNA distribution will accordingly change in time. This would mean that the DNA distribution of a population of cells will be different for each time measurement. Conversely, if the population's cells are independently progressing through interphase, temporal differences between the population's DNA distribution become indistinguishable, rendering its DNA distribution into a static steady-state (**Figure 3.1a**).

With this in mind, we can create a set of assumptions: Let $\{\mathbf{X}_t\}$ denote sets of observations generated from an evolving probability distribution at any point in time t. We define the auto-similarity function (ASF) between times t_1 and t_2 as

$$\mathbf{\Sigma_{XX}}(t_1, t_2) = \max_{-\infty < x < \infty} \left(F_{\mathbf{X}_{t_1}}(x) - F_{\mathbf{X}_2}(x) \right) + \max_{-\infty < x < \infty} \left(F_{\mathbf{X}_2}(x) - F_{\mathbf{X}_{t_1}}(x) \right)$$

where $F_{\mathbf{X}_t}$ denotes the cumulative distribution function of a given set of observations $\mathbf{X}_t$.

Essentially, the auto-similarity function is the Kuiper two-sample test statistic, which measures the similarity between two sets of data, performed on a single, time evolving variable $\mathbf{X}_t$ rather than two distinct variables. The Kuiper test statistic is rotation-invariant, making its application insensitive to the "starting points" of the data to be compared. As the DNA content measured in our cell populations cycle between 2N to 4N, the data collected from our cell cycle experiments

are inherently cyclical, making the use of a rotation-invariance test statistic ideal. If the evolving distribution eventually converges to a steady-state, we expect $\mathbf{\Sigma_{XX}}(t_i, t_{i+1}) \to 0$ for some successive time measurements t_i and t_{i+1} as $t \to \infty$, where a value of 0 indicates full asynchrony. Conversely, we interpret non-zero, positive evaluations of the ASF to indicate dissimilarity, where, in the case of a cyclically evolving sets of data, evidence that the underlying probability distribution is in a transient state, where a maximum value of 1 indicates full synchrony (**Figures 3.2a**).

In our experiments, $\{\mathbf{X}_t\}$ is variable DNA fluorescently measured by flow cytometry in PI-stained populations of cells, where $t_i = \{0, 8, 16, \ldots, 88\}$ indicates the hour corresponding to the i_{th} measurement of data collected with respect to their release from cycle arrest via double thymidine block at $t_0 = 0$. We expect that the ASF evaluation of times t_0 and t_1 to be the greatest as the population of cells synchronously progress through the cell cycle, resulting in markedly dissimilar distributions of DNA in observation sets $\mathbf{X}_{t_0}$ and $\mathbf{X}_{t_1}$.

As the individual cells within a population variably progress through the cell cycle, we expect population DNA distributions to diverge, eventually settling to the classic asynchronous distribution profile (**Figure 3.1a-d**), where successive measurements of a no-longer-evolving variable are expected to be near-zero. We calculated the ASF between each temporally successive pair of data for both the synchronized cell population and the asynchronous control population (**Figure 3.2c**). We found that the ASF converges to a minimum of 0.127 from an initial value of 0.869, following a logistics curve. We observed an expected linear ASF from the

asynchronous population with slight oscillations, most likely emerging from unintended loss of mitotic cells during harvesting (mitotic shake off) positive slope (**Figure 3.2c**).

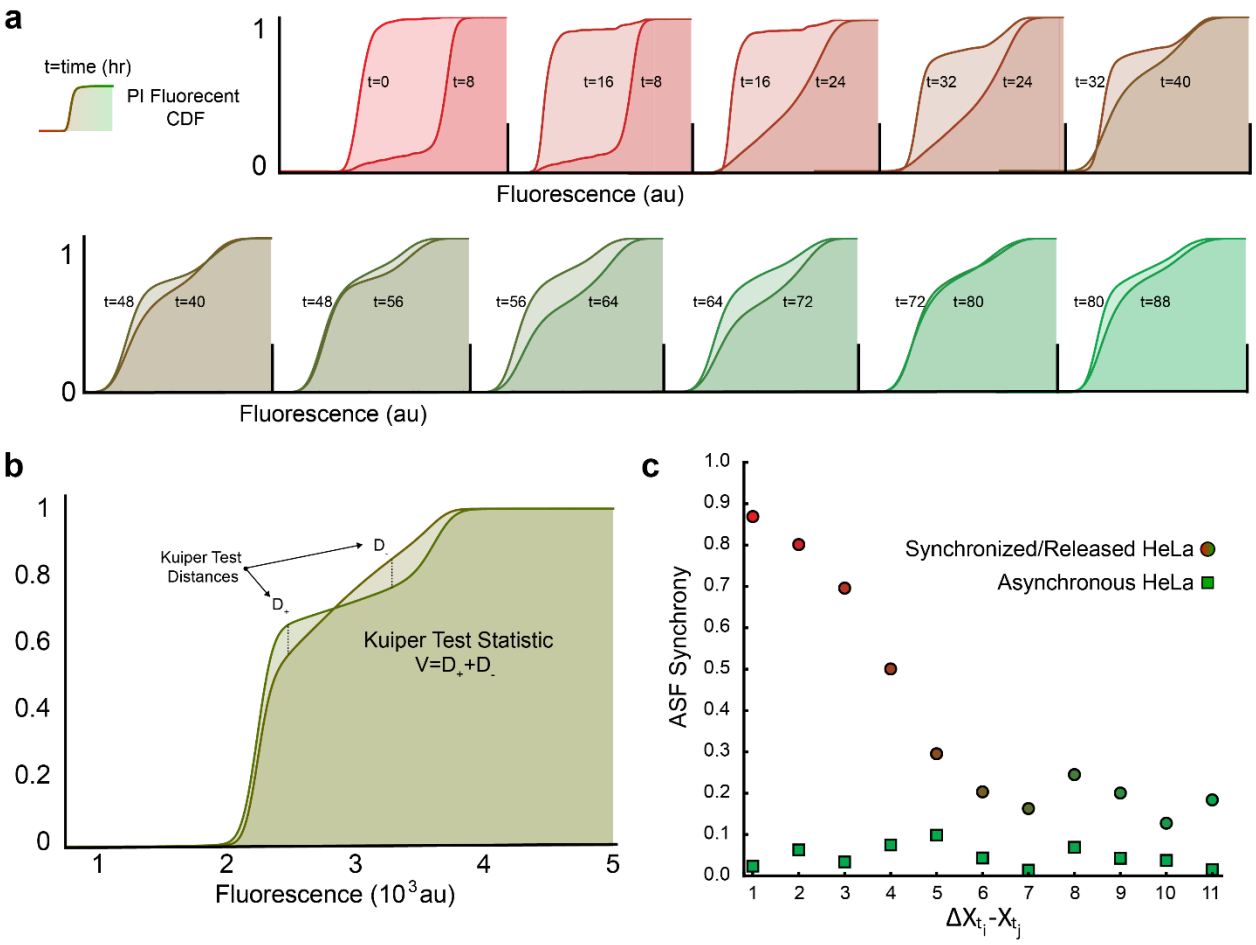

Figure 3.2: Rate of desynchronization using Kuiper Test Statistic. a) Pairwise comparison of PI CDFs for each time point (data shown is from synchronized cells). b) Visual representation of Kuiper Test Statistic determination between time points. c) Rate of desynchronization between asynchronous (green) and synchronized (red) Hela cells. Over time (~60 hours) synchronized cells being to reach an asynchronous state

3.5.3 A single cell interphase model

Cell cycle progression is intimately linked to a cell's dynamically changing DNA content. Temporal transitions from a cell's state of 2N to 4N define cell cycle phases, where G_1, S, and

G_2, correspond to genetic quantities of 2N, 2N+, and 4N, respectively, where the event of mitosis restarts the cell cycle for two progeny cells. Deterministically, we model a single cell's dynamic DNA content as

$$dna(t) = dna_0 + \frac{dna_{max} - dna_0}{1 + e^{-\beta(t-s)}} \qquad t_0 \le t \le \tau$$

where dna_0 is the initial genetic content in phase G_1, dna_{max} is the maximum genetic content after synthesis, β parameterizes the synthesis rate, s is the time in which the cell is halfway through synthesis and determines the periods of G_1, S, and G_2, and t is time. We assume that synthesis faithfully duplicates the genetic content, where $dna_{max} = 2\ dna_0$, thus reducing the above equation to:

$$dna(t) = dna_0 \left(1 + \frac{1}{1 + e^{-\beta(t-s)}}\right) \qquad t_0 \le t \le \tau$$

We can further reduce Eq. 2 by representing β and s as functions of the cycle period τ as:

$$dna(t) = dna_0 \left(1 + \frac{1}{1 + e^{-24\left(t - \frac{2\tau}{3}\right)}}\right) \qquad t_0 \le t \le \tau$$

where we assume that the duration of S is ~1/3 of the total cycle period. Accordingly, this single cell model captures DNA concentration during interphase using two parameters, the initial DNA concentration and the cell cycle period (**Figure 3.3a**).

To study the impact of the cell cycle period to the rate of asynchrony we use the Error-in-Variables (EIV) modeling approach to add noise to the cycle periodicity:

$$dna(t) = (dna_0 + \varepsilon_{dna_0}) \left(1 + \frac{1}{1 + e^{-24\left(t - \frac{2\tau + \varepsilon_\tau}{3}\right)}}\right) \qquad t_0 \le t \le \tau$$

where $\varepsilon_\tau \sim N(0, \sigma_\tau^2)$ is a normally distributed error term with variance σ_τ^2 and $\varepsilon_{dna_0} \sim N(0, \sigma_{dna_0}^2)$ is additionally added to capture fluorescent variability seen as broadened peaks around G_1 and G_2 (**Figure 3.1a**). We simulate a population of 1,000 cells, each starting synchronously at G_1 with extrinsically varying initial DNA content and cell cycle periodicity, as they repetitively progress through interphase (**Figure 3.3b**). We then take temporal slices of the DNA content of the population of cells and plot the populations distribution of DNA content intermittently (**Figure 3.3b-c**). We finally apply ASF to the slices in a pairwise manner as done in the experiment (**Figure 3.2**). An observation from these simulations is that a Poisson distributed error term for variance, as opposed to normal distribution, did not accurately capture the DNA dynamics of desynchronized cells using our ASF analysis.

Importantly, we found that only by including a variance term to cell cycle periodicity were we able to capture population dynamics that recapitulates the experimental results. Moreover, our model revealed that increasing the magnitude of variance resulted in increasing rates of desynchronization (**Figure B.2**). In order to further evaluate our model's prediction, we sought to experimentally introduce an additional source of noise that might impact the overall variance of cell cycle duration.

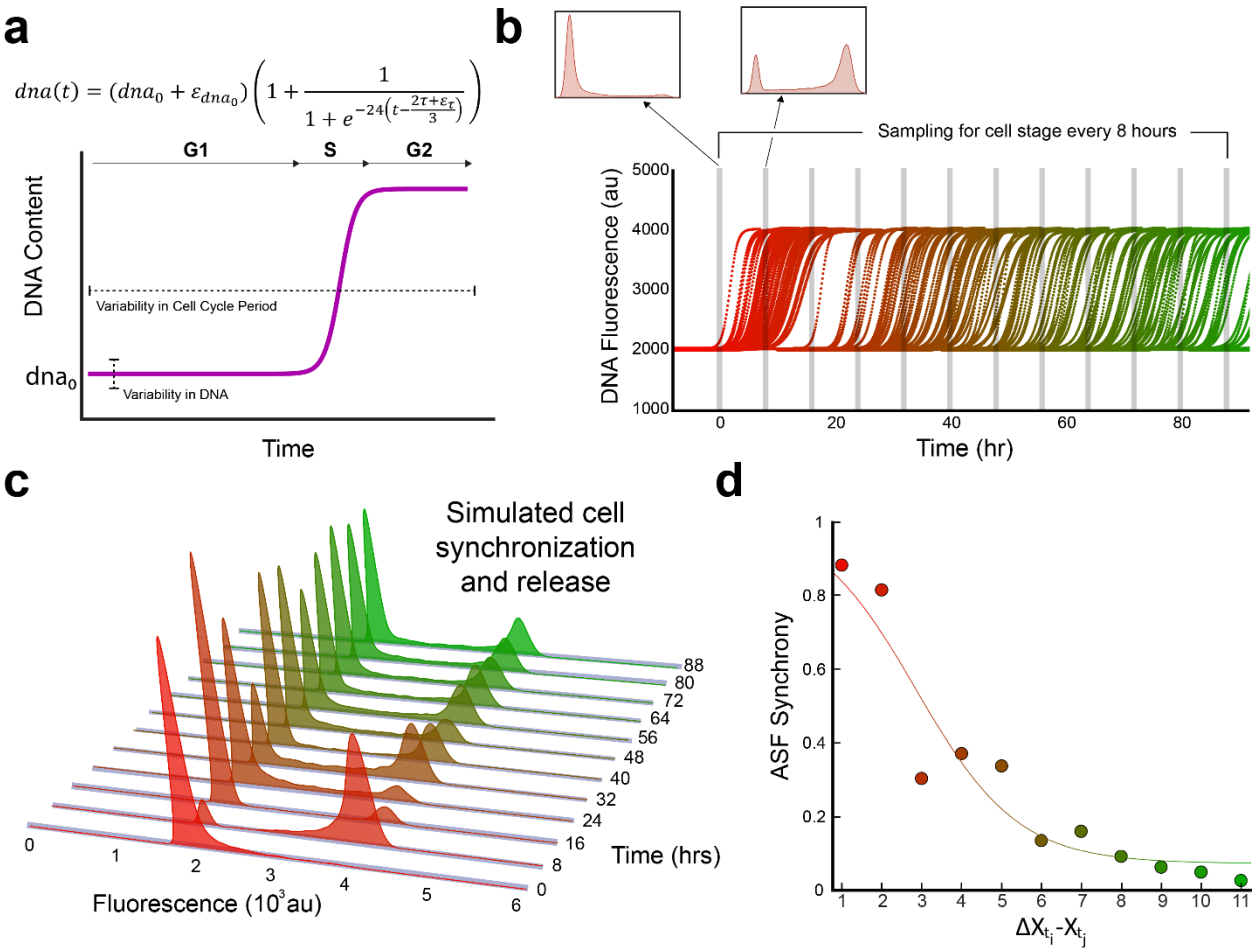

Figure 3.3: Single cell model of desynchronization. a) DNA synthesis is captured by the Gaussian error function where the relative durations of cycle phase are tunable. b) Cell cycle pace inheritance following a Gaussian distribution. c) Simulated data of PI staining of multiple lineages with normally distributed initial gene content. d) Desynchronization rate of simulated cell population.

3.5.4 Impact of LPS on cell cycle duration variability

Lipopolysaccharide (LPS) is a major component of the outer membrane of Gram-negative bacteria that can bind to TLR4 receptors initiating a signaling cascade that ultimately results in NFκB translocation from the cytoplasm to the nucleus, where as a transcription factor, it initiates the upregulation of inflammation regulatory genes (Y. Wang et al. 2014; Savinova, Hoffmann,

and Ghosh 2009; N et al. 2017). Additionally, NFκB activation can be induced by cytokines such as TNFα (Hayden and Ghosh 2014), which has been reported with contrasting roles, whereby NFκB induction is associated with both the activation of pro-survival genes as well pro-apoptotic genes (R. E. C. Lee et al. 2016). In addition to regulating inflammation signaling pathways, NFκB regulates major cell cycle regulatory factors (Bash, Zong, and Gélinas 1997; Ankers et al. 2016; Ledoux and Perkins 2014; Kenter and Watson 1987). Interestingly, components of NF-κB, such as RelA, have shown to interact with key cell cycle regulators, such as E2F transcription factors that are crucial in controlling progression through the G_1/S boundary (Ankers et al. 2016).

We therefore hypothesized that the contrasting nature of LPS stimulation in HeLa cells would result in a greater variance in overall cell cycle duration. Accordingly, if LPS is a viable approach for introducing cellular noise we would expect the desynchronization rate to increase compared to untreated synchronized cells (**Figure B.3**). Thus, in order to determine if LPS simulation had any effect on cell cycle duration, we conducted a time-lapse experiment to track individual cells cell cycle duration. In order to have a better indication of relative position of each cell in relation to the cell cycle, we integrated a fluorescence tracker using lentiviral transduction that express the histone protein H2B fused to a fluorescent protein (H2B-FT) (Eastman et al. 2020). Upon expression, the H2B protein is incorporated into nucleosomes, which binds DNA, and therefore could more easily distinguish cells undergoing mitosis. Next, we treated asynchronously-growing HeLa cells with 1.0 μg/mL of LPS derived from *E. coli.* O111:B4, and monitored the duration of the cell cycle for individual cells with timelapse microscopy for 72 hours every 20 minutes (**Figure B.4**). We found that the overall variance was

higher in treated cells versus untreated cells with an accompanying increase in the mean duration 23.7±4.73 and 21.7±3.42 hours, respectively (**Figure 3.4a**). Additionally, we also found that the addition of LPS appeared to enhance cell motility, as LPS treated cells showed an increase in overall cell displacement (**Figure B.5**), which supports the notion that LPS can induce epithelial-mesenchymal transition via TLR4 signaling (Jing et al. 2012; H. Li et al. 2014; Cho et al. 2015).

We next sought to test if the predictability of our simulation model with the values obtained from the time-lapse microscopy would result in an increased desynchronization rate under LPS stimulation. In order to compare multiple synchronous cell samples, we normalized each sample to its initial ASF value ($\mathbf{X}_{t_0} - \mathbf{X}_{t_8}$, **Figure B.6**). Upon inputting our new values obtained from the time-lapse microscopy, our model indeed predicted an increase in desynchronization when treated with LPS compared to the untreated sample (**Figure 3.4b**).

Given that we were able to increase the variance of cell cycle duration with LPS, and that our simulation model predicted an increase in desynchronization due to increased cell cycle duration variance, we next tested if we could experimentally obtain higher rates of desynchronization using the previous approach of PI-staining time-separated synchronized cells. Therefore, we again synchronized HeLa cells via the double-thymidine block method, and immediately following release of the arrested cells, we treated with varying concentrations of LPS (0.0, 0.1, 0.5, 1.0 μg/mL) and collected timepoints every 8 hours for 88 hours. We then analyzed the PI-stained cell populations via FlowJo cell cycle classifier that uses the Dean-Jett-Fox algorithm, and while it was not able to detect substantial changes in the overall phase distributions at the

early timepoints (0-32 hours), the effects of LPS were more evident at the later timepoints (40-88 hours) (**Figure 3.4c**). Interestingly, our ASF analysis methodology (**Figure B.7-B.8**) was able to differentiate the impact on cell cycle desynchronization at all timepoints tested for all LPS concentrations, with each increase in LPS having a greater impact in cell cycle desynchronization (**Figure 3.4d**).

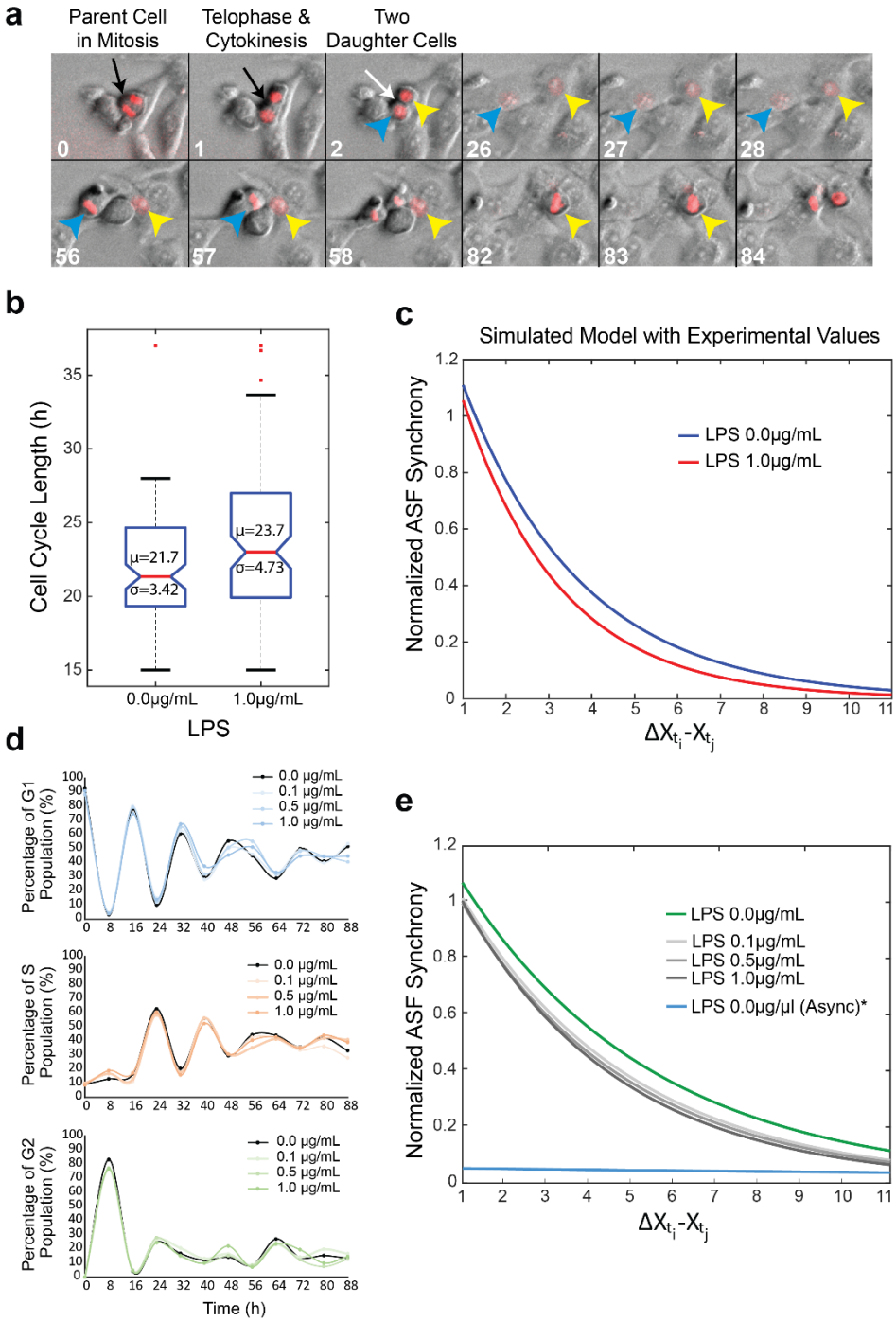

Figure 3.4: Noise variation of cell periodicity. a) Representative images of time lapse experiments. Once the septum (white arrow) is visible following cytokinesis, the cell cycle duration recording begins for both daughter cells (yellow and blue arrow). Both cells being cell cycle at Frame 2, and both daughter cells can be seen progressing through interphase in Frames 26-28. By the end of Frame 57, the first daughter cell completes the cell cycle and record

ends. The second daughter cell (yellow arrow) had a substantially longer cell cycle duration, which concluded at the end of Frame 84, thus demonstrating the inherent variability of cell cycle duration between identical cells within the population. b) Asynchronous cells were wither treated with 1 μg/mL of LPS or left untreated and cell cycle duration was recorded as described in Figure 4a. 100 cells were tracked for each condition and the population mean and standard deviation of cell cycle duration is shown. c) Values obtained from time lapse microscopy for cell cycle mean and standard deviation were used in our model to predict the impact on cell cycle desynchronization. The model revealed the LPS administration should result in an increased rate of cell cycle desynchronization d) Cell cycle phase distribution of various LPS concentrations following cell cycle synchronization for 88 hours post release. e) Normalized ASF scores for LPS-treated desynchronizing cells. The asynchronous population was not normalized in order to capture the overall linear trend.

3.6 Discussion

The cell cycle and subsequent daughter cell division is a central facet of cell biology from development and cellular differentiation to disease initiation and progression. While the process is tightly regulated and robust in a single cell, across a population we observe significant variability in period. Each cell within a given population contains measurable variations in their cellular content and housekeeping genes (e.g., differences in their RNA polymerases, ribosomes). These variations impact the expression of genes in what is known as extrinsic noise (Quarton et al. 2020; M. B. Elowitz et al. 2002; Kang et al. 2020; Raser and O'Shea 2004; Swain, Elowitz, and Siggia 2002). Furthermore, the cellular machinery responsible for progressing a cell through its cycle is intrinsically noisy as well. These intra and inter-cellular differences cause an initially synchronously in-phase population of cells to diverge as each progresses independently through their life cycle at varying rates (Chao et al. 2019).

Moreover, cell synchronicity is an essential aspect of mammalian biological homeostasis. The circadian rhythm is a molecular orchestrated process present in various tissues that synchronizes

biological outputs to the 24-hour day-night cycle (Patke, Young, and Axelrod 2019). It is composed of multiple master transcription factor regulators that are involved in robust feedback networks that enable these oscillatory functions is cells (Partch, Green, and Takahashi 2014). Importantly, cancer cells can become compromised with respect to these molecular actuators the enable cellular synchronization, and there is evidence that this disruption can enhance tumorigenesis (Sulli, Lam, and Panda 2019). For example, DNA repair mechanisms are tied to the circadian regulation (Sancar et al. 2010) and if these processes are disrupted it may lead to accumulating mutations and overall genome instability (Gery et al. 2006). Thus, understanding and modeling cell desynchronization at a single-cell level is a decisive approach to quantifying cellular changes that may impact oncogenesis (Barberis and Verbruggen 2017).

Here, using a combination of simulations and experiments we show that the variability in cell cycle period directly impacts the rate of desynchronization in a population of cells. The next line of investigation will include studying the factors that contribute to this variability at a single cell level, and the distribution between intrinsic and extrinsic sources of noise. Finally, a key direction of research is not just on how such a tightly regulated process can rely on stochastic variations, but also how diseased states such as cancer cells, utilize noise and if noise itself can become a contributor to disease progression. More specifically an intriguing hypothesis is that cancer cells obtain benefit by having higher noise in cell cycle periodicity, which yields ultra-slow and fast diving cells. Moreover, this hypothesis opens the path for potential means to exploit variability in cell cycle period for therapeutic purposes.

3.7 Acknowledgements

We thank Khai Nguyen and Bleris lab members for support and discussions. This work was funded by US National Science Foundation (NSF) grants (1351354, 1361355, 2029121), a Cecil H. and Ida Green Endowment, and the University of Texas at Dallas

APPENDIX A

SUPPLEMENTAL MATERIAL FOR CHAPTER 2

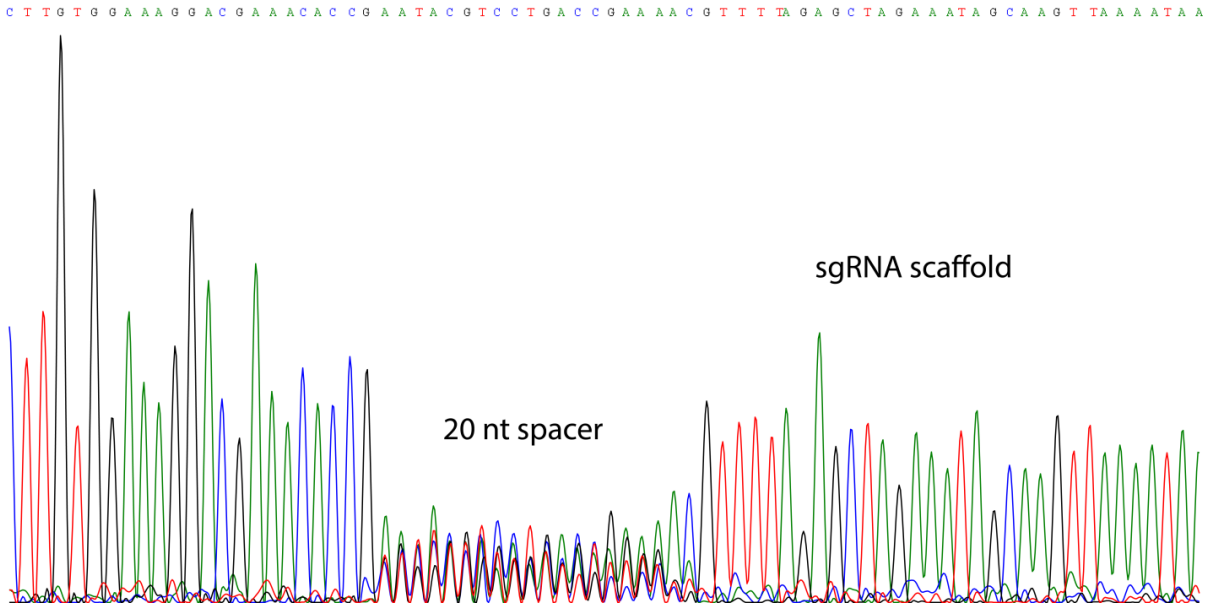

Figure A.1: Confirming the complexity of the CRISPR plasmid library. The CRISPR plasmid library was subjected to Sanger sequencing using primer P1, resulting in a 20-nt "noisy" target sequence closely matching the expected pattern from the 93 sgRNA oligonucleotide mixture.

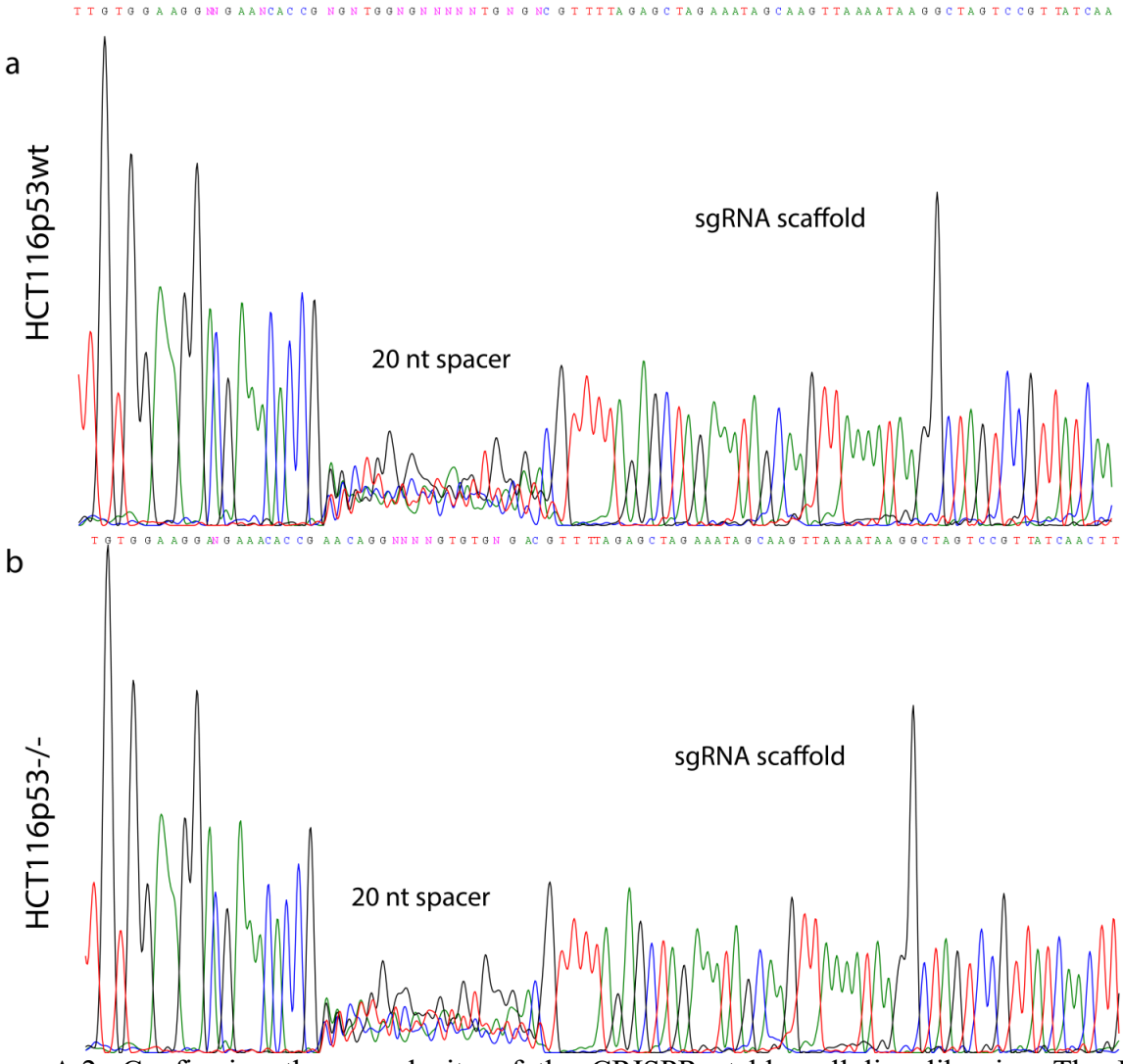

Figure A.2: Confirming the complexity of the CRISPR stable cell line libraries. The PCR fragments harboring the sgRNA constructs were amplified from the (a) WT-LIB and (b) KO-LIB cells by PCR and subjected to Sanger sequencing using primer P2, resulting in a 20-nt "noisy" sgRNA target sequence closely matching the expected pattern.

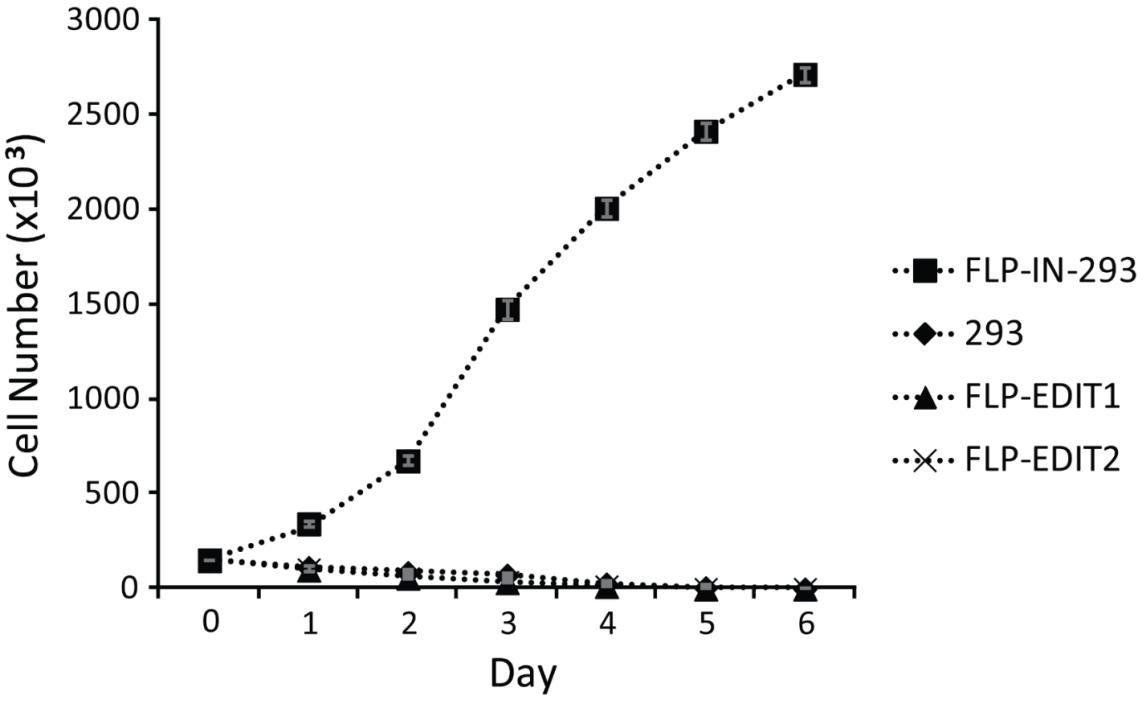

Figure A.3: Efficacy of the LentiCRISPRv2 system. Lentivirus was prepared targeting the open reading frame (ORF) of the zeocin resistance gene. On stable integration of these CRISPR constructs, the zeocin resistance cassette in the Flp-In-293 cells was effectively disrupted and the cells (FLP-EDIT1 and FLP-EDIT2) became sensitive to treatment with 100 μg/mL zeocin.

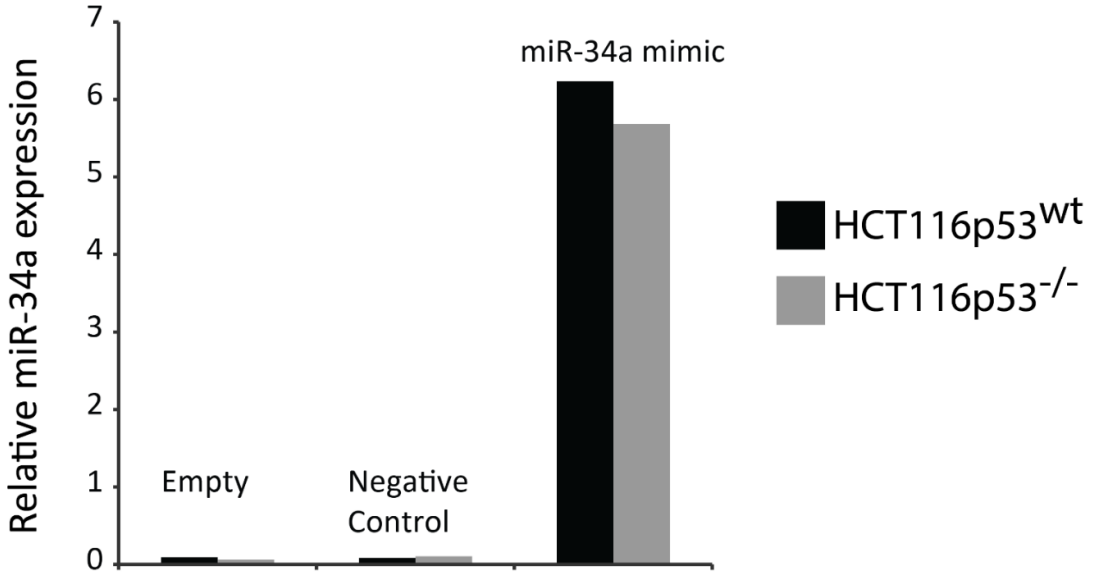

Figure A.4: Endogenous and ectopic miR-34a expression in HCT116p53 wild-type and p53-/- cells. Empty represents cells that were not transfected with anything. Negative control represents cells that were transfected with 25nM of a miRNA mimic derived from *C. elgans* (cel-miR-67). miR-34a levels were measured relative to the small nuclear RNA U6.

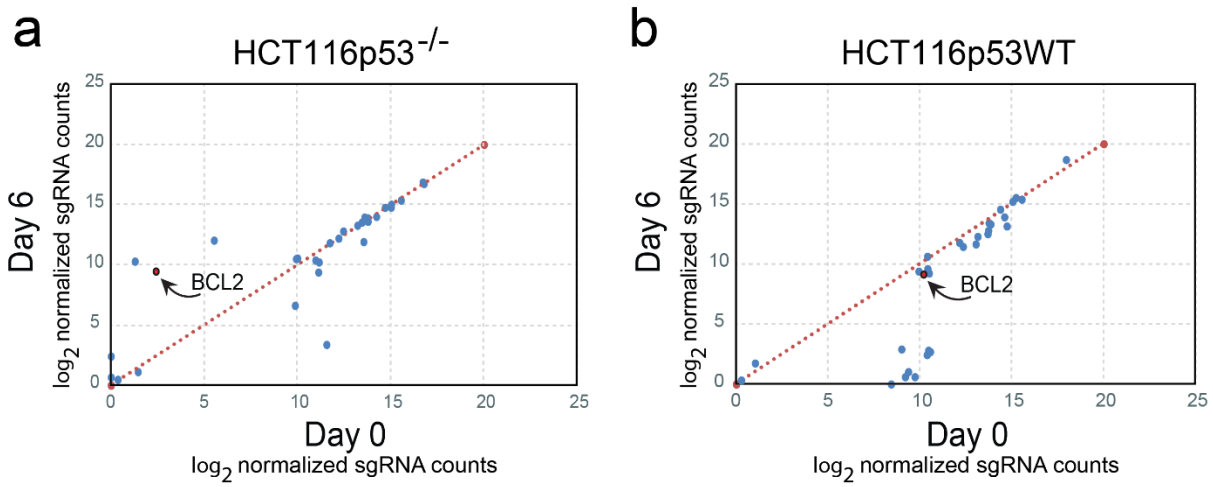

Figure A.5: High-throughput editing of edges with CRISPR libraries in (a) HCT116p53-/- (LIB-p53-/-) and (b) HCT116p53WT (LIB-WT) cells. 34 sgRNAs corresponding to direct miR-34a targets are shown. After 6 days treatment with 25nM of miR-34a mimic, LIB-p53$^{-/-}$ cells showed an enrichment of the sgRNA targeting the miR-34a target site in the BCL2 3'UTR.

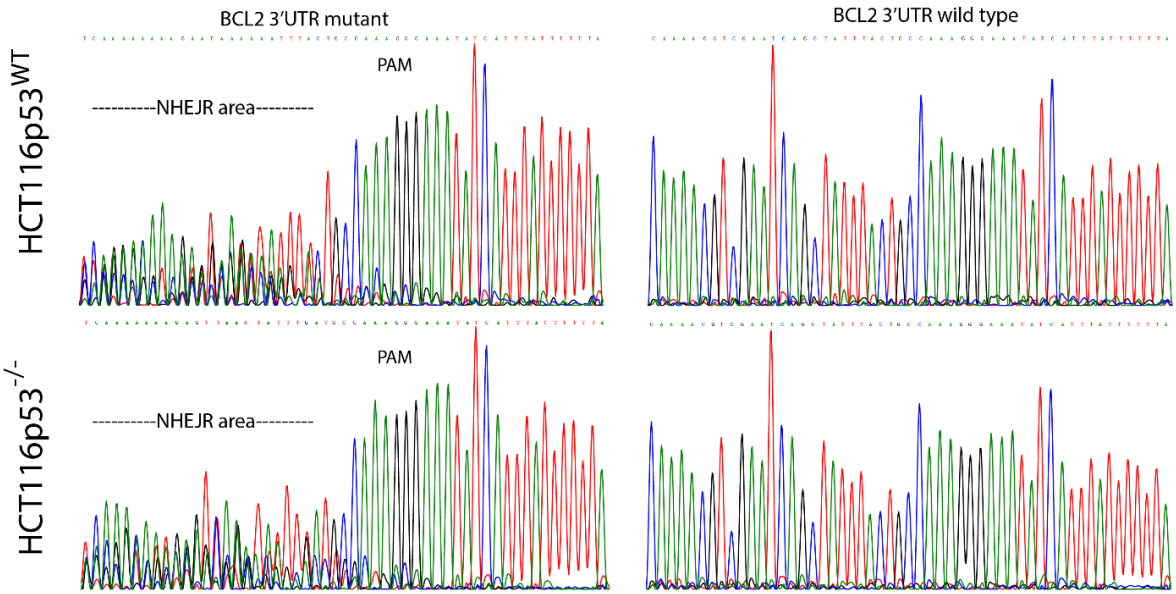

Figure A.6: Preparation of BCL2tgt-WT and BCL2tgt-p53-/- stable cells. Sanger sequencing results for PCR products harboring the miR-34a target sites within the 3'UTR of BCL2 in BCL2tgt-WT (left, upper panel) and BCL2tgt-p53$^{-/-}$ cells (left, lower panel) were included. Additionally, Sanger sequencing results for their corresponding parental cells (right, upper panel: HCT116p53WT; right, lower panel: HCT116p53$^{-/-}$) at the same genomic location were included

BCL2tgt-WT

13.20%	CAGGCAAAACGTCGAATCAGCTATTTACTGCCAAAGGGAAATATCA
12.00%	CAGGCAAAACGTCGAATCAGCTAT-----GCCAAAGGGAAATATCA
10.00%	CAGGCAAAACGTCGAAT------TTTACTGCCAAAGGGAAATATCA
9.50%	CAGGCAAAACGTCGAATCAGCTATTTACTGC---AGGGAAATATCA
9.40%	CAGGCAAAACGTCGAATCAGCTATTTA----CAAAGGGAAATATCA
9.00%	CAGGCAAAACGTCGAATCAGCTATTTACTGCCAAA-----ATATCA
7.10%	CAGGCAAAACGTCGAATCAG----TTACTGCCAAAGGGAAATATCA
6.20%	CAGGCAAAACGTCGAATC---TGTTTACTGCCAAAGGGAAATATCA
5.60%	CAGGCAAAACGTCGAA--AGCTATTTACTGCCAAAGGGAAATATCA
1.60%	CAGGCA----------GCCAAAGGGAAATATCA

BCL2tgt-p53-/-

14.40%	CAGGCAAAACGTCGAATCAGCTATTT ACTGCCAAAGGGAAATATCA
13.60%	CAGGCAAAACGTCGA---------- --TGCCAAAGGGAAATATCA
9.20%	CAGGCAAAACGTCGAATCAGCTATTT ACTG-GAAAGGGAAATATCA
9.00%	CAGGCAAAACGTCGAATCAGCTATTTGA-TGCCAAAGGGAAATATCA
9.00%	CAGGCAAAACGTC-----AGCTATTT ACTGCCAAAGGGAAATATCA
7.70%	CAGGCAAAACGTCGAATCAGCTAT-- -CCACCAAAGGGAAATATCA
7.70%	CAGGCAAAACGTCGAATCAGCTATTT ACTGCCAAA-----ATATCA
6.40%	CAGGCAAAACGTCG--T-TGCTATTT ACTGCCAAAGGGAAATATCA
5.50%	CAGGCAAAACGTCGA-T-AGCTATTT ACTGCCAAAGGGAAATATCA
4.40%	CAGGCAAAACGTCGAATCAGCTATTT ACTGCCAAAGG-AAATATCA

Figure A.7: Alignment of wild-type and the most frequently detected indel sequences in BCL2tgt-WT and BCL2tgt-p53-/- stable cells. NGS amplicon sequencing results for PCR products harboring the miR-34a target sites within the 3'UTR of BCL2 in BCL2tgt-WT and BCL2tgt-p53$^{-/-}$ cells.

.

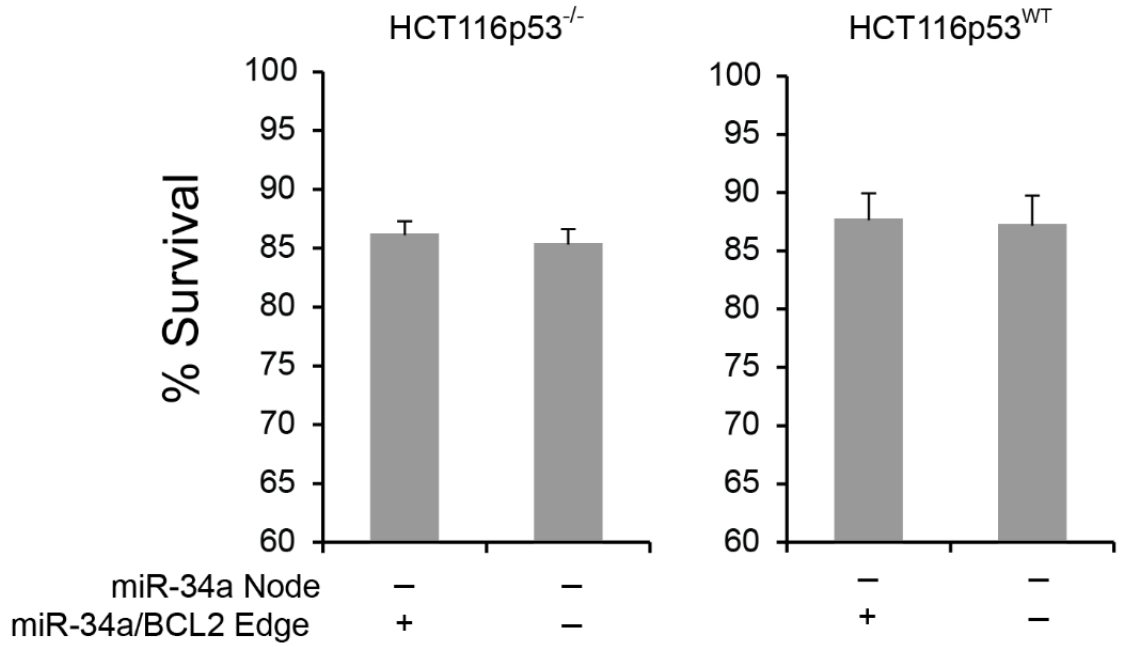

Figure A.8: Cell survival after miR-34a/BCL2 edge removal. In both WT and $p53^{-/-}$ cells, the removal of miR-34a/BCL2 edge alone did not induce apoptosis.

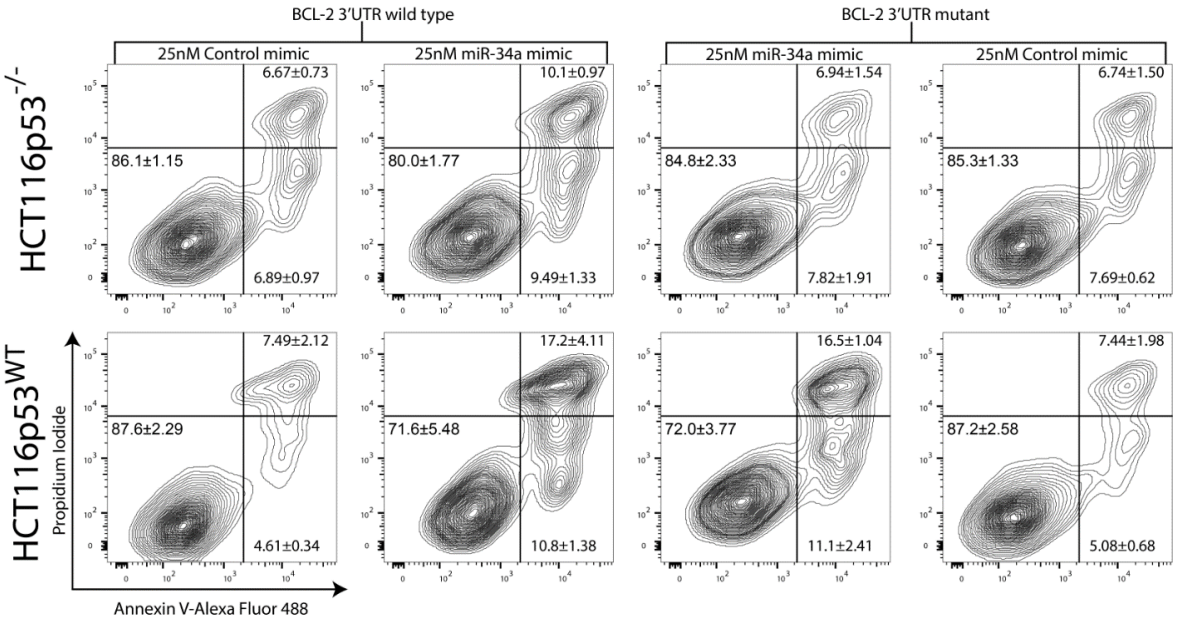

Figure A.9: miR-34a-induced apoptosis in WT, p53-/-, BCL2tgt-WT and BCL2tgt-p53-/- cells. As the cell initiates apoptosis it flips phosphatidylserine (PS) from the inner leaflet of the cell membrane to the outer leaflet. Annexin V binds externalized PS, giving a positive Alexa-Fluor 488 signal. As apoptosis progresses, the outer membrane loses its integrity such that the propidium iodide, which is typically impermeable to the cell, is able to enter the cell and bind nucleic acids giving a positive propidium iodide signal. Transfection of 25nM of miR-34a mimics induces apoptosis in the WT and $p53^{-/-}$ cells. This effect is mitigated in BCL2tgt-$p53^{-/-}$ cells, but not in BCL2tgt-WT cells

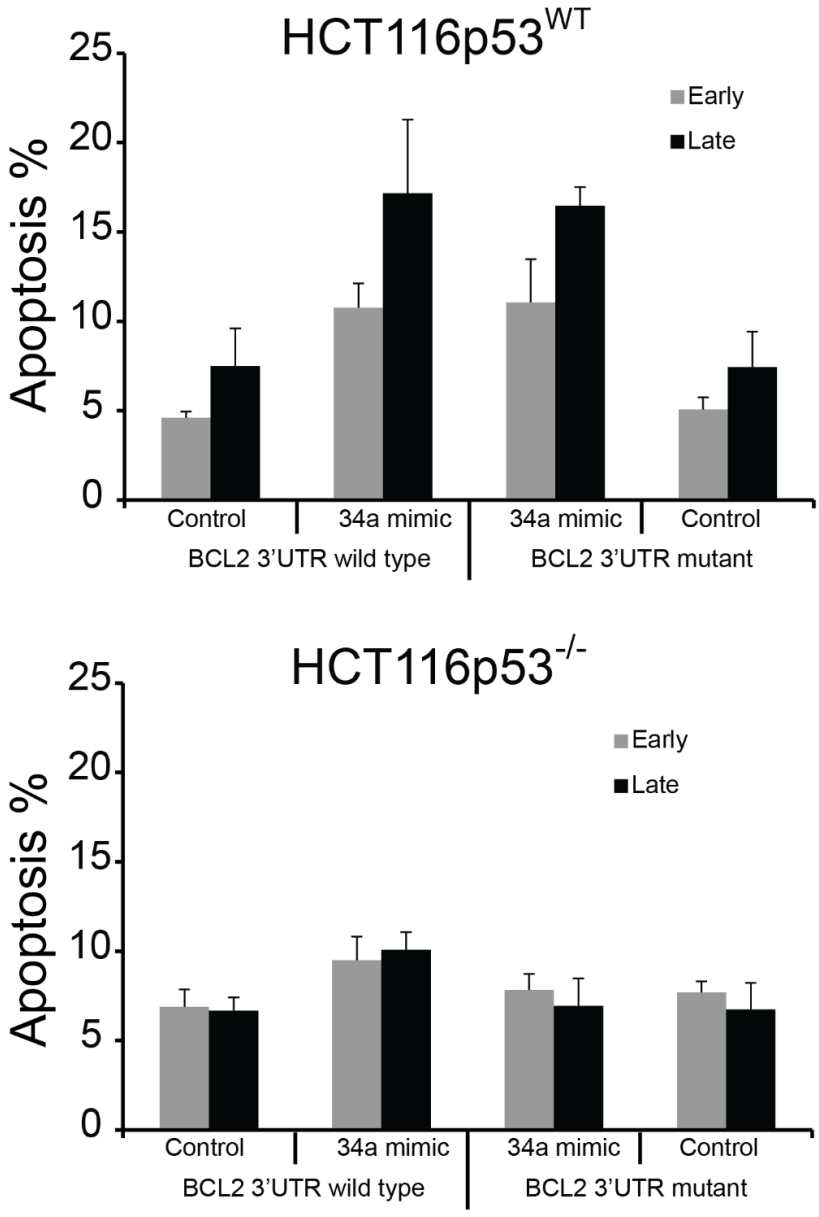

Figure A.10: Cells undergoing early and late apoptosis after miR-34a delivery. Ectopic miR-34a delivery induces early and late apoptosis in WT and $p53^{-/-}$ cells. This effect is mostly abolished in BCL2tgt-$p53^{-/-}$ cells, but not in BCL2tgt-WT cells, where the miR-34a target sites within the 3'UTR of BCL2 are disrupted.

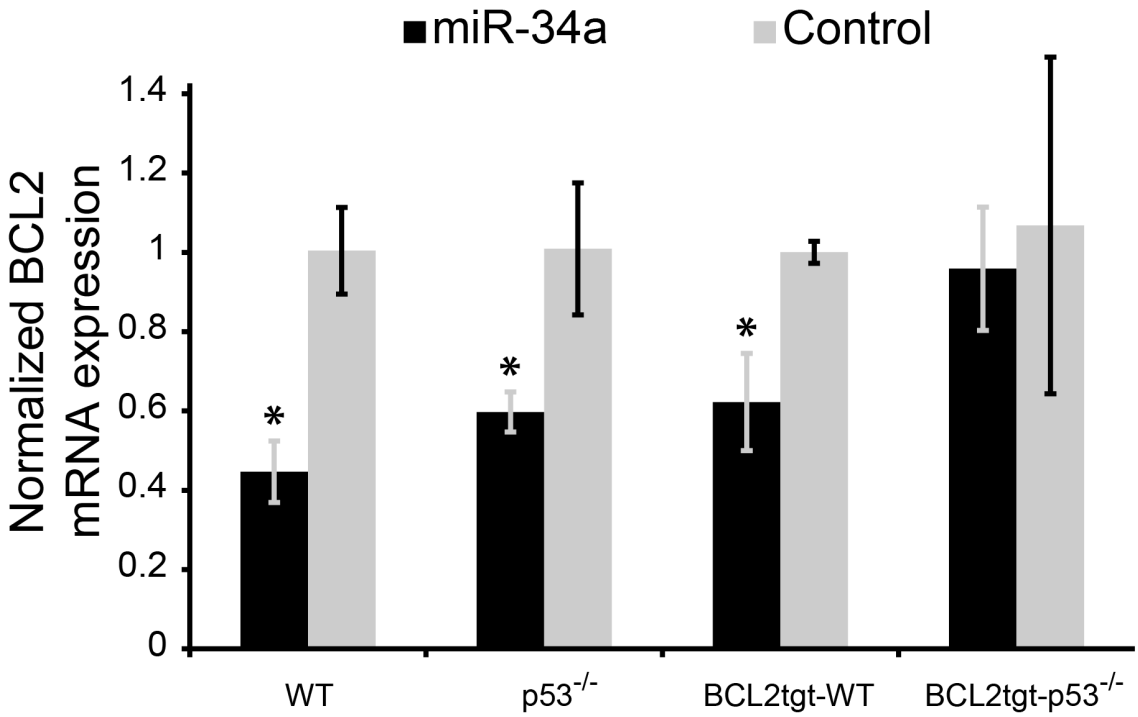

Figure A.11: Expression of BCL2 after miR-34a delivery. Treatment with miR-34a suppresses the expression of BCL2 in WT and $p53^{-/-}$ cells. This effect is abolished in BCL2tgt-$p53^{-/-}$ cells, but not in BCL2tgt-WT cells (* indicates $p < 0.05$).

Table A.1: Target genes for miR-34a and the corresponding sgRNA sequences.

Gene name	miRNA seed	sgRNA target	PAM
AXL	CACTGCCA	TCCAAGCTAAGCACTGCCAC	TGG
BCL2	ACTGCCA	AATCAGCTATTTACTGCCAA	AGG
CCND1	ACTGCCA	AGAAAACTAAAACTAGTACA	TGG
CDK6	CACTGCCT	TTTGCCAACAAGGCAGTGTG	TGG
DLL1-1	CACTGCC	TGCAACGGCGACGTCACGGA	AGG
DLL1-2	CACTGCCT	AGAATCCAAAATATACACTC	AGG
DLL1-3	CACTGCCT	CGTATCAAAAAGGACAATAA	AGG
E2F3	CACTGCCA	AAAGCAGCTAGAAAGTATTC	TGG
FOSL1	CACTGCCA	TCACCTGCTGCTGCTGGCAG	TGG
FUT8	CACTGCCA	GTCACTTAAATTACACAATA	TGG
GALNT7	CACTGCCA	TCTTTTTGAAGCACTGCCAC	AGG
GAS1	CACTGCCA	CATAAAGAGACTTTCATACA	TGG
HDAC1	GAGCCAAGAAA	AGAGGGCAGGCAGTGTTTCT	TGG
HNF4A	CCACTGCC	GAAGGTGAAGGTGAAGGCAG	TGG
INHBB	ACTGCCA	AAAAATAACTTTTTTTCAAA	TGG
JAG1-1	CACTGCC	CCTCAGACTCTACCTAGCGG	CGG
JAG1-2	CACTGCCT	TTGATTTCCTCACTTAAGGC	AGG
KLF4	CACTGCCA	AAAAATACTGAATTCTCTTC	TGG
MAP2K1	CACTGCCA	TGGTGAAGCCCCAGCTATCA	TGG
MET-1	CACTGCCT	TCGATGGCCTTTTAAAGGTC	AGG
MET-2	CACTGCCT	TTCAGTTCAGCTGCAGGTAT	AGG
NOTCH1	CACTGCCT	AACAGTACATATAAATAAAA	AGG
NOTCH2	CACTGCCT	AGATCAGTAAAAAGTTTGAA	AGG
PDGFRA-1	ACTGCCA	ACAGCTTGTCATAAATGTTT	TGG
PDGFRA-2	CACTGCC	AGTTAAAAAAATATAAACGA	AGG
YY1	ACTGCCA	TTACACTGAACATCAGCATC	TGG
MDM4	CACTGCCA	AGTAACCTTAACATTCCCTA	TGG
MYCN-1	CACTGCC	AAAAATCAAAATGTGCAAAG	TGG
MYCN-2	CACTGCC	AGCGTCATACTAAAGTATAC	AGG
PDGFRB	CACTGCC	GAGATGTCACTGCTAGGTCT	GGG
SNAI1	CACTGCC	CCACATCCTTCTCACTGCCA	TGG
SRC-1	CACTGCC	CAGCTGGGCTGAGCGGGCAG	CGG
SRC-2	CACTGCC	ACACAGCCAGTCCTGGTGCA	TGG
SRC-3	CACTGCC	CTGGCTGGCTCAAGAACCCC	TGG

Table A.2: Target genes for miR-145 and the corresponding sgRNA sequences.

Gene name	miRNA seed	sgRNA target	PAM
ADAM17	AACTGGAA	CATTTATTTGTGATGACAAC	TGG
ADD3-1	AACTGGA	GATTGGGGGATGTAGCAAAC	TGG
ADD3-2	AACTGGAA	GCAAACTGGACTTTAAGAAC	TGG
ADD3-3	ACTGGAA	TTCTAGATCTCACTAACTAC	TGG
CDK6-1	AACTGGAA	AAAATGCAGCTGTTCTGAAC	TGG
CDK6-2	AACTGGA	ACCAATAATCCTTTGGAAAC	TGG
CTNND1	AACTGGA	AAAGCTCTGTTCCATGCAAC	TGG
DDX6	ACTGGAA	TTATCTCAATAAAAGCCCAC	TGG
DDX17	ACTGGAA	TATATATATATATAGCTGAC	TGG
E2F3	ACTGGAA	GCTTTGTGTTAAGTGCCTAC	TGG
ETS1	ACTGGAA	GTGGTGGGTGGTTTATACAC	TGG
FLI1-1	AACTGGA	CCTTGAAGGGAAGACAAAAC	TGG
FLI1-2	AACTGGAA	CAAATTCAGTGGATGGCAAC	TGG
FLI1-3	AACTGGAA	CAGTGAAGTTTTCACCCAAC	TGG
FSCN1-1	AACTGGAA	AGCCCCCTTGCCTTTCAAAC	TGG
FSCN1-2	AACTGGAA	CCCTGGGCGTGTAGTGTAAC	TGG
FSCN1-3	ACTGGAA	TCCTTTCACCCTAGCCTGAC	TGG
FSCN1-4	AACTGGAA	CCATGATAGTAGCTTCAAAC	TGG
IGF1R	AACTGGAT	TACCTACCGGTTTCCACAAC	TGG
IRS1	AACTGGAA	TCAAACTACCGATTTAAAAC	TGG
ITGB8	AACTGGAA	CACTTTTAAACAAAATTAAC	TGG
KLF4	ACTGGAA	CAAAATGCCAAGGGGGTGAC	TGG
KLF5	AACTGGAA	AAGAAAACCACAACTAAAAC	TGG
MYO6-1	AACTGGA	ATGGCACAGTACCATATAAC	TGG
MYO6-2	AACTGGA	AGGTGGCATAGTGGCTTAAC	TGG
NEDD9	AACTGGAA	TAACGGTTACTAAGGAAAAC	TGG
NRAS	AACTGGAA	GATGTTTAAAAAATAAAAAC	TGG
PAK4	ACTGGAA	GGCAGCGGCCCTCCCATCAC	TGG
RREB1	AACTGGAA	GGGTACCCATAGCCAATAAC	TGG
RTKN	AACTGGAA	AACCCTTCCTGGAAGAAAAC	TGG
SERPINE1	AACTGGA	GCCTTCATCTGGGACAAAAC	TGG
SMAD3-1	AACTGGAA	CTAGTCTAAATTATTTCAAC	TGG
SMAD3-2	AACTGGA	GAAACTTGCCTCATGTAAAC	TGG
SOX9	AACTGGAA	TGTTTTTGTTGAAAACAAAC	TGG
SP1	ACTGGAA	TCTTCACATTGTGTGAATAC	TGG
SRGAP1-1	AACTGGA	CTTAGTTTTGTGCTTATAAC	TGG
SRGAP1-2	AACTGGA	TTGTAATTTTTTTAAATAAC	TGG

Table A.2, continued

SRGAP1-3	AACTGGAA	GTCAGATCCATAAAGCAAAC	TGG
SWAP70	AACTGGAA	TTATTTACATGAGAGGAAAC	TGG
TGFBR2	AACTGGAA	TCTGGGTTATCAGCATAAAC	TGG
TNFSF13	ACTGGAA	CAGACCTGGTCGGGGCCCAC	TGG
YES1	AACTGGAA	GCATGTTTTTAATGGTAAAC	TGG
BNIP3-1	AACTGGA	TGAAGAACTGGAGTCTGACT	TGG
BNIP3-2	AACTGGA	CTGTGTCTACTTTAAAAAAC	TGG

Table A.3: Target genes for miR-192 and the corresponding sgRNA sequences.

Gene name	miRNA seed	sgRNA target	PAM
ALCAM	TAGGTCA	GTTTTGGCAGCCATGATAAT	AGG
DICER1	TAGGTCA	TATACTCGCACAACTTAAAT	AGG
RB1	TAGGTCAA	TCAGTTAGTTTTTAGGTCAA	GGG
WNK1	TAGGTCA	GTGCAACTCTTTCTTATGAT	AGG

Table A.4: Target genes for miR-194 and the corresponding sgRNA sequences.

Gene name	miRNA seed	sgRNA target	PAM
DNMT3A	CTGTTAC	CTGTAAACAAGAGGTAACAG	CGG
HBEGF-1	CTGTTAC	AAGTGCCTAGACTGTTACTT	TGG
HBEGF-2	CTGTTACA	AAGTTGTAACAGTTCAGAAA	TGG
IGF1R	CTGTTACA	ATCATGTCTTGCACTGTAAC	AGG
ITGA9	CTGTTAC	TATATTTATAAAAATACTTT	AGG
PTPN12	CTGTTACA	TCTACAAGCAGCGTGTAACA	GGG
RBX1	CTGTTAC	ATTTGTAATTAGGTAACAGC	AGG

Table A.5: Target genes for miR-215 and the corresponding sgRNA sequences.

Gene name	miRNA seed	sgRNA target	PAM
ALCAM	TAGGTCA	GTTTTGGCAGCCATGATAAT	AGG
PTPRT	AGGTCAA	AGCAGAAGGTAAATAATGTC	AGG
RB1	TAGGTCAA	ATACAAATCAGTTAGTTTTT	AGG
WNK1	TAGGTCA	GTGCAACTCTTTCTTATGAT	AGG

Table A.6: Relative abundance of the 93 sgRNA target sequences as determined by NGS amplicon sequencing.

sgRNA Target	LIB-WT-D0	LIB-WT-D6	LIB-p53$^{-/-}$-D0	LIB-p53$^{-/-}$-D6
AXL	0.0014406	0.00059977	0.002269509	0.001206818
BCL2	0.00116582	0.00056636	4.30E-06	0.000712584
CCND1	0.00900663	0.00499026	0.00949756	0.009996992
CDK6	0.02117193	0.02389951	0.013848337	0.015336366
DLL1-1	0.02707046	0.00908714	0.012335809	0.015994559
DLL1-2	0.00034274	0	2.87E-07	3.93E-07
DLL1-3	0.00083966	5.22E-07	1.43E-06	1.26E-03
E2F3	0.2536203	0.4203797	0.107535808	0.120319506
FOSL1	0.00050852	6.52E-06	4.51E-05	0.004232699
FUT8	1.04E-06	2.35E-06	0.000968178	0.00145796
GALNT7	0	0	0	0
GAS1	0	0	0	0
HDAC1	0.00134714	0.00158086	0.011911693	0.003894962
HNF4A	0.00451927	0.00352503	0.004715781	0.004747746
INHBB	0.00097331	0.00067076	0.003390633	0.003639304
JAG1-1	0.03373529	0.03751129	0.04793143	0.042674737
JAG1-2	0.01346623	0.00703596	0.033127253	0.028289924
KLF4	2.07E-07	2.61E-07	0	4.32E-06
MAP2K1	0.00133036	4.44E-06	0.001998339	1.35E-03
MET-1	0	0	0	0
MET-2	0.02470359	0.01539126	0.026401943	0.02801031
NOTCH1	0.00058333	5.22E-07	0	5.89E-07
NOTCH2	0.01315187	0.00582154	0.005607343	7.16E-03
PDGFRA-1	0.00135937	0.00077464	0.003011282	9.43E-06
PDGFRA-2	0.00518839	0.00278823	0.001020404	1.51E-03
YY1	0.00150318	5.48E-06	0.000932883	9.80E-05
MDM4	0	0	0	0.00E+00
MYCN-1	0.00065751	1.04E-06	1.72E-06	1.18E-06
MYCN-2	0.03807698	0.04691867	0.019170735	1.66E-02
PDGFRB	0.01467391	0.01018045	0.013979474	0.012529424
SNAI1	0.00841004	0.00322097	0.011193738	0.011962931
SRC-1	0.04748313	0.04273201	0.112325622	0.11057778
SRC-2	0.01374659	0.01093526	0.033329842	0.033475549
SRC-3	0.00140268	6.00E-06	0.002223023	0.000672527
ALCAM	0.06371658	0.03938864	0.154566206	0.162712666
PTPRT	0.02649791	0.00757988	0.00808604	0.01155588

Table A.6, continued

RB1	0.00546938	0.00276683	0.019628425	0.019041057
WNK1	0.05712116	0.12653401	0.034930751	0.028601937
DNMT3A	0	0	0	0
HBEGF-1	0.01392978	0.00583433	0.022108844	0.030726926
HBEGF-2	0.00363133	0.00146524	0.001297313	0.001815136
IGF1R	0.04630529	0.02288684	0.017214005	0.014285063
ITGA9	2.07E-07	2.61E-07	8.61E-07	3.93E-07
PTPN12	0	0	5.74E-07	3.93E-07
RBX1	2.69E-06	0.00084876	5.17E-06	1.05E-03
ALCAM	0	0	0	0
DICER1	0.00203428	0.00108392	0.004851222	0.002461744
RB1	0	0	0	0
WNK1	0	0	0	0
ADAM17	0	0	0	0
ADD3-1	0.05134075	0.03375423	0.046668551	0.040806192
ADD3-2	0.00764727	0.00157355	0.003598387	0.007044156
ADD3-3	0.00165093	0.00189693	0.000831589	0.00068529
CDK6-1	0.00268496	0.00530503	0.012269523	0.012464626
CDK6-2	0.00036782	0.00182646	0.000681226	0.001165779
CTNND1	0.00561568	0.00324863	0.000961005	0.002768259
DDX6	0	0	0	0
DDX17	0	0	0	0
E2F3	0.00673632	0.00292604	0.00464806	0.003046891
ETS1	6.22E-07	0.00021558	0.001169619	2.55E-06
FLI1-1	0.00068818	0.0005139	8.61E-07	1.18E-06
FLI1-2	0.00546979	0.00058176	0.006579538	2.74E-03
FLI1-3	0.01225461	0.00828796	0.010742074	0.023490928
FSCN1-1	0.00355632	0.00351328	0.008916768	0.004905815
FSCN1-2	0.01821365	0.011475	0.006625164	0.000846304
FSCN1-3	0.04537135	0.02319768	0.017552896	0.016474458
FSCN1-4	0	0	0	0
IGF1R	0.00130238	0.0015699	0.003967695	0.005591694
IRS1	0	0	0	0
ITGB8	0.00063513	3.65E-06	4.59E-06	2.10E-05
KLF4	0.00538048	0.00146785	0.002142102	4.84E-04
KLF5	0.00077956	0.00152892	0.001459728	0.000650535
MYO6-1	0.00095176	2.87E-06	2.87E-06	3.53E-06
MYO6-2	0.00216442	0.00144305	1.43E-05	2.12E-03

Table A.6, continued

NEDD9	0.00143894	0.00103355	0.00345118	0.003832913
NRAS	0	0	0	0
PAK4	0.00852567	0.00340158	0.008635267	0.010401686
RREB1	0.00348628	1.23E-05	0.003863818	0.002857405
RTKN	0.00699307	0.00510954	0.017313578	0.019979846
SERPINE1	0.00997974	0.00689737	0.028574462	0.033511679
SMAD3-1	4.99E-05	2.61E-07	2.18E-05	0
SMAD3-2	0.00034523	0.0010265	1.15E-06	0.000134505
SOX9	0	0	0	0
SP1	0.02086669	0.00795023	0.041485898	0.038913298
SRGAP1-1	0	0	0	0
SRGAP1-2	1.45E-06	7.83E-07	7.49E-05	0.00084061
SRGAP1-3	1.04E-06	0.00055201	5.74E-07	3.93E-07
SWAP70	0.00351529	0.00146002	0.009548351	8.10E-03
TGFBR2	0	0	0	0
TNFSF13	0.00254715	0.00144566	0.005597012	0.002562279
YES1	0.00444343	0.00724502	0.004088502	0.000642288
BNIP3-1	0.00480544	0.0025074	0.007038089	0.002951461
BNIP3-2	0	0	0	0

Table A.7: log-transformed counts per million reads for the 93 sgRNA target sequences as determined by NGS amplicon sequencing.

sgRNA Target	LIB-WT-D0	LIB-WT-D6	LIB-p53$^{-/-}$-D0	LIB-p53$^{-/-}$-D6
AXL	10.49345223	9.230672244	11.14879994	10.23818721
BCL2	10.18836955	9.148130131	2.407159755	9.478939719
CCND1	13.13693225	12.28518973	13.21349313	13.28742263
CDK6	14.36993313	14.54475352	13.75752928	13.90476308
DLL1-1	14.72448504	13.14976879	13.59068169	13.96538375
DLL1-2	8.425185406	0	0.363959021	0.477901637
DLL1-3	9.715374381	0.605962886	1.283781618	10.30397784
E2F3	17.95231638	18.68133691	16.71447103	16.87652302
FOSL1	8.992992549	2.911677746	5.525178517	12.04770288
FUT8	1.025810247	1.743719184	9.920618414	10.5107247
GALNT7	0	0	0	0
GAS1	0	0	0	0
HDAC1	10.39675522	10.62740576	13.54021199	11.92776406
HNF4A	12.14219395	11.78382781	12.20358676	12.213331
INHBB	9.928244117	9.391807626	11.72776435	11.82984322
JAG1-1	15.04201383	15.19507564	15.54871445	15.38112846
JAG1-2	13.71716501	12.78073663	15.01577453	14.78805166
KLF4	0.271689229	0.334564973	0	2.411394177
MAP2K1	10.37868037	2.442797807	10.96530707	10.39599311
MET-1	0	0	0	0
MET-2	14.59249129	13.90991753	14.68841114	14.77372181
NOTCH1	9.190629063	0.605962886	0	0.668187021
NOTCH2	13.6830902	12.50743308	12.45335875	12.8053138
PDGFRA-1	10.40977976	9.59924234	11.5566409	3.382002676
PDGFRA-2	12.34134849	11.44565231	9.996337575	10.56184554
YY1	10.55475922	2.69620294	9.867098315	6.629105545
MDM4	0	0	0	0
MYCN-1	9.363063066	1.031387046	1.444516614	1.123103023
MYCN-2	15.21666921	15.51790519	14.22669331	14.0173545
PDGFRB	13.84106368	13.3136559	13.77112568	13.61314765
SNAI1	13.03806928	11.65372528	13.45053308	13.54640384
SRC-1	15.53515782	15.38306343	16.77734037	16.75471504
SRC-2	13.74689159	13.41683144	15.02457015	15.0308632
SRC-3	10.45499392	2.80795941	11.11895567	9.395592066
ALCAM	15.95940382	15.26552862	17.23787474	17.3119759
PTPRT	14.69364534	12.88814926	12.98139601	13.49646435
RB1	12.41742489	11.43453983	14.26073029	14.21690171

Table A.7, continued

WNK1	15.80176302	16.94917709	15.09225135	14.80387567
DNMT3A	0	0	0	0
HBEGF-1	13.76598816	12.5105984	14.43240123	14.90726278
HBEGF-2	11.82668049	10.51790338	10.34242265	10.82665634
IGF1R	15.49892053	14.4822935	14.07137898	13.80232082
ITGA9	0.271689229	0.334564973	0.895968027	0.477901637
PTPN12	0	0	0.654348814	0.477901637
RBX1	1.885131808	9.73091606	2.624135633	10.0374476
ALCAM	0	0	0	0
DICER1	10.99101427	10.0833743	12.2444299	11.26605067
RB1	0	0	0	0
WNK1	0	0	0	0
ADAM17	0	0	0	0
ADD3-1	15.64784479	15.04282363	15.51019397	15.31653582
ADD3-2	12.90091697	10.62072532	11.81353541	12.78241599
ADD3-3	10.68993322	10.8902088	9.701460515	9.42267522
CDK6-1	11.39122008	12.37341639	13.58290914	13.60566772
CDK6-2	8.526759061	10.83562238	9.414105272	10.18831561
CTNND1	12.45550086	11.66606022	9.909899928	11.43528415
DDX6	0	0	0	0
DDX17	0	0	0	0
E2F3	12.71796008	11.51522607	12.18272324	11.57359566
ETS1	0.69747275	7.758780298	10.1930561	1.828898567
FLI1-1	9.42873563	9.008157752	0.895968027	1.123103023
FLI1-2	12.41753419	9.186764397	12.68398988	11.41789165
FLI1-3	13.58115431	13.01697597	13.39111924	14.51987749
FSCN1-1	11.79657443	11.77901431	13.12246694	12.2605711
FSCN1-2	14.15281144	13.48633214	12.69395814	9.726736049
FSCN1-3	15.46952565	14.50175537	14.09950366	14.00803096
FSCN1-4	0	0	0	0
IGF1R	10.34804309	10.61737346	11.95444893	12.44932773
IRS1	0	0	0	0
ITGB8	9.313179815	2.218458683	2.483169064	4.460109129
KLF4	12.39378747	10.52046916	11.06548469	8.920741087
KLF5	9.608372342	10.57924153	10.51247218	9.347698692
MYO6-1	9.895974835	1.952694473	1.952157195	2.180927158
MYO6-2	11.08043002	10.49590802	3.939944415	11.05391849
NEDD9	10.49179224	10.01478566	11.75329198	11.90460198

Table A.7, continued

NRAS	0	0	0	0
PAK4	13.05776733	11.73241141	13.07619219	13.34466849
RREB1	11.76788565	3.72975552	11.91618476	11.48099484
RTKN	12.77191668	12.31926016	14.07969957	14.28633003
SERPINE1	13.28493108	12.75203995	14.80248921	15.0324194
SMAD3-1	5.670731143	0.334564973	4.511493629	0
SMAD3-2	8.435584341	10.00492499	1.10286689	7.08220663
SOX9	0	0	0	0
SP1	14.34898339	12.95696289	15.34036818	15.24801273
SRGAP1-1	0	0	0	0
SRGAP1-2	1.293101822	0.834299696	6.245926332	9.71700755
SRGAP1-3	1.025810247	9.111158875	0.654348814	0.477901637
SWAP70	11.77983787	10.51275809	13.22118694	12.98436926
TGFBR2	0	0	0	0
TNFSF13	11.31523709	10.49851318	12.45069893	11.32377477
YES1	12.11778253	12.82297285	11.99770944	9.32932068
BNIP3-1	12.23075414	11.29255129	12.78117294	11.5277023
BNIP3-2	0	0	0	0

Table A.8: sgRNA target genes showing differential responses to treatment with miR-34a between WT-LIB and KO-LIB cells. Direct miR-34a targets are in bold and underlined. For each gene, the number of target sites for miR-34a is in parenthesis.

WT-LIB (D6 vs. D0)				**KO-LIB (D6 vs. D0)**			
Enriched	**Fold (X)**	**Depleted**	**Fold (X)**	**Enriched**	**Fold (X)**	**Depleted**	**Fold (X)**
SRGAP1-3 (0)	271.60	**DLL1-3 (3)**	552.34	**DLL1-3 (3)**	519.22	ETS1 (0)	329.51
RBX1 (0)	230.05	**NOTCH1 (2)**	383.92	RBX1 (0)	170.46	**PDGFRA-1 (2)**	288.94
ETS1 (0)	133.56	**DLL1-2 (3)**	343.74	MYO6-2 (0)	138.52	SMAD3-1 (0)	22.81
		MYCN-1 (2)	322.17	**BCL2 (1)**	134.53		
		RREB1 (0)	262.86	**FOSL1 (1)**	91.93		
		MYO6-1 (0)	246.13	SMAD3-2 (0)	63.09		
		MAP2K1 (1)	244.87	SRGAP1-2 (0)	11.09		
		YY1 (1)	232.09				
		SRC-3 (3)	200.44				
		ITGB8 (0)	136.69				
		FOSL1 (1)	67.71				
		SMAD3-1 (0)	40.40				

Table A.9: Oligonucleotide pairs for the 93 sgRNA target sequences.

sgRNA Target	Forward Primer	Reverse Primer
AXL	CACCGTCCAAGCTAAGCACTGCCAC	AAACGTGGCAGTGCTTAGCTTGGAC
BCL2	CACCGAATCAGCTATTTACTGCCAA	AAACTTGGCAGTAAATAGCTGATTC
CCND1	CACCGAGAAAACTAAAACTAGTACA	AAACTGTACTAGTTTTAGTTTTCTC
CDK6	CACCGTTTGCCAACAAGGCAGTGTG	AAACCACACTGCCTTGTTGGCAAAC
DLL1-1	CACCGTGCAACGGCGACGTCACGGA	AAACTCCGTGACGTCGCCGTTGCAC
DLL1-2	CACCGAGAATCCAAAATATACACTC	AAACGAGTGTATATTTTGGATTCTC
DLL1-3	CACCGCGTATCAAAAAGGACAATAA	AAACTTATTGTCCTTTTTGATACGC
E2F3	CACCGAAAGCAGCTAGAAAGTATTC	AAACGAATACTTTCTAGCTGCTTTC
FOSL1	CACCGTCACCTGCTGCTGCTGGCAG	AAACCTGCCAGCAGCAGCAGGTGAC
FUT8	CACCGGTCACTTAAATTACACAATA	AAACTATTGTGTAATTTAAGTGACC
GALNT7	CACCGTCTTTTTGAAGCACTGCCAC	AAACGTGGCAGTGCTTCAAAAAGAC
GAS1	CACCGCATAAAGAGACTTTCATACA	AAACTGTATGAAAGTCTCTTTATGC
HDAC1	CACCGAGAGGGCAGGCAGTGTTTCT	AAACAGAAACACTGCCTGCCCTCTC
HNF4A	CACCGGAAGGTGAAGGTGAAGGCAG	AAACCTGCCTTCACCTTCACCTTCC
INHBB	CACCGAAAAATAACTTTTTTTCAAA	AAACTTTGAAAAAAAGTTATTTTTC
JAG1-1	CACCGCCTCAGACTCTACCTAGCGG	AAACCCGCTAGGTAGAGTCTGAGGC
JAG1-2	CACCGTTGATTTCCTCACTTAAGGC	AAACGCCTTAAGTGAGGAAATCAAC
KLF4	CACCGAAAAATACTGAATTCTCTTC	AAACGAAGAGAATTCAGTATTTTTC
MAP2K1	CACCGTGGTGAAGCCCCAGCTATCA	AAACTGATAGCTGGGGCTTCACCAC
MET-1	CACCGTCGATGGCCTTTTAAAGGTC	AAACGACCTTTAAAAGGCCATCGAC
MET-2	CACCGTTCAGTTCAGCTGCAGGTAT	AAACATACCTGCAGCTGAACTGAAC
NOTCH1	CACCGAACAGTACATATAAATAAAA	AAACTTTTATTTATATGTACTGTTC
NOTCH2	CACCGAGATCAGTAAAAAGTTTGAA	AAACTTCAAACTTTTTACTGATCTC
PDGFRA-1	CACCGACAGCTTGTCATAAATGTTT	AAACAAACATTTATGACAAGCTGTC
PDGFRA-2	CACCGAGTTAAAAAAATATAAACGA	AAACTCGTTTATATTTTTTTAACTC
YY1	CACCGTTACACTGAACATCAGCATC	AAACGATGCTGATGTTCAGTGTAAC
MDM4	CACCGAGTAACCTTAACATTCCCTA	AAACTAGGGAATGTTAAGGTTACTC
MYCN-1	CACCGAAAAATCAAAATGTGCAAAG	AAACCTTTGCACATTTTGATTTTTC
MYCN-2	CACCGAGCGTCATACTAAAGTATAC	AAACGTATACTTTAGTATGACGCTC
PDGFRB	CACCGGAGATGTCACTGCTAGGTCT	AAACAGACCTAGCAGTGACATCTCC
SNAI1	CACCGCCACATCCTTCTCACTGCCA	AAACTGGCAGTGAGAAGGATGTGGC
SRC-1	CACCGCAGCTGGGCTGAGCGGGCAG	AAACCTGCCCGCTCAGCCCAGCTGC
SRC-2	CACCGACACAGCCAGTCCTGGTGCA	AAACTGCACCAGGACTGGCTGTGTC
SRC-3	CACCGCTGGCTGGCTCAAGAACCCC	AAACGGGGTTCTTGAGCCAGCCAGC
ALCAM	CACCGGTTTTGGCAGCCATGATAAT	AAACATTATCATGGCTGCCAAAACC

Table A.9, continued

PTPRT	CACCGAGCAGAAGGTAAATAATGTC	AAACGACATTATTTACCTTCTGCTC
RB1	CACCGATACAAATCAGTTAGTTTTT	AAACAAAAACTAACTGATTTGTATC
WNK1	CACCGGTGCAACTCTTTCTTATGAT	AAACATCATAAGAAAGAGTTGCACC
DNMT3A	CACCGCTGTAAACAAGAGGTAACAG	AAACCTGTTACCTCTTGTTTACAGC
HBEGF-1	CACCGAAGTGCCTAGACTGTTACTT	AAACAAGTAACAGTCTAGGCACTTC
HBEGF-2	CACCGAAGTTGTAACAGTTCAGAAA	AAACTTTCTGAACTGTTACAACTTC
IGF1R	CACCGATCATGTCTTGCACTGTAAC	AAACGTTACAGTGCAAGACATGATC
ITGA9	CACCGTATATTTATAAAAATACTTT	AAACAAAGTATTTTTATAAATATAC
PTPN12	CACCGTCTACAAGCAGCGTGTAACA	AAACTGTTACACGCTGCTTGTAGAC
RBX1	CACCGATTTGTAATTAGGTAACAGC	AAACGCTGTTACCTAATTACAAATC
ALCAM	CACCGGTTTTGGCAGCCATGATAAT	AAACATTATCATGGCTGCCAAAACC
DICER1	CACCGTATACTCGCACAACTTAAAT	AAACATTTAAGTTGTGCGAGTATAC
RB1	CACCGTCAGTTAGTTTTTAGGTCAA	AAACTTGACCTAAAAACTAACTGAC
WNK1	CACCGGTGCAACTCTTTCTTATGAT	AAACATCATAAGAAAGAGTTGCACC
ADAM17	CACCGCATTTATTTGTGATGACAAC	AAACGTTGTCATCACAAATAAATGC
ADD3-1	CACCGGATTGGGGGATGTAGCAAAC	AAACGTTTGCTACATCCCCCAATCC
ADD3-2	CACCGGCAAACTGGACTTTAAGAAC	AAACGTTCTTAAAGTCCAGTTTGCC
ADD3-3	CACCGTTCTAGATCTCACTAACTAC	AAACGTAGTTAGTGAGATCTAGAAC
CDK6-1	CACCGAAAATGCAGCTGTTCTGAAC	AAACGTTCAGAACAGCTGCATTTTC
CDK6-2	CACCGACCAATAATCCTTTGGAAAC	AAACGTTTCCAAAGGATTATTGGTC
CTNND1	CACCGAAAGCTCTGTTCCATGCAAC	AAACGTTGCATGGAACAGAGCTTTC
DDX6	CACCGTTATCTCAATAAAAGCCCAC	AAACGTGGGCTTTTATTGAGATAAC
DDX17	CACCGTATATATATATATAGCTGAC	AAACGTCAGCTATATATATATATAC
E2F3	CACCGGCTTTGTGTTAAGTGCCTAC	AAACGTAGGCACTTAACACAAAGCC
ETS1	CACCGGTGGTGGGTGGTTTATACAC	AAACGTGTATAAACCACCCACCACC
FLI1-1	CACCGCCTTGAAGGGAAGACAAAAC	AAACGTTTTGTCTTCCCTTCAAGGC
FLI1-2	CACCGCAAATTCAGTGGATGGCAAC	AAACGTTGCCATCCACTGAATTTGC
FLI1-3	CACCGCAGTGAAGTTTTCACCCAAC	AAACGTTGGGTGAAAACTTCACTGC
FSCN1-1	CACCGAGCCCCCTTGCCTTTCAAAC	AAACGTTTGAAAGGCAAGGGGGCTC
FSCN1-2	CACCGCCCTGGGCGTGTAGTGTAAC	AAACGTTACACTACACGCCCAGGGC
FSCN1-3	CACCGTCCTTTCACCCTAGCCTGAC	AAACGTCAGGCTAGGGTGAAAGGAC
FSCN1-4	CACCGCCATGATAGTAGCTTCAAAC	AAACGTTTGAAGCTACTATCATGGC
IGF1R	CACCGTACCTACCGGTTTCCACAAC	AAACGTTGTGGAAACCGGTAGGTAC
IRS1	CACCGTCAAACTACCGATTTAAAAC	AAACGTTTTAAATCGGTAGTTTGAC
ITGB8	CACCGCACTTTTAAACAAAATTAAC	AAACGTTAATTTTGTTTAAAAGTGC
KLF4	CACCGCAAAATGCCAAGGGGGTGAC	AAACGTCACCCCCTTGGCATTTTGC
KLF5	CACCGAAGAAAACCACAACTAAAAC	AAACGTTTTAGTTGTGGTTTTCTTC
MYO6-1	CACCGATGGCACAGTACCATATAAC	AAACGTTATATGGTACTGTGCCATC

Table A.9, continued

MYO6-2	CACCGAGGTGGCATAGTGGCTTAAC	AAACGTTAAGCCACTATGCCACCTC
NEDD9	CACCGTAACGGTTACTAAGGAAAAC	AAACGTTTTCCTTAGTAACCGTTAC
NRAS	CACCGGATGTTTAAAAAATAAAAAC	AAACGTTTTTATTTTTTAAACATCC
PAK4	CACCGGGCAGCGGCCCTCCCATCAC	AAACGTGATGGGAGGGCCGCTGCCC
RREB1	CACCGGGGTACCCATAGCCAATAAC	AAACGTTATTGGCTATGGGTACCCC
RTKN	CACCGAACCCTTCCTGGAAGAAAAC	AAACGTTTTCTTCCAGGAAGGGTTC
SERPINE1	CACCGGCCTTCATCTGGGACAAAAC	AAACGTTTTGTCCCAGATGAAGGCC
SMAD3-1	CACCGCTAGTCTAAATTATTTCAAC	AAACGTTGAAATAATTTAGACTAGC
SMAD3-2	CACCGGAAACTTGCCTCATGTAAAC	AAACGTTTACATGAGGCAAGTTTCC
SOX9	CACCGTGTTTTTGTTGAAAACAAAC	AAACGTTTGTTTTCAACAAAAACAC
SP1	CACCGTCTTCACATTGTGTGAATAC	AAACGTATTCACACAATGTGAAGAC
SRGAP1-1	CACCGCTTAGTTTTGTGCTTATAAC	AAACGTTATAAGCACAAAACTAAGC
SRGAP1-2	CACCGTTGTAATTTTTTTAAATAAC	AAACGTTATTTAAAAAAATTACAAC
SRGAP1-3	CACCGGTCAGATCCATAAAGCAAAC	AAACGTTTGCTTTATGGATCTGACC
SWAP70	CACCGTTATTTACATGAGAGGAAAC	AAACGTTTCCTCTCATGTAAATAAC
TGFBR2	CACCGTCTGGGTTATCAGCATAAAC	AAACGTTTATGCTGATAACCCAGAC
TNFSF13	CACCGCAGACCTGGTCGGGGCCCAC	AAACGTGGGCCCCGACCAGGTCTGC
YES1	CACCGGCATGTTTTTAATGGTAAAC	AAACGTTTACCATTAAAAACATGCC
BNIP3-1	CACCGTGAAGAACTGGAGTCTGACT	AAACAGTCAGACTCCAGTTCTTCAC
BNIP3-2	CACCGCTGTGTCTACTTTAAAAAAC	AAACGTTTTTTAAAGTAGACACAGC

Table A.10: Primers used in this study.

primer	sequence (5'->3')
P1	GGGCCTATTTCCCATGATTCCTTCA
P2	CATATGCTTACCGTAACTTGAAAGT
P3	GAATTCAAAAAAGCACCGACTCGGTG
P4	CATGCTGGGGCCGTACAG
P5	GAACCGGCACCTGCACAC
P6	AATCCCATCACCATCTTCCA
P7	TGGACTCCACGACGTACTCA
P8	CAATTAACAGTCTTCAGGCA
P9	GCACAGAACATCCAGGTGGAGCCACACG
P10	TCGTCGGCAGCGTCAGATGTGTATAAGAGACAGCATATGCTTACCGTAACTTGAAAGT
P11	GTCTCGTGGGCTCGGAGATGTGTATAAGAGACAGGAATTCAAAAAAGCACCGACTCGGTG
P12	CAGTACGGTACCGAGGGCCTATTTCCCATGATTCCTTC
P13	TAACTTGCTATTTCTAGCTCTAAAACGAACTCGACCGCTCCGGCGACGGTGTTTCGTCCTTTCCACAAGATATA
P14	TAACTTGCTATTTCTAGCTCTAAAACGCGACGTCGCGCGCGGTGAGCGGTGTTTCGTCCTTTCCACAAGATATA
P15	CAGTACGAATTCAAAAAAGCACCGACTCGGTGCCACTTTTTCAAGTTGATAACGGACTAGCCTTATTTTAACTTGCTATTTCTAGCTCTAAAAC
P16	TCGTCGGCAGCGTCAGATGTGTATAAGAGACAGCAATTAACAGTCTTCAGGCA
P17	GTCTCGTGGGCTCGGAGATGTGTATAAGAGACAGGCACAGAACATCCAGGTGGAGCCACACG

APPENDIX B

SUPPLEMENTAL MATERIAL FOR CHAPTER 3

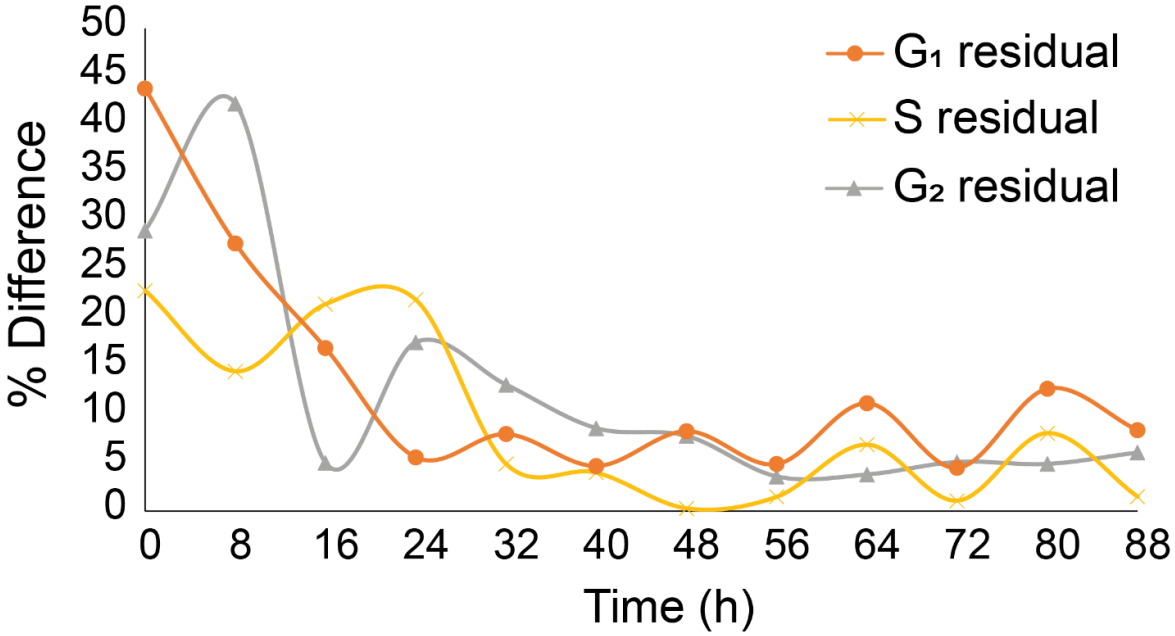

Figure B.1: Residual plot comparison of synchronous cells to asynchronous cells. The difference for each phase distribution for each time point demonstrates that overtime an initially synchronous population will converge to a static stead-state DNA distribution indicative of cells passing through the cell cycle asynchronously.

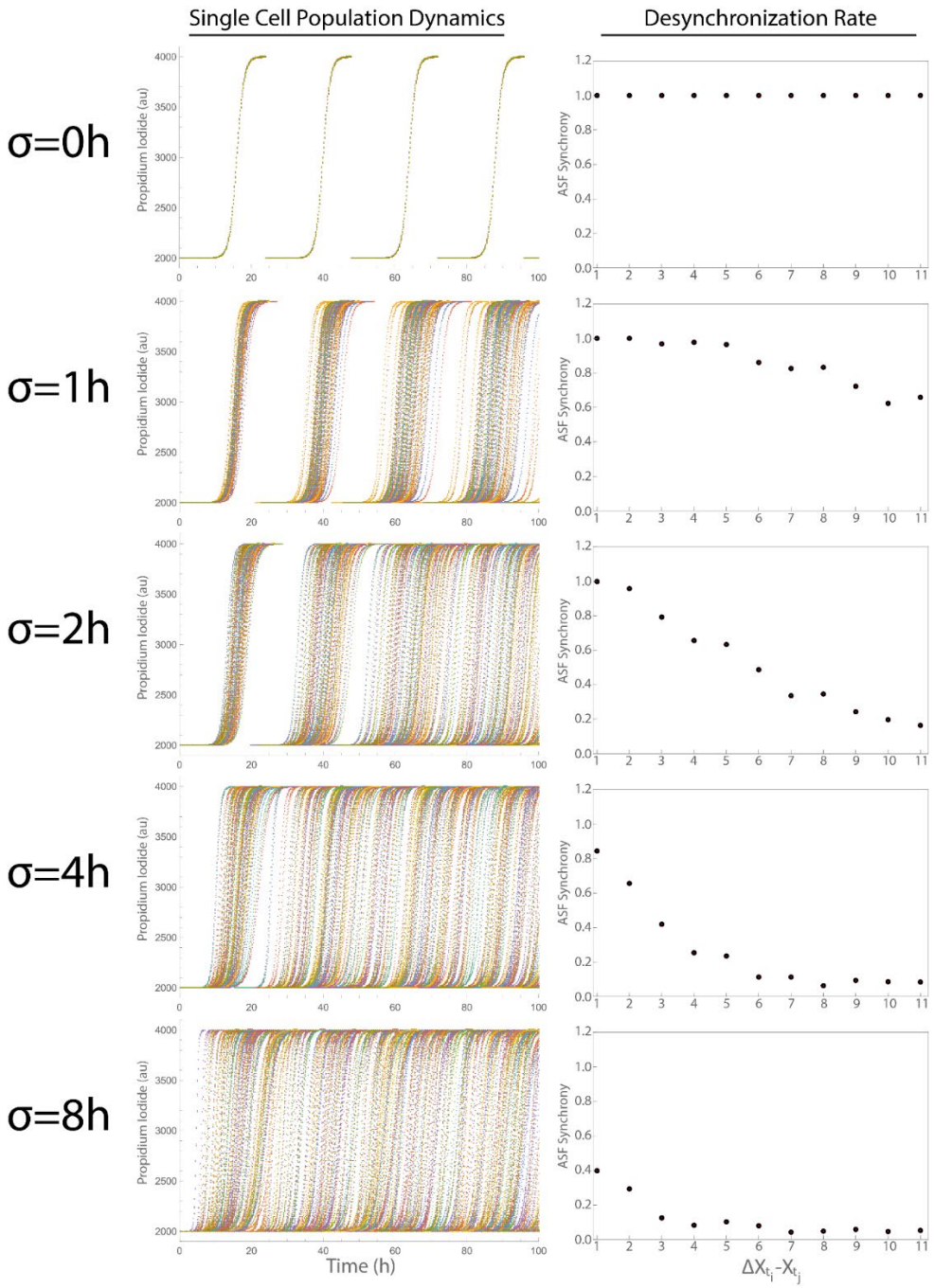

Figure B.2: Effect of population variance of cell cycle duration**.** If variance of the cell cycle is not incorporated into the model, not only does the model not capitulate experimental observation, but the population of cells will never desynchronize. Therefore, we can assume that single-cell variance of the cell cycle is core component driving cell cycle desynchronization. Importantly, as variance is increased, the desynchronization rates increase. A standard deviation of 4 hours most accurately captures experimental observations. Furthermore, as the variance increases, desynchronization begins to approach an asynchronous trend.

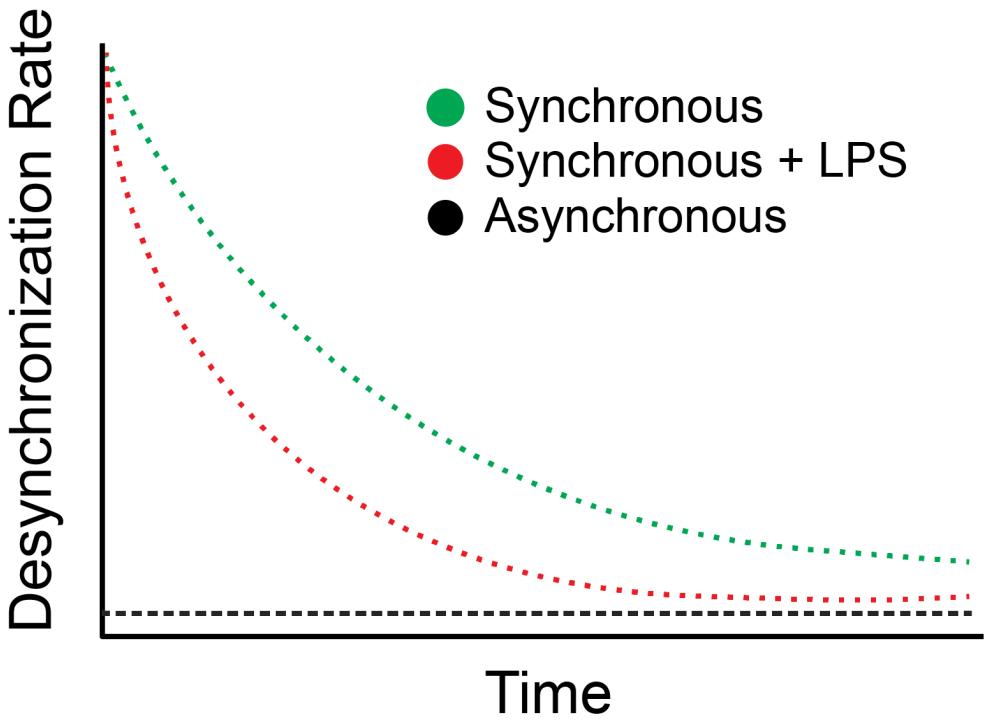

Figure B.3: Graphical hypothesis of LPS exposure to synchronous cell populations. If LPS exposure induces a greater degree of cell cycle variation starting from the same point of synchronicity, it would be expected that the desynchronization rates would increase, or rather reach an asynchronous trend sooner than cells not treated with LPS.

Figure B.4: Overall scheme of single-cell tracking of cell cycle duration. Timelapse microscopy of asynchronous cells performed for 72 hours at 20 minutes per frame. Frame 0 depicts a parent cell undergoing mitosis. Frame 1 show the parent cell undergoing telophase and cytokinesis. Once the septum is visible between the two daughter cells (yellow and blue arrow), the cell cycle duration begins being recorded. Frames 26-28 depicts cells progressing through interphase. At frame 56, one of the two daughter cells (blue arrow) begins metaphase, and by frame 58, the two resulting daughter cells are apparent and the cell cycle duration ends. Thus, the (blue arrow) daughter cell had a cell cycle duration of 18.3 hours (57 frames – 2 frames, multiplied by 20 minutes per frame). The other daughter cell (yellow arrow) had a substantially longer cell cycle duration of 27 hours, thus highlighting the inherent heterogeneity of cell cycle duration between identical cells within the population.

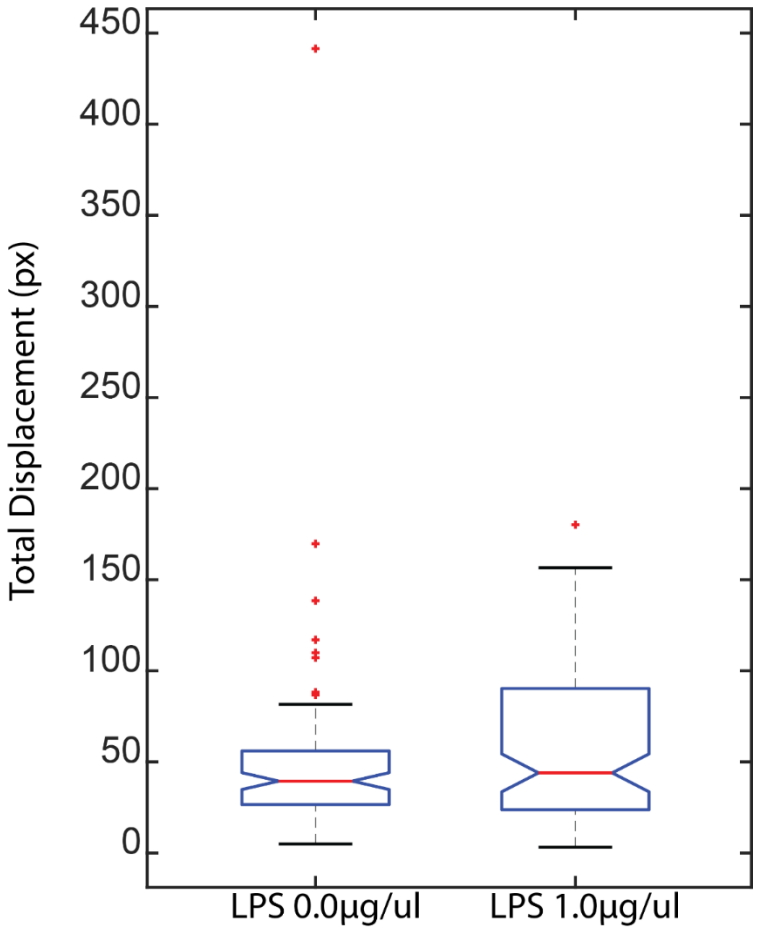

Figure B.5: Total displacement of single cells from time-lapse analysis. Cell coordinates were recorded both at the start and end of each cell that was recorded for single-cell cell cycle duration, and the total displacement was plotted for 100 cells for both conditions. LPS exposure had a large impact on the overall motility of cells. Total displacement was calculated with pixel coordinates using $d = \sqrt{(x_{start} - x_{end})^2 + (y_{start} - y_{end})^2}$.

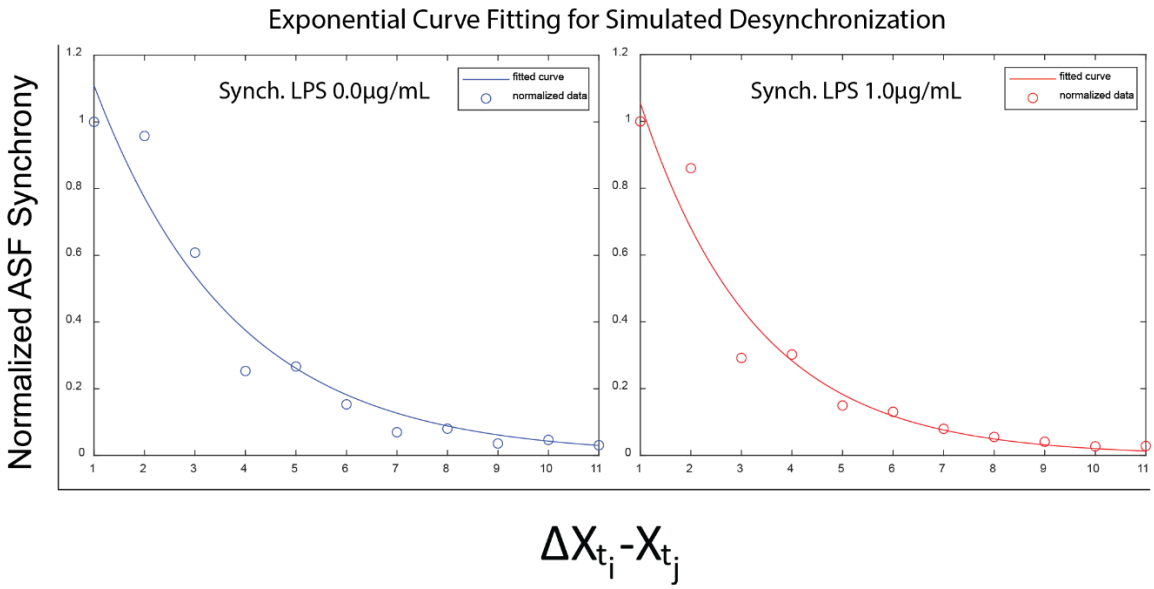

Figure B.6: Normalized and curve fitted desynchronization rates from simulated model using experimental values. The mean and standard deviation of the cell cycle duration obtained from single-cell time-lapse analysis were used in the simulated model to predict if the model was accurate in predicting resulting desynchronization rate. All ASF scores were normalized to the first value ($\mathbf{X}_{t_0} - \mathbf{X}_{t_8}$) in order to compare synchronous population trends to asynchrony. The normalized data points were fit with exponential curves.

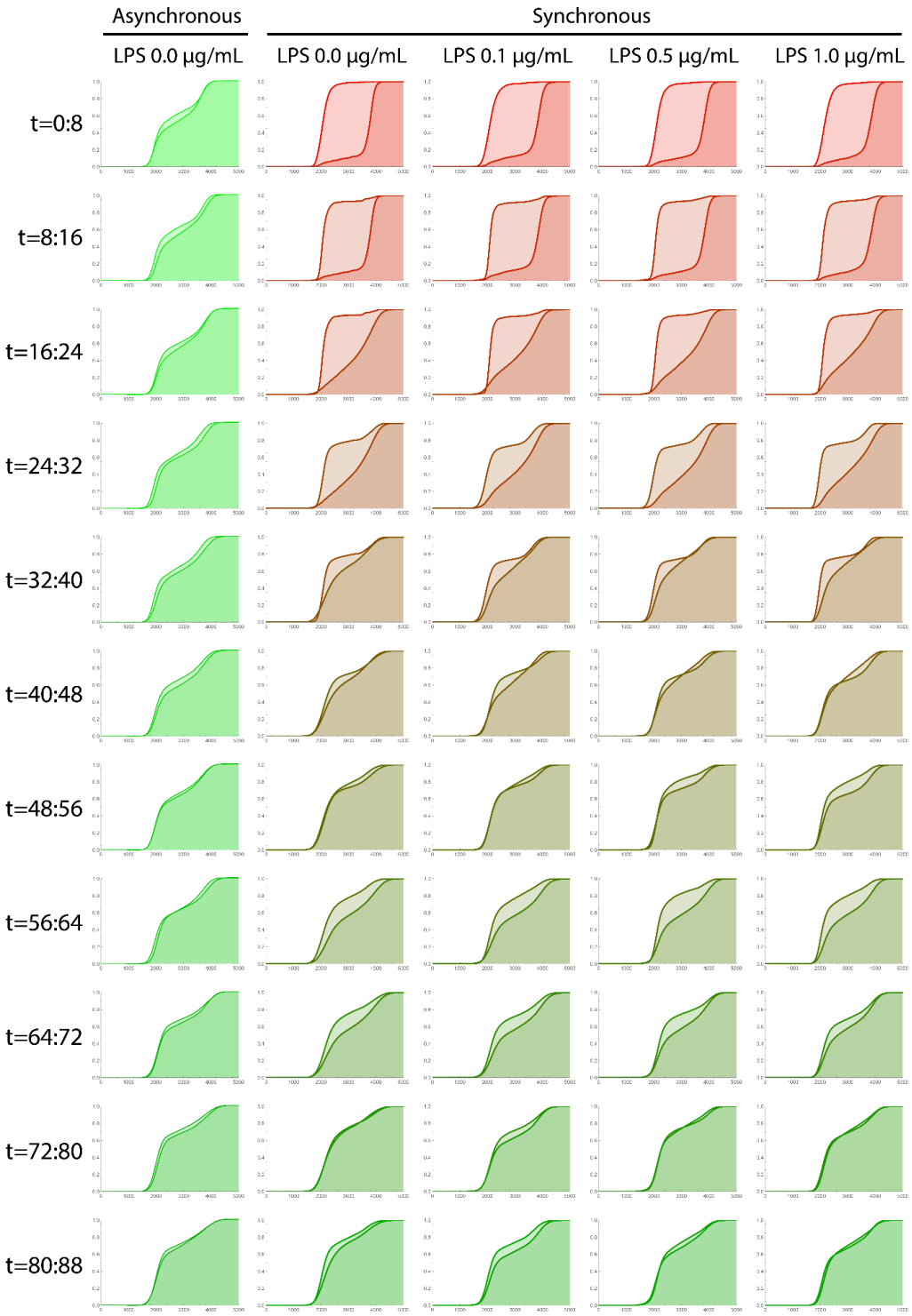

Figure B.7: ASF methodology for cell cycle desynchronization for LPS treated cells. Pairwise comparison of cumulative distribution function for propidium iodide-stained cells for each condition tested.

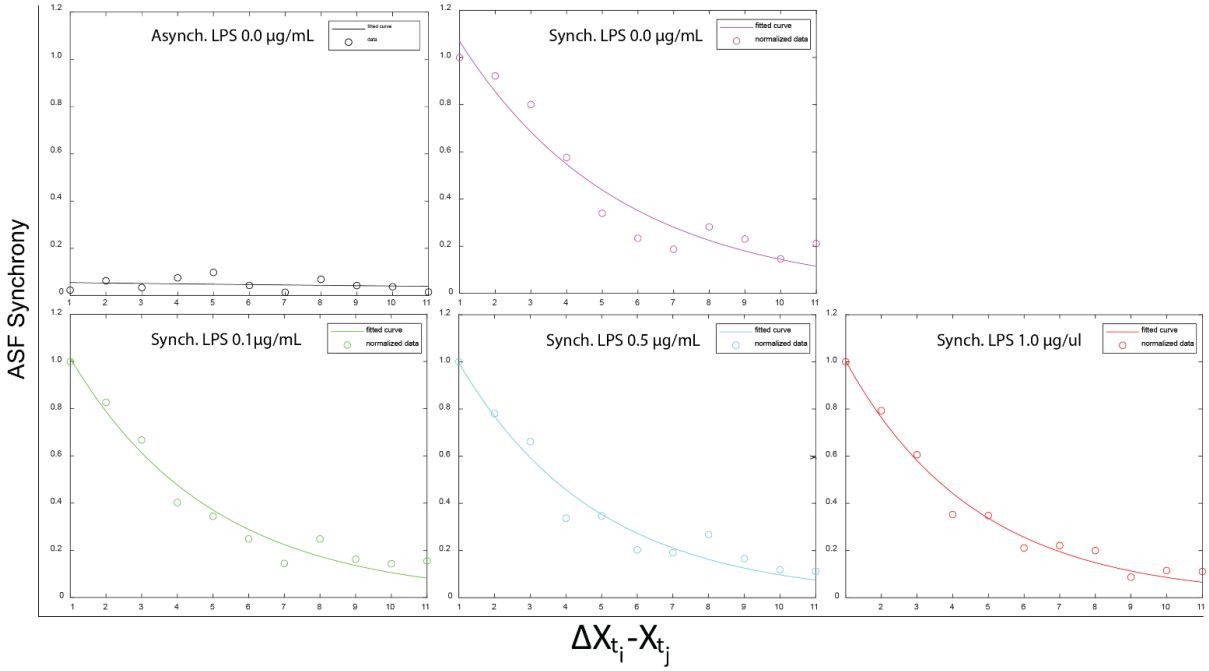

Figure B.8: Normalized and curved fitted desynchronization rates for synchronized cells. All ASF scores for synchonized cell populations treated with varying concentrations of LPS were normalized to the first value ($\mathbf{X}_{t_0} - \mathbf{X}_{t_8}$) in order to compare synchronous population trends to asynchrony. The normalized data points were fit with exponential curves. Asynchronous population was not normalized to retain linear trend.

REFERENCES

Abelson, Jesse F, Kenneth Y Kwan, Brian J O'Roak, Danielle Y Baek, Althea A Stillman, Thomas M Morgan, Carol A Mathews, et al. 2005. "Sequence Variants in SLITRK1 Are Associated with Tourette's Syndrome." *Science (New York, N.Y.)* 310 (5746): 317–20. https://doi.org/10.1126/science.1116502.

Agarwal, Vikram, George W Bell, Jin-Wu Nam, and David P Bartel. 2015. "Predicting Effective MicroRNA Target Sites in Mammalian MRNAs." *ELife* 4 (August): e05005. https://doi.org/10.7554/eLife.05005.

Agostino, Silvia Di, Sabrina Strano, Velia Emiliozzi, Valentina Zerbini, Marcella Mottolese, Ada Sacchi, Giovanni Blandino, and Giulia Piaggio. 2006. "Gain of Function of Mutant P53: The Mutant P53/NF-Y Protein Complex Reveals an Aberrant Transcriptional Mechanism of Cell Cycle Regulation." *Cancer Cell* 10 (3): 191–202. https://doi.org/10.1016/J.CCR.2006.08.013.

Alberghina, Lilia, Luigi Mariani, and Enzo Martegani. 1985. "Modeling Controls and Variability of the Cell Cycle," 239–46. https://doi.org/10.1007/978-3-642-93287-8_32.

Anders, Carolin, Ole Niewoehner, Alessia Duerst, and Martin Jinek. 2014. "Structural Basis of PAM-Dependent Target DNA Recognition by the Cas9 Endonuclease." *Nature* 513 (7519): 569–73. https://doi.org/10.1038/nature13579.

Ankers, John M., Raheela Awais, Nicholas A. Jones, James Boyd, Sheila Ryan, Antony D. Adamson, Claire V. Harper, et al. 2016. "Dynamic NF-Kb and E2F Interactions Control the Priority and Timing of Inflammatory Signalling and Cell Proliferation." *ELife* 5 (MAY2016). https://doi.org/10.7554/eLife.10473.

Anzalone, Andrew V., Peyton B. Randolph, Jessie R. Davis, Alexander A. Sousa, Luke W. Koblan, Jonathan M. Levy, Peter J. Chen, et al. 2019. "Search-and-Replace Genome Editing without Double-Strand Breaks or Donor DNA." *Nature 2019 576:7785* 576 (7785): 149–57. https://doi.org/10.1038/s41586-019-1711-4.

Bader, Andreas G. 2012. "MiR-34 - a MicroRNA Replacement Therapy Is Headed to the Clinic." *Frontiers in Genetics* 3: 120. https://doi.org/10.3389/fgene.2012.00120.

Barberis, Matteo, and Paul Verbruggen. 2017. "Quantitative Systems Biology to Decipher Design Principles of a Dynamic Cell Cycle Network: The 'Maximum Allowable Mammalian Trade–Off–Weight' (MAmTOW)." *Npj Systems Biology and Applications 2017 3:1* 3 (1): 1–14. https://doi.org/10.1038/s41540-017-0028-x.

Barrangou, Rodolphe, Christophe Fremaux, Hélène Deveau, Melissa Richards, Patrick Boyaval, Sylvain Moineau, Dennis A Romero, and Philippe Horvath. 2007. "CRISPR Provides Acquired Resistance against Viruses in Prokaryotes." *Science (New York, N.Y.)* 315 (5819): 1709–12. https://doi.org/10.1126/science.1138140.

Bartel, D P. 2009. "MicroRNAs: Target Recognition and Regulatory Functions." *Cell* 136 (2): 215–33.

Bartel, David P. 2009. "MicroRNAs: Target Recognition and Regulatory Functions." *Cell* 136 (2): 215–33. https://doi.org/10.1016/j.cell.2009.01.002.

Bash, J, W X Zong, and C Gélinas. 1997. "C-Rel Arrests the Proliferation of HeLa Cells and Affects Critical Regulators of the G1/S-Phase Transition." *Molecular and Cellular Biology* 17 (11): 6526. https://doi.org/10.1128/MCB.17.11.6526.

Batchelor, Eric, Alexander Loewer, and Galit Lahav. 2009. "The Ups and Downs of P53: Understanding Protein Dynamics in Single Cells." *Nature Reviews Cancer* 9 (5): 371–77. https://doi.org/10.1038/nrc2604.

Bieging, Kathryn T., Stephano Spano Mello, and Laura D. Attardi. 2014. "Unravelling Mechanisms of P53-Mediated Tumour Suppression." *Nature Reviews Cancer* 14 (5): 359–70. https://doi.org/10.1038/nrc3711.

Bjursell, G., and P. Reichard. 1973. "Effects of Thymidine on Deoxyribonucleoside Triphosphate Pools and Deoxyribonucleic Acid Synthesis in Chinese Hamster Ovary Cells." *Journal of Biological Chemistry* 248 (11): 3904–9. https://doi.org/10.1016/s0021-9258(19)43819-2.

Bohnsack, Markus T, Kevin Czaplinski, and Dirk Gorlich. 2004. "Exportin 5 Is a RanGTP-Dependent DsRNA-Binding Protein That Mediates Nuclear Export of Pre-MiRNAs." *RNA (New York, N.Y.)* 10 (2): 185–91. https://doi.org/10.1261/rna.5167604.

Bolotin, Alexander, Benoit Quinquis, Alexei Sorokin, and S. Dusko Ehrlich. 2005. "Clustered Regularly Interspaced Short Palindrome Repeats (CRISPRs) Have Spacers of Extrachromosomal Origin." *Microbiology* 151 (8): 2551–61. https://doi.org/10.1099/mic.0.28048-0.

Brennecke, Julius, Alexander Stark, Robert B Russell, and Stephen M Cohen. 2005. "Principles of MicroRNA-Target Recognition." *PLoS Biology* 3 (3): e85. https://doi.org/10.1371/journal.pbio.0030085.

Brest, Patrick, Pierre Lapaquette, Mouloud Souidi, Kevin Lebrigand, Annabelle Cesaro, Valerie Vouret-Craviari, Bernard Mari, et al. 2011. "A Synonymous Variant in IRGM Alters a Binding Site for MiR-196 and Causes Deregulation of IRGM-Dependent Xenophagy in Crohn's Disease." *Nature Genetics* 43 (3): 242–45. https://doi.org/10.1038/ng.762.

Briner, Alexandra E, Paul D Donohoue, Ahmed A Gomaa, Kurt Selle, Euan M Slorach, Christopher H Nye, Rachel E Haurwitz, Chase L Beisel, Andrew P May, and Rodolphe Barrangou. 2014. "Guide RNA Functional Modules Direct Cas9 Activity and Orthogonality." *Molecular Cell* 56 (2): 333–39. https://doi.org/10.1016/j.molcel.2014.09.019.

Brooks, R. F., D. C. Bennett, and J. A. Smith. 1980. "Mammalian Cell Cycles Need Two Random Transitions." *Cell* 19 (2): 493–504. https://doi.org/10.1016/0092-8674(80)90524-3.

Brooks, Robert F. 2021. "Cell Cycle Commitment and the Origins of Cell Cycle Variability." *Frontiers in Cell and Developmental Biology* 9 (July): 698066. https://doi.org/10.3389/FCELL.2021.698066.

Brouns, Stan J J, Matthijs M Jore, Magnus Lundgren, Edze R Westra, Rik J H Slijkhuis, Ambrosius P L Snijders, Mark J Dickman, Kira S Makarova, Eugene V Koonin, and John van der Oost. 2008. "Small CRISPR RNAs Guide Antiviral Defense in Prokaryotes." *Science (New York, N.Y.)* 321 (5891): 960–64. https://doi.org/10.1126/science.1159689.

Castor, La Roy N. 1980. "A G1 Rate Model Accounts for Cell-Cycle Kinetics Attributed to 'Transition Probability.'" *Nature* 287 (5785): 857–59. https://doi.org/10.1038/287857a0.

Chang, Tsung-Cheng, Erik A. Wentzel, Oliver A. Kent, Kalyani Ramachandran, Michael Mullendore, Kwang Hyuck Lee, Georg Feldmann, et al. 2007. "Transactivation of MiR-34a by P53 Broadly Influences Gene Expression and Promotes Apoptosis." *Molecular Cell* 26 (5): 745–52. https://doi.org/10.1016/j.molcel.2007.05.010.

Chao, Hui Xiao, Randy I Fakhreddin, Hristo K Shimerov, Katarzyna M Kedziora, Rashmi J Kumar, Joanna Perez, Juanita C Limas, et al. 2019. "Evidence That the Human Cell Cycle Is a Series of Uncoupled, Memoryless Phases." *Molecular Systems Biology* 15 (3): e8604. https://doi.org/10.15252/MSB.20188604.

Chatzikyriakidou, Anthoula, Paraskevi V Voulgari, Ioannis Georgiou, and Alexandros A Drosos. 2010. "A Polymorphism in the 3'-UTR of Interleukin-1 Receptor-Associated Kinase (IRAK1), a Target Gene of MiR-146a, Is Associated with Rheumatoid Arthritis Susceptibility." *Joint, Bone, Spine : Revue Du Rhumatisme* 77 (5): 411–13. https://doi.org/10.1016/j.jbspin.2010.05.013.

Chen, Baohui, Luke A Gilbert, Beth A Cimini, Joerg Schnitzbauer, Wei Zhang, Gene-Wei Li, Jason Park, et al. 2013. "Dynamic Imaging of Genomic Loci in Living Human Cells by an Optimized CRISPR/Cas System." *Cell* 155 (7): 1479–91. https://doi.org/10.1016/j.cell.2013.12.001.

Chen, Guo, and Xingming Deng. 2018. "Cell Synchronization by Double Thymidine Block." *BIO-PROTOCOL* 8 (17). https://doi.org/10.21769/bioprotoc.2994.

Chen, Sidi, Neville E Sanjana, Kaijie Zheng, Ophir Shalem, Kyungheon Lee, Xi Shi, David A Scott, et al. 2015. “Genome-Wide CRISPR Screen in a Mouse Model of Tumor Growth and Metastasis.” *Cell* 160 (6): 1246–60. https://doi.org/10.1016/j.cell.2015.02.038.

Chin, Lena J., Elena Ratner, Shuguang Leng, Rihong Zhai, Sunitha Nallur, Imran Babar, Roman-Ulrich Muller, et al. 2008. “A SNP in a Let-7 MicroRNA Complementary Site in the KRAS 3′ Untranslated Region Increases Non–Small Cell Lung Cancer Risk.” *Cancer Research* 68 (20). http://cancerres.aacrjournals.org/content/68/20/8535.

Chiorino, G., J. A.J. Metz, D. Tomasoni, and P. Ubezio. 2001. “Desynchronization Rate in Cell Populations: Mathematical Modeling and Experimental Data.” *Journal of Theoretical Biology* 208 (2): 185–99. https://doi.org/10.1006/jtbi.2000.2213.

Cho, In-Hye, Eun Hyang Jang, Darong Hong, Bom Jung, Min-Ju Park, and Jong-Ho Kim. 2015. “Suppression of LPS-Induced Epithelial-Mesenchymal Transition by Aqueous Extracts of Prunella Vulgaris through Inhibition of the NF-KB/Snail Signaling Pathway and Regulation of EMT-Related Protein Expression.” *Oncology Reports* 34 (5): 2445–50. https://doi.org/10.3892/OR.2015.4218.

Chou, Chih-Hung, Nai-Wen Chang, Sirjana Shrestha, Sheng-Da Hsu, Yu-Ling Lin, Wei-Hsiang Lee, Chi-Dung Yang, et al. 2016. “MiRTarBase 2016: Updates to the Experimentally Validated MiRNA-Target Interactions Database.” *Nucleic Acids Research* 44 (D1): D239--D247. https://doi.org/10.1093/nar/gkv1258.

Christoffersen, N R, R Shalgi, L B Frankel, E Leucci, M Lees, M Klausen, Y Pilpel, F C Nielsen, M Oren, and A H Lund. 2010. “P53-Independent Upregulation of MiR-34a during Oncogene-Induced Senescence Represses MYC.” *Cell Death Differ* 17: 236–45.

Clark, Peter M., Phillipe Loher, Kevin Quann, Jonathan Brody, Eric R. Londin, and Isidore Rigoutsos. 2015. “Argonaute CLIP-Seq Reveals MiRNA Targetome Diversity across Tissue Types.” *Scientific Reports* 4 (1): 5947. https://doi.org/10.1038/srep05947.

Concepcion, Carla P., Yoon-Chi Han, Ping Mu, Ciro Bonetti, Evelyn Yao, Aleco D’Andrea, Joana A. Vidigal, et al. 2012. “Intact P53-Dependent Responses in MiR-34–Deficient Mice.” Edited by H. Leighton Grimes. *PLoS Genetics* 8 (7): e1002797. https://doi.org/10.1371/journal.pgen.1002797.

Cong, Le, F Ann Ran, David Cox, Shuailiang Lin, Robert Barretto, Naomi Habib, Patrick D Hsu, et al. 2013. “Multiplex Genome Engineering Using CRISPR/Cas Systems.” *Science (New York, N.Y.)* 339 (6121): 819–23. https://doi.org/10.1126/science.1231143.

Consiglio, C R, T D Veit, O A Monticielo, T Mucenic, R M Xavier, J C T Brenol, and J A B Chies. 2011. “Association of the HLA-G Gene +3142C>G Polymorphism with Systemic Lupus Erythematosus.” *Tissue Antigens* 77 (6): 540–45. https://doi.org/10.1111/j.1399-0039.2011.01635.x.

Conti, Anastasia, and Raffaella Di Micco. 2018. “P53 Activation: A Checkpoint for Precision Genome Editing?” *Genome Medicine 2018 10:1* 10 (1): 1–4. https://doi.org/10.1186/S13073-018-0578-6.

Cooper, Stephen. 2003. “Reappraisal of Serum Starvation, the Restriction Point, G0, and G1 Phase Arrest Points.” *The FASEB Journal* 17 (3): 333–40. https://doi.org/10.1096/fj.02-0352rev.

Cory, S, and J M Adams. 2002. “The Bcl-2 Family: Regulators of the Cellular Life-or-Death Switch.” *Nat Rev Cancer* 2: 647–56.

Dean, Phillip N., and James H. Jett. 1974. “Mathematical Analysis of Dna Distributions Derived from Flow Microfluorometry.” *Journal of Cell Biology* 60 (2): 528–527. https://doi.org/10.1083/jcb.60.2.523.

DeLeo, A B, G Jay, E Appella, G C Dubois, L W Law, and L J Old. 1979. “Detection of a Transformation-Related Antigen in Chemically Induced Sarcomas and Other Transformed Cells of the Mouse.” *Proceedings of the National Academy of Sciences of the United States of America* 76 (5): 2420–24.

Deltcheva, Elitza, Krzysztof Chylinski, Cynthia M Sharma, Karine Gonzales, Yanjie Chao, Zaid A Pirzada, Maria R Eckert, Jörg Vogel, and Emmanuelle Charpentier. 2011. “CRISPR RNA Maturation by Trans-Encoded Small RNA and Host Factor RNase III.” *Nature* 471 (7340): 602–7. https://doi.org/10.1038/nature09886.

Deveau, Hélène, Rodolphe Barrangou, Josiane E Garneau, Jessica Labonté, Christophe Fremaux, Patrick Boyaval, Dennis A Romero, Philippe Horvath, and Sylvain Moineau. 2008. “Phage Response to CRISPR-Encoded Resistance in Streptococcus Thermophilus.” *Journal of Bacteriology* 190 (4): 1390–1400. https://doi.org/10.1128/JB.01412-07.

Eastman, Anna E., Xinyue Chen, Xiao Hu, Amaleah A. Hartman, Aria M. Pearlman Morales, Cindy Yang, Jun Lu, Hao Yuan Kueh, and Shangqin Guo. 2020. “Resolving Cell Cycle Speed in One Snapshot with a Live-Cell Fluorescent Reporter.” *Cell Reports* 31 (12): 107804. https://doi.org/10.1016/J.CELREP.2020.107804.

Elowitz, Michael B., Arnold J. Levine, Eric D. Siggia, and Peter S. Swain. 2002. “Stochastic Gene Expression in a Single Cell.” *Science* 297 (5584): 1183–86. https://doi.org/10.1126/SCIENCE.1070919.

Enache, Oana M., Veronica Rendo, Mai Abdusamad, Daniel Lam, Desiree Davison, Sangita Pal, Naomi Currimjee, et al. 2020. “Cas9 Activates the P53 Pathway and Selects for P53-Inactivating Mutations.” *Nature Genetics 2020 52:7* 52 (7): 662–68. https://doi.org/10.1038/s41588-020-0623-4.

Feng, Zhaohui, Cen Zhang, Rui Wu, and Wenwei Hu. 2011. “Tumor Suppressor P53 Meets MicroRNAs.” *Journal of Molecular Cell Biology* 3 (1): 44–50. https://doi.org/10.1093/jmcb/mjq040.

Ferrell, James E., and Jr. 2013. “Feedback Loops and Reciprocal Regulation: Recurring Motifs in the Systems Biology of the Cell Cycle.” *Current Opinion in Cell Biology* 25 (6): 676–86. https://doi.org/10.1016/J.CEB.2013.07.007.

Filipowicz, Witold, Suvendra N Bhattacharyya, and Nahum Sonenberg. 2008. “Mechanisms of Post-Transcriptional Regulation by MicroRNAs: Are the Answers in Sight?” *Nat Rev Genet* 2008 (2): 102–14. http://dx.doi.org/10.1038/nrg2290.

Fox, Michael H. 1980. “A Model for the Computer Analysis of Synchronous DNA Distributions Obtained by Flow Cytometry.” *Cytometry* 1 (1): 71–77. https://doi.org/10.1002/cyto.990010114.

Garneau, Josiane E, Marie-Ève Dupuis, Manuela Villion, Dennis A Romero, Rodolphe Barrangou, Patrick Boyaval, Christophe Fremaux, Philippe Horvath, Alfonso H Magadán, and Sylvain Moineau. 2010. “The CRISPR/Cas Bacterial Immune System Cleaves Bacteriophage and Plasmid DNA.” *Nature* 468 (7320): 67–71. https://doi.org/10.1038/nature09523.

Gasiunas, Giedrius, Rodolphe Barrangou, Philippe Horvath, and Virginijus Siksnys. 2012. “Cas9-CrRNA Ribonucleoprotein Complex Mediates Specific DNA Cleavage for Adaptive Immunity in Bacteria.” *Proceedings of the National Academy of Sciences of the United States of America* 109 (39): E2579-86. https://doi.org/10.1073/pnas.1208507109.

Gaudelli, Nicole M., Alexis C. Komor, Holly A. Rees, Michael S. Packer, Ahmed H. Badran, David I. Bryson, and David R. Liu. 2017. “Programmable Base Editing of A•T to G•C in Genomic DNA without DNA Cleavage.” *Nature* 551 (7681): 464–71. https://doi.org/10.1038/nature24644.

Gérard, Claude, Didier Gonze, and Albert Goldbeter. 2012. “Effect of Positive Feedback Loops on the Robustness of Oscillations in the Network of Cyclin-Dependent Kinases Driving the Mammalian Cell Cycle.” *The FEBS Journal* 279 (18): 3411–31. https://doi.org/10.1111/J.1742-4658.2012.08585.X.

Gery, Sigal, Naoki Komatsu, Lilit Baldjyan, Andrew Yu, Danielle Koo, and H. Phillip Koeffler. 2006. “The Circadian Gene Per1 Plays an Important Role in Cell Growth and DNA Damage Control in Human Cancer Cells.” *Molecular Cell* 22 (3): 375–82. https://doi.org/10.1016/J.MOLCEL.2006.03.038.

Gilbert, D. A. 1982. “Cell Cycle Variability: The Oscillator Model of the Cell Cycle Yields Transition Probability Alpha and Beta Type Curves.” *Biosystems* 15 (4): 317–30. https://doi.org/10.1016/0303-2647(82)90046-6.

Gilbert, Luke A A, Matthew H H Larson, Leonardo Morsut, Zairan Liu, Gloria A A Brar, Sandra E E Torres, Noam Stern-Ginossar, et al. 2013. "CRISPR-Mediated Modular RNA-Guided Regulation of Transcription in Eukaryotes." *Cell* 154 (2): 442–51. https://doi.org/http://dx.doi.org/10.1016/j.cell.2013.06.044.

Gonze, Didier, Claude Gérard, Benjamin Wacquier, Aurore Woller, Alen Tosenberger, Albert Goldbeter, and Geneviève Dupont. 2018. "Modeling-Based Investigation of the Effect of Noise in Cellular Systems." *Frontiers in Molecular Biosciences* 0 (APR): 34. https://doi.org/10.3389/FMOLB.2018.00034.

Guo, Fei, Hongwei Chen, Qiaoying Gong, Huijun Zuo, Jieqi Xiong, and Sisun Liu. 2015. "The Involvement of P53-MiR-34a-CDK4 Signaling During the Development of Cervical Cancer." *Cancer Translational Medicine* 1 (2): 67. https://doi.org/10.4103/2395-3977.155928.

Haapaniemi, Emma, Sandeep Botla, Jenna Persson, Bernhard Schmierer, and Jussi Taipale. 2018. "CRISPR–Cas9 Genome Editing Induces a P53-Mediated DNA Damage Response." *Nature Medicine 2018 24:7* 24 (7): 927–30. https://doi.org/10.1038/s41591-018-0049-z.

Hai, Tang, Fei Teng, Runfa Guo, Wei Li, and Qi Zhou. 2014. "One-Step Generation of Knockout Pigs by Zygote Injection of CRISPR/Cas System." *Cell Research* 24 (3): 372–75. https://doi.org/10.1038/cr.2014.11.

Hainaut, Pierre, and Monica Hollstein. 1999. "P53 and Human Cancer: The First Ten Thousand Mutations." *Advances in Cancer Research* 77 (C): 81–137. https://doi.org/10.1016/S0065-230X(08)60785-X.

Hamm, Jörg, and Iain W. Mattaj. 1990. "Monomethylated Cap Structures Facilitate RNA Export from the Nucleus." *Cell* 63 (1): 109–18. https://doi.org/10.1016/0092-8674(90)90292-M.

Hanin, Geula, Shani Shenhar-Tsarfaty, Nadav Yayon, Yin Hoe Yau, Estelle R Bennett, Ella H Sklan, Dabeeru C Rao, et al. 2014. "Competing Targets of MicroRNA-608 Affect Anxiety and Hypertension." *Human Molecular Genetics* 23 (17): 4569–80. https://doi.org/10.1093/hmg/ddu170.

Hargraves, Kris G., Lin He, and Gary L. Firestone. 2016. "Phytochemical Regulation of the Tumor Suppressive MicroRNA, MiR-34a, by P53-Dependent and Independent Responses in Human Breast Cancer Cells." *Molecular Carcinogenesis* 55 (5): 486–98. https://doi.org/10.1002/mc.22296.

Haronikova, Lucia, Vanesa Olivares-Illana, Lixiao Wang, Konstantinos Karakostis, Sa Chen, and Robin Fåhraeus. 2019. "The P53 MRNA: An Integral Part of the Cellular Stress Response." *Nucleic Acids Research* 47 (7): 3257–71. https://doi.org/10.1093/NAR/GKZ124.

Haupt, Ygal, Ruth Maya, Anat Kazaz, and Moshe Oren. 1997. “Mdm2 Promotes the Rapid Degradation of P53.” *Nature 1997 387:6630* 387 (6630): 296–99. https://doi.org/10.1038/387296a0.

Hayden, Matthew S, and Sankar Ghosh. 2014. “Regulation of NF-KB by TNF Family Cytokines.” *Seminars in Immunology* 26 (3): 253. https://doi.org/10.1016/J.SMIM.2014.05.004.

He, Guangan, Zahid H Siddik, Zaifeng Huang, Ruoning Wang, John Koomen, Ryuji Kobayashi, Abdul R Khokhar, and Jian Kuang. 2005. “Induction of P21 by P53 Following DNA Damage Inhibits Both Cdk4 and Cdk2 Activities.” *Oncogene* 24 (18): 2929–43. https://doi.org/10.1038/sj.onc.1208474.

He, Lin, Xingyue He, Lee P. Lim, Elisa de Stanchina, Zhenyu Xuan, Yu Liang, Wen Xue, et al. 2007. “A MicroRNA Component of the P53 Tumour Suppressor Network.” *Nature* 447 (7148): 1130–34. https://doi.org/10.1038/nature05939.

Hermeking, H. 2010. “The MiR-34 Family in Cancer and Apoptosis.” *Cell Death and Differentiation* 17 (2): 193–99. https://doi.org/10.1038/cdd.2009.56.

Hilton, Isaac B, Anthony M D’Ippolito, Christopher M Vockley, Pratiksha I Thakore, Gregory E Crawford, Timothy E Reddy, and Charles A Gersbach. 2015. “Epigenome Editing by a CRISPR-Cas9-Based Acetyltransferase Activates Genes from Promoters and Enhancers.” *Nature Biotechnology* 33 (5): 510–17. https://doi.org/10.1038/nbt.3199.

Höck, Julia, and Gunter Meister. 2008. “The Argonaute Protein Family.” *Genome Biology* 9 (2): 210. https://doi.org/10.1186/gb-2008-9-2-210.

Hong, Bo, A Pieter J van den Heuvel, Varun V Prabhu, Shengliang Zhang, and Wafik S El-Deiry. 2014. “Targeting Tumor Suppressor P53 for Cancer Therapy: Strategies, Challenges and Opportunities.” *Current Drug Targets* 15 (1): 80–89.

Horvath, Philippe, and Rodolphe Barrangou. 2010. “CRISPR/Cas, the Immune System of Bacteria and Archaea.” *Science (New York, N.Y.)* 327 (5962): 167–70. https://doi.org/10.1126/science.1179555.

Hsieh, Meng Hsiung, Joshua H. Choe, Jashkaran Gadhvi, Yoon Jung Kim, Marcus A. Arguez, Madison Palmer, Haleigh Gerold, et al. 2019. “P63 and SOX2 Dictate Glucose Reliance and Metabolic Vulnerabilities in Squamous Cell Carcinomas.” *Cell Reports* 28 (7): 1860-1878.e9. https://doi.org/10.1016/J.CELREP.2019.07.027.

Jansen, Ruud., Jan. D. A. van Embden, Wim. Gaastra, and Leo. M. Schouls. 2002. “Identification of Genes That Are Associated with DNA Repeats in Prokaryotes.” *Molecular Microbiology* 43 (6): 1565–75. https://doi.org/10.1046/j.1365-2958.2002.02839.x.

Jia, Lijun, and Yi Sun. 2009. “RBX1/ROC1-SCF E3 Ubiquitin Ligase Is Required for Mouse Embryogenesis and Cancer Cell Survival.” *Cell Division* 4 (1): 16. https://doi.org/10.1186/1747-1028-4-16.

Jinek, Martin, Krzysztof Chylinski, Ines Fonfara, Michael Hauer, Jennifer A Doudna, and Emmanuelle Charpentier. 2012. “A Programmable Dual-RNA-Guided DNA Endonuclease in Adaptive Bacterial Immunity.” *Science (New York, N.Y.)* 337 (6096): 816–21. https://doi.org/10.1126/science.1225829.

Jinek, Martin, Alexandra East, Aaron Cheng, Steven Lin, Enbo Ma, and Jennifer Doudna. 2013. “RNA-Programmed Genome Editing in Human Cells.” *ELife* 2 (January): e00471. https://doi.org/10.7554/eLife.00471.

Jinek, Martin, Fuguo Jiang, David W Taylor, Samuel H Sternberg, Emine Kaya, Enbo Ma, Carolin Anders, et al. 2014. “Structures of Cas9 Endonucleases Reveal RNA-Mediated Conformational Activation.” *Science (New York, N.Y.)* 343 (6176): 1247997. https://doi.org/10.1126/science.1247997.

Jing, Ying-Ying, Zhi-Peng Han, Kai Sun, Shan-Shan Zhang, Jing Hou, Yan Liu, Rong Li, et al. 2012. “Toll-like Receptor 4 Signaling Promotes Epithelial-Mesenchymal Transition in Human Hepatocellular Carcinoma Induced by Lipopolysaccharide.” *BMC Medicine 2012 10:1* 10 (1): 1–12. https://doi.org/10.1186/1741-7015-10-98.

Kang, Taek, Richard Moore, Yi Li, Eduardo Sontag, and Leonidas Bleris 2015. “Discriminating Direct and Indirect Connectivities in Biological Networks.” *Proceedings of the National Academy of Sciences of the United States of America* 112 (41): 201507168. https://doi.org/10.1073/pnas.1507168112.

Kang, Taek, Tyler Quarton, Chance M. Nowak, Kristina Ehrhardt, Abhyudai Singh, Yi Li, and Leonidas Bleris. 2020. “Robust Filtering and Noise Suppression in Intragenic MiRNA-Mediated Host Regulation.” *IScience* 23 (10): 101595. https://doi.org/10.1016/J.ISCI.2020.101595.

Kenter, Amy L., and James V. Watson. 1987. “Cell Cycle Kinetics Model of LPS-Stimulated Spleen Cells Correlates Switch Region Rearrangements with S Phase.” *Journal of Immunological Methods* 97 (1): 111–17. https://doi.org/10.1016/0022-1759(87)90112-8.

Kloosterman, Wigard P., and Ronald H.A. Plasterk. 2006. “The Diverse Functions of MicroRNAs in Animal Development and Disease.” *Developmental Cell* 11 (4): 441–50. https://doi.org/10.1016/j.devcel.2006.09.009.

Koch, Arthur L. 1980. “Does the Variability of the Cell Cycle Result from One or Many Chance Events?” *Nature 1980 286:5768* 286 (5768): 80–82. https://doi.org/10.1038/286080a0.

Komor, Alexis C., Yongjoo B. Kim, Michael S. Packer, John A. Zuris, and David R. Liu. 2016. "Programmable Editing of a Target Base in Genomic DNA without Double-Stranded DNA Cleavage." *Nature* 533 (7603): 420–24. https://doi.org/10.1038/nature17946.

Kubbutat, Michael H. G., Stephen N. Jones, and Karen H. Vousden. 1997. "Regulation of P53 Stability by Mdm2." *Nature 1997 387:6630* 387 (6630): 299–303. https://doi.org/10.1038/387299a0.

Kulkarni, Smita, Ying Qi, Colm O'hUigin, Florencia Pereyra, Veron Ramsuran, Paul McLaren, Jacques Fellay, et al. 2013. "Genetic Interplay between HLA-C and MIR148A in HIV Control and Crohn Disease." *Proceedings of the National Academy of Sciences of the United States of America* 110 (51): 20705–10. https://doi.org/10.1073/pnas.1312237110.

Lander, Eric S. 2016. "The Heroes of CRISPR." *Cell* 164 (1–2): 18–28. https://doi.org/10.1016/j.cell.2015.12.041.

Lane, D. P. 1992. "P53, Guardian of the Genome." *Nature 1992 358:6381* 358 (6381): 15–16. https://doi.org/10.1038/358015a0.

Leal-Esteban, Lucia C., and Lluis Fajas. 2020. "Cell Cycle Regulators in Cancer Cell Metabolism." *Biochimica et Biophysica Acta (BBA) - Molecular Basis of Disease* 1866 (5): 165715. https://doi.org/10.1016/J.BBADIS.2020.165715.

Ledoux, Adeline C., and Neil D. Perkins. 2014. "NF-KB and the Cell Cycle." *Biochemical Society Transactions* 42 (1): 76–81. https://doi.org/10.1042/BST20130156.

Lee, J., J. Lee, K. S. Farquhar, J. Yun, C. A. Frankenberger, E. Bevilacqua, K. Yeung, E.-J. Kim, G. Balazsi, and M. R. Rosner. 2014. "Network of Mutually Repressive Metastasis Regulators Can Promote Cell Heterogeneity and Metastatic Transitions." *Proceedings of the National Academy of Sciences* 111 (3): E364–73. https://doi.org/10.1073/pnas.1304840111.

Lee, Robin E. C., Mohammad A. Qasaimeh, Xianfang Xia, David Juncker, and Suzanne Gaudet. 2016. "NF-KB Signalling and Cell Fate Decisions in Response to a Short Pulse of Tumour Necrosis Factor." *Scientific Reports 2016 6:1* 6 (1): 1–12. https://doi.org/10.1038/srep39519.

Lee, Tae J., Guang Yao, Dorothy C. Bennett, Joseph R. Nevins, and Lingchong You. 2010. "Stochastic E2F Activation and Reconciliation of Phenomenological Cell-Cycle Models." Edited by Andre Levchenko. *PLoS Biology* 8 (9): e1000488. https://doi.org/10.1371/journal.pbio.1000488.

Levine, A J. 1997. "P53, the Cellular Gatekeeper for Growth and Division." *Cell* 88 (3): 323–31. http://www.ncbi.nlm.nih.gov/pubmed/9039259.

Li, Hangyu, Yan Li, Dan Liu, and Jingang Liu. 2014. “LPS Promotes Epithelial–Mesenchymal Transition and Activation of TLR4/JNK Signaling.” *Tumor Biology 2014 35:10* 35 (10): 10429–35. https://doi.org/10.1007/S13277-014-2347-5.

Li, Jian-Feng, Julie E Norville, John Aach, Matthew McCormack, Dandan Zhang, Jenifer Bush, George M Church, and Jen Sheen. 2013. “Multiplex and Homologous Recombination-Mediated Genome Editing in Arabidopsis and Nicotiana Benthamiana Using Guide RNA and Cas9.” *Nature Biotechnology* 31 (8): 688–91. https://doi.org/10.1038/nbt.2654.

Li, Yi, Saurabh Mendiratta, Kristina Ehrhardt, Neha Kashyap, Michael A White, and Leonidas Bleris. 2016. “Exploiting the CRISPR/Cas9 PAM Constraint for Single-Nucleotide Resolution Interventions.” *PloS One* 11 (1): e0144970. https://doi.org/10.1371/journal.pone.0144970.

Li, Yi, Chance M. Nowak, Daniel Withers, Alexander Pertsemlidis, and Leonidas Bleris. 2018. “CRISPR-Based Editing Reveals Edge-Specific Effects in Biological Networks.” *The CRISPR Journal* 1 (4): 286–93. https://doi.org/10.1101/265710.

Li, Yunqing, Fadila Guessous, Ying Zhang, Charles DiPierro, Benjamin Kefas, Elizabeth Johnson, Lukasz Marcinkiewicz, et al. 2009. “MicroRNA-34a Inhibits Glioblastoma Growth by Targeting Multiple Oncogenes.” *Cancer Research* 69 (19). http://cancerres.aacrjournals.org/content/69/19/7569.long.

Lim, Lee P., Nelson C. Lau, Philip Garrett-Engele, Andrew Grimson, Janell M. Schelter, John Castle, David P. Bartel, Peter S. Linsley, and Jason M. Johnson. 2005. “Microarray Analysis Shows That Some MicroRNAs Downregulate Large Numbers of Target MRNAs.” *Nature* 433 (7027): 769–73. https://doi.org/10.1038/nature03315.

Lin, Xiaojie, Hongyu Guan, Zhimin Huang, Juan Liu, Hai Li, Guohong Wei, Xiaopei Cao, and Yanbing Li. 2014. “Downregulation of Bcl-2 Expression by Mir-34a Mediates Palmitate-Induced Min6 Cells Apoptosis.” *Journal of Diabetes Research* 2014. https://doi.org/10.1155/2014/258695.

Lv, Ke, Yingjun Guo, Yiliang Zhang, Kaiyu Wang, Yin Jia, and Shuhan Sun. 2008. “Allele-Specific Targeting of Hsa-MiR-657 to Human IGF2R Creates a Potential Mechanism Underlying the Association of ACAA-Insertion/Deletion Polymorphism with Type 2 Diabetes.” *Biochemical and Biophysical Research Communications* 374 (1): 101–5. https://doi.org/10.1016/j.bbrc.2008.06.102.

Macias, Everardo, Aiwen Jin, Chad Deisenroth, Krishna Bhat, Hua Mao, Mikael S. Lindström, and Yanping Zhang. 2010. “An ARF-Independent c-MYC-Activated Tumor Suppression Pathway Mediated by Ribosomal Protein-Mdm2 Interaction.” *Cancer Cell* 18 (3): 231–43. https://doi.org/10.1016/J.CCR.2010.08.007.

Makarova, Kira S, Nick V Grishin, Svetlana A Shabalina, Yuri I Wolf, Eugene V Koonin, A Fire, GJ Hannon, et al. 2006. "A Putative RNA-Interference-Based Immune System in Prokaryotes: Computational Analysis of the Predicted Enzymatic Machinery, Functional Analogies with Eukaryotic RNAi, and Hypothetical Mechanisms of Action." *Biology Direct* 1 (1): 7. https://doi.org/10.1186/1745-6150-1-7.

Mali, Prashant, Luhan Yang, Kevin M Esvelt, John Aach, Marc Guell, James E DiCarlo, Julie E Norville, and George M Church. 2013. "RNA-Guided Human Genome Engineering via Cas9." *Science (New York, N.Y.)* 339 (6121): 823–26. https://doi.org/10.1126/science.1232033 [doi].

Marraffini, Luciano A, and Erik J Sontheimer. 2010. "Self versus Non-Self Discrimination during CRISPR RNA-Directed Immunity." *Nature* 463 (7280): 568–71. https://doi.org/10.1038/nature08703.

Marzi, Matteo J, Francesco Ghini, Benedetta Cerruti, Stefano de Pretis, Paola Bonetti, Chiara Giacomelli, Marcin M Gorski, et al. 2016. "Degradation Dynamics of MicroRNAs Revealed by a Novel Pulse-Chase Approach." *Genome Research* 26 (4): 554–65. https://doi.org/10.1101/gr.198788.115.

McCracken, S, N Fong, K Yankulov, S Ballantyne, G Pan, J Greenblatt, S D Patterson, M Wickens, and D L Bentley. 1997. "The C-Terminal Domain of RNA Polymerase II Couples MRNA Processing to Transcription." *Nature* 385 (6614): 357–61. https://doi.org/10.1038/385357a0.

Mitschka, Sibylle, and Christine Mayr. 2021. "Endogenous P53 Expression in Human and Mouse Is Not Regulated by Its 3'UTR." *ELife* 10 (May). https://doi.org/10.7554/ELIFE.65700.

Mojica, F J M, C Díez-Villaseñor, J García-Martínez, and C Almendros. 2009. "Short Motif Sequences Determine the Targets of the Prokaryotic CRISPR Defence System." *Microbiology (Reading, England)* 155 (Pt 3): 733–40. https://doi.org/10.1099/mic.0.023960-0.

Moore, Richard;, Hsu Kiang; Ooi, Taek; Kang, Leonidas; Bleris, and Lan; Ma. 2015. "MicroRNA-192-Mediated Positive Feedback Loop Controls the Robustness of Stress-Induced P53 Oscillations in Breast Cancer Cells." *PLoS Computational Biology* 11 (12): e1004653. https://doi.org/10.1371/journal.pcbi.1004653. eCollection 2015.

Moore, Richard, Alec Spinhirne, Michael J Lai, Samantha Preisser, Yi Li, Taek Kang, and Leonidas Bleris. 2015. "CRISPR-Based Self-Cleaving Mechanism for Controllable Gene Delivery in Human Cells." *Nucleic Acids Research* 43 (2): 1297–1303. https://doi.org/10.1093/nar/gku1326.

Muller, Patricia A. J., and Karen H. Vousden. 2013. “P53 Mutations in Cancer.” *Nature Cell Biology* 15 (1): 2–8. https://doi.org/10.1038/ncb2641.

N, Jiang, Xie F, Guo Q, Li MQ, Xiao J, and Sui L. 2017. “Toll-like Receptor 4 Promotes Proliferation and Apoptosis Resistance in Human Papillomavirus-Related Cervical Cancer Cells through the Toll-like Receptor 4/Nuclear Factor-KB Pathway.” *Tumour Biology : The Journal of the International Society for Oncodevelopmental Biology and Medicine* 39 (6). https://doi.org/10.1177/1010428317710586.

Navarro, Francisco, David Gutman, Eti Meire, Mario Cáceres, Isidore Rigoutsos, Zvi Bentwich, and Judy Lieberman. 2009. “MiR-34a Contributes to Megakaryocytic Differentiation of K562 Cells Independently of P53.” *Blood* 114 (10). http://www.bloodjournal.org/content/114/10/2181.long?sso-checked=true.

Navarro, Francisco, and Judy Lieberman. 2015. “MiR-34 and P53: New Insights into a Complex Functional Relationship.” Edited by Fabio Martelli. *PLOS ONE* 10 (7): e0132767. https://doi.org/10.1371/journal.pone.0132767.

Nguyen, Alexander, Mitsukuni Yoshida, Hani Goodarzi, and Sohail F. Tavazoie. 2016. “Highly Variable Cancer Subpopulations That Exhibit Enhanced Transcriptome Variability and Metastatic Fitness.” *Nature Communications* 7 (May). https://doi.org/10.1038/NCOMMS11246.

Nishimasu, Hiroshi, F Ann Ran, Patrick D Hsu, Silvana Konermann, Soraya I Shehata, Naoshi Dohmae, Ryuichiro Ishitani, Feng Zhang, and Osamu Nureki. 2014. “Crystal Structure of Cas9 in Complex with Guide RNA and Target DNA.” *Cell* 156 (5): 935–49. https://doi.org/10.1016/j.cell.2014.02.001.

Niu, Yuyu, Bin Shen, Yiqiang Cui, Yongchang Chen, Jianying Wang, Lei Wang, Yu Kang, et al. 2014. “Generation of Gene-Modified Cynomolgus Monkey via Cas9/RNA-Mediated Gene Targeting in One-Cell Embryos.” *Cell* 156 (4): 836–43. https://doi.org/10.1016/j.cell.2014.01.027.

O’Duibhir, Eoghan, Philip Lijnzaad, Joris J Benschop, Tineke L Lenstra, Dik van Leenen, Marian JA Groot Koerkamp, Thanasis Margaritis, Mariel O Brok, Patrick Kemmeren, and Frank CP Holstege. 2014. “Cell Cycle Population Effects in Perturbation Studies.” *Molecular Systems Biology* 10 (6): 732. https://doi.org/10.15252/MSB.20145172.

Okada, Nobuhiro, Chao-Po Lin, Marcelo C Ribeiro, Anne Biton, Gregory Lai, Xingyue He, Pengcheng Bu, et al. 2014. “A Positive Feedback between P53 and MiR-34 MiRNAs Mediates Tumor Suppression.” *Genes & Development* 28 (5): 438–50. https://doi.org/10.1101/gad.233585.113.

Otto, Tobias, and Piotr Sicinski. 2017. “Cell Cycle Proteins as Promising Targets in Cancer Therapy.” *Nature Reviews. Cancer* 17 (2): 93. https://doi.org/10.1038/NRC.2016.138.

Pardee, Arthur B. 1974. “A Restriction Point for Control of Normal Animal Cell Proliferation (Growth Control/Cell Survival/Cancer).” Vol. 71.

Parrales, Alejandro, and Tomoo Iwakuma. 2015. “Targeting Oncogenic Mutant P53 for Cancer Therapy.” *Frontiers in Oncology* 5 (December): 288. https://doi.org/10.3389/fonc.2015.00288.

Partch, Carrie L., Carla B. Green, and Joseph S. Takahashi. 2014. “Molecular Architecture of the Mammalian Circadian Clock.” *Trends in Cell Biology* 24 (2): 90. https://doi.org/10.1016/J.TCB.2013.07.002.

Patke, Alina, Michael W. Young, and Sofia Axelrod. 2019. “Molecular Mechanisms and Physiological Importance of Circadian Rhythms.” *Nature Reviews Molecular Cell Biology 2019 21:2* 21 (2): 67–84. https://doi.org/10.1038/s41580-019-0179-2.

Perez-Carrasco, Ruben, Casper Beentjes, and Ramon Grima. 2020. “Effects of Cell Cycle Variability on Lineage and Population Measurements of Messenger RNA Abundance.” *Journal of the Royal Society Interface* 17 (168). https://doi.org/10.1098/RSIF.2020.0360.

PK, Davis, Ho A, and Dowdy SF. 2001. “Biological Methods for Cell-Cycle Synchronization of Mammalian Cells.” *BioTechniques* 30 (6): 1322–31. https://doi.org/10.2144/01306RV01.

Polager, Shirley, and Doron Ginsberg. 2009. “P53 and E2f: Partners in Life and Death.” *Nature Reviews Cancer* 9 (10): 738–48. https://doi.org/10.1038/nrc2718.

Pomerening, Joseph R. 2009. “Positive Feedback Loops in Cell Cycle Progression.” *FEBS Letters* 583 (21): 3388. https://doi.org/10.1016/J.FEBSLET.2009.10.001.

Pomerening, Joseph R., Sun Young Kim, and James E. Ferrell. 2005. “Systems-Level Dissection of the Cell-Cycle Oscillator: Bypassing Positive Feedback Produces Damped Oscillations.” *Cell* 122 (4): 565–78. https://doi.org/10.1016/J.CELL.2005.06.016.

Prescott, David M. 1968. “Regulation of Cell Reproduction.” *Cancer Research* 28 (9).

Pu, Xia, Jack A Roth, Michelle A T Hildebrandt, Yuanqing Ye, Hua Wei, John D Minna, Scott M Lippman, and Xifeng Wu. 2013. “MicroRNA-Related Genetic Variants Associated with Clinical Outcomes in Early-Stage Non-Small Cell Lung Cancer Patients.” *Cancer Research* 73 (6): 1867–75. https://doi.org/10.1158/0008-5472.CAN-12-0873.

Qi, Lei S, Matthew H Larson, Luke A Gilbert, Jennifer A Doudna, Jonathan S Weissman, Adam P Arkin, and Wendell A Lim. 2013. “Repurposing CRISPR as an RNA-Guided Platform for Sequence-Specific Control of Gene Expression.” *Cell* 152 (5): 1173–83. https://doi.org/10.1016/j.cell.2013.02.022.

Quarton, Tyler, Taek Kang, Vasileios Papakis, Khai Nguyen, Chance Nowak, Yi Li, and Leonidas Bleris. 2020. “Uncoupling Gene Expression Noise along the Central Dogma Using Genome Engineered Human Cell Lines.” *Nucleic Acids Research* 48 (16): 9406–13. https://doi.org/10.1093/NAR/GKAA668.

Raser, J M, and E K O’Shea. 2004. “Control of Stochasticity in Eukaryotic Gene Expression.” *Science* 304 (5678): 1811–14. http://dx.doi.org/10.1126/science.1098641.

Richardson, Kris, Qiong Louie-Gao, Donna K Arnett, Laurence D Parnell, Chao-Qiang Lai, Alberto Davalos, Caroline S Fox, et al. 2011. “The PLIN4 Variant Rs8887 Modulates Obesity Related Phenotypes in Humans through Creation of a Novel MiR-522 Seed Site.” *PloS One* 6 (4): e17944. https://doi.org/10.1371/journal.pone.0017944.

Rokavec, M., H. Li, L. Jiang, and H. Hermeking. 2014. “The P53/MiR-34 Axis in Development and Disease.” *Journal of Molecular Cell Biology* 6 (3): 214–30. https://doi.org/10.1093/jmcb/mju003.

Rong, Zhili, Shengyun Zhu, Yang Xu, and Xuemei Fu. 2014. “Homologous Recombination in Human Embryonic Stem Cells Using CRISPR/Cas9 Nickase and a Long DNA Donor Template.” *Protein & Cell* 5 (4): 258–60. https://doi.org/10.1007/s13238-014-0032-5.

Ruda, Vera M., Rohit Chandwani, Alfica Sehgal, Roman L. Bogorad, Akin Akinc, Klaus Charisse, Alexander Tarakhovsky, Tatiana I. Novobrantseva, and Victor Koteliansky. 2014. “The Roles of Individual Mammalian Argonautes in RNA Interference In Vivo.” Edited by Alexandre H. Kihara. *PLoS ONE* 9 (7): e101749. https://doi.org/10.1371/journal.pone.0101749.

Ryan, Brid M, Ana I Robles, Andrew C McClary, Majda Haznadar, Elise D Bowman, Sharon R Pine, Derek Brown, et al. 2015. “Identification of a Functional SNP in the 3’UTR of CXCR2 That Is Associated with Reduced Risk of Lung Cancer.” *Cancer Research* 75 (3): 566–75. https://doi.org/10.1158/0008-5472.CAN-14-2101.

Sahni, Nidhi, Song Yi, Quan Zhong, Noor Jailkhani, Benoit Charloteaux, Michael E Cusick, and Marc Vidal. 2013. “Edgotype: The Link between Genotype and Phenotype.” *Current Opinion in Genetics & Development* 23 (6): 649. https://doi.org/10.1016/J.GDE.2013.11.002.

Sancar, Aziz, Laura A. Lindsey-Boltz, Tae-Hong Kang, Joyce T. Reardon, Jin Hyup Lee, and Nuri Ozturk. 2010. “Circadian Clock Control of the Cellular Response to DNA Damage.” *FEBS Letters* 584 (12): 2618. https://doi.org/10.1016/J.FEBSLET.2010.03.017.

Sanjana, Neville E, Ophir Shalem, and Feng Zhang. 2014. “Improved Vectors and Genome-Wide Libraries for CRISPR Screening.” *Nature Methods* 11 (8): 783–84. https://doi.org/10.1038/nmeth.3047.

Savinova, Olga V., Alexander Hoffmann, and Gourisankar Ghosh. 2009. “The Nfkb1 and Nfkb2 Proteins P105 and P100 Function as the Core of High-Molecular-Weight Heterogeneous Complexes.” *Molecular Cell* 34 (5): 591. https://doi.org/10.1016/J.MOLCEL.2009.04.033.

Schorl, Christoph, and John M. Sedivy. 2007. “Analysis of Cell Cycle Phases and Progression in Cultured Mammalian Cells.” *Methods (San Diego, Calif.)* 41 (2): 143. https://doi.org/10.1016/J.YMETH.2006.07.022.

Seok, Heeyoung, Juyoung Ham, Eun-Sook Jang, and Sung Wook Chi. 2016. “MicroRNA Target Recognition: Insights from Transcriptome-Wide Non-Canonical Interactions.” *Molecules and Cells* 39 (5): 375–81. https://doi.org/10.14348/molcells.2016.0013.

Sethupathy, Praveen, Christelle Borel, Maryline Gagnebin, Gregory R Grant, Samuel Deutsch, Terry S Elton, Artemis G Hatzigeorgiou, and Stylianos E Antonarakis. 2007. “Human MicroRNA-155 on Chromosome 21 Differentially Interacts with Its Polymorphic Target in the AGTR1 3’ Untranslated Region: A Mechanism for Functional Single-Nucleotide Polymorphisms Related to Phenotypes.” *American Journal of Human Genetics* 81 (2): 405–13. https://doi.org/10.1086/519979.

Shalem, Ophir, Neville E Sanjana, Ella Hartenian, Xi Shi, David A Scott, Tarjei S Mikkelsen, Dirk Heckl, et al. 2014. “Genome-Scale CRISPR-Cas9 Knockout Screening in Human Cells.” *Science (New York, N.Y.)* 343 (6166): 84–87. https://doi.org/10.1126/science.1247005.

Shields, Robert, and James A Smith. 1977. “Cells Regulate Theri Proliferation through Alterations in Transition Probability.” *Journal of Cellular Physiology* 91 (3): 345–55. https://doi.org/10.1002/jcp.1040910304.

Smith, J A, and L Martin. 1973. “Do Cells Cycle? (Cell Kinetics/Control of Growth/DNA Replication/Cell Culture).” *DETERMINATE Downloaded at LIBRARY SERIALS*. Vol. 70.

Soltani, Mohammad, Cesar A. Vargas-Garcia, Duarte Antunes, and Abhyudai Singh. 2016. “Intercellular Variability in Protein Levels from Stochastic Expression and Noisy Cell Cycle Processes.” *PLOS Computational Biology* 12 (8): e1004972. https://doi.org/10.1371/JOURNAL.PCBI.1004972.

Sorek, Rotem, Victor Kunin, and Philip Hugenholtz. 2008. “CRISPR--a Widespread System That Provides Acquired Resistance against Phages in Bacteria and Archaea.” *Nature Reviews. Microbiology* 6 (3): 181–86. https://doi.org/10.1038/nrmicro1793.

Sotillo, E, T Laver, H Mellert, J M Schelter, M A Cleary, S McMahon, and A Thomas-Tikhonenko. 2011. “Myc Overexpression Brings out Unexpected Antiapoptotic Effects of MiR-34a.” *Oncogene* 30 (22): 2587–94. https://doi.org/10.1038/onc.2010.634.

Sternberg, Samuel H., Benjamin LaFrance, Matias Kaplan, and Jennifer A. Doudna. 2015. "Conformational Control of DNA Target Cleavage by CRISPR–Cas9." *Nature* 527 (7576): 110–13. https://doi.org/10.1038/nature15544.

Sternberg, Samuel H, Sy Redding, Martin Jinek, Eric C Greene, and Jennifer A Doudna. 2014. "DNA Interrogation by the CRISPR RNA-Guided Endonuclease Cas9." *Nature* 507 (7490): 62–67. https://doi.org/10.1038/nature13011.

Sulli, Gabriele, Michael Tun Yin Lam, and Satchidananda Panda. 2019. "Interplay between Circadian Clock and Cancer: New Frontiers for Cancer Treatment." *Trends in Cancer* 5 (8): 475. https://doi.org/10.1016/J.TRECAN.2019.07.002.

Sun, Fang, Hanjiang Fu, Qin Liu, Yi Tie, Jie Zhu, Ruiyun Xing, Zhixian Sun, and Xiaofei Zheng. 2008. "Downregulation of CCND1 and CDK6 by MiR-34a Induces Cell Cycle Arrest." *FEBS Letters* 582 (10): 1564–68. https://doi.org/10.1016/j.febslet.2008.03.057.

Sundaram, P, S Hultine, L M Smith, M Dews, J L Fox, D Biyashev, J M Schelter, et al. 2011. "P53-Responsive MiR-194 Inhibits Thrombospondin-1 and Promotes Angiogenesis in Colon Cancers." *Cancer Research* 71 (24): 7490–7501. https://doi.org/10.1158/0008-5472.CAN-11-1124.

Swain, Peter S., Michael B. Elowitz, and Eric D. Siggia. 2002. "Intrinsic and Extrinsic Contributions to Stochasticity in Gene Expression." *Proceedings of the National Academy of Sciences* 99 (20): 12795–800. https://doi.org/10.1073/PNAS.162041399.

Tarasov, Valery, Peter Jung, Berlinda Verdoodt, Dmitri Lodygin, Alexey Epanchintsev, Antje Menssen, Gunter Meister, and Heiko Hermeking. 2007. "Differential Regulation of MicroRNAs by P53 Revealed by Massively Parallel Sequencing: MiR-34a Is a P53 Target That Induces Apoptosis and G(1)-Arrest." *Cell Cycle* 6 (13). http://view.ncbi.nlm.nih.gov/pubmed/17554199.

Tazawa, Hiroshi, Naoto Tsuchiya, Masashi Izumiya, and Hitoshi Nakagama. 2007. "Tumor-Suppressive MiR-34a Induces Senescence-like Growth Arrest through Modulation of the E2F Pathway in Human Colon Cancer Cells." *Proceedings of the National Academy of Sciences* 104 (39): 15472–77. https://doi.org/10.1073/PNAS.0707351104.

Temin, Howard M. 1971. "Stimulation by Serum of Multiplication of Stationary Chicken Cells." *Journal of Cellular Physiology* 78 (2): 161–70. https://doi.org/10.1002/jcp.1040780202.

Vousden, K H, and C Prives. 2009. "Blinded by the Light: The Growing Complexity of P53." *Cell* 137 (3): 413–31. http://www.ncbi.nlm.nih.gov/entrez/query.fcgi?cmd=Retrieve&db=PubMed&dopt=Citation&list_uids=19410540.

Wang, Gaofeng, Joelle M van der Walt, Gregory Mayhew, Yi-Ju Li, Stephan Zuchner, William K Scott, Eden R Martin, and Jeffery M Vance. 2008. "Variation in the MiRNA-433 Binding Site of FGF20 Confers Risk for Parkinson Disease by Overexpression of Alpha-Synuclein." *American Journal of Human Genetics* 82 (2): 283–89. https://doi.org/10.1016/j.ajhg.2007.09.021.

Wang, Tianyou. 2014. "A Correlation Analysis of MiRNA-34a and Its Predicted Target Genes in Leukemia." *Molecular Medicine Reports*, February. https://doi.org/10.3892/mmr.2014.1931.

Wang, Tim, Jenny J Wei, David M Sabatini, and Eric S Lander. 2014. "Genetic Screens in Human Cells Using the CRISPR-Cas9 System." *Science* 343 (6166): 80–84. https://doi.org/10.1126/science.1246981.

Wang, Yongjun, Yanjie Weng, Ying Shi, Xi Xia, Shixuan Wang, and Hua Duan. 2014. "Expression and Functional Analysis of Toll-like Receptor 4 in Human Cervical Carcinoma." *The Journal of Membrane Biology 2014 247:7* 247 (7): 591–99. https://doi.org/10.1007/S00232-014-9675-7.

Watson, James V., Stephen H. Chambers, and Paul J. Smith. 1987. "A Pragmatic Approach to the Analysis of DNA Histograms with a Definable G1 Peak." *Cytometry* 8 (1): 1–8. https://doi.org/10.1002/cyto.990080101.

Wu, Li-Sha, Fang-Fang Li, Liang-Dan Sun, Dai Li, Juan Su, Ye-Hong Kuang, Gang Chen, Xiao-Ping Chen, and Xiang Chen. 2011. "A MiRNA-492 Binding-Site Polymorphism in BSG (Basigin) Confers Risk to Psoriasis in Central South Chinese Population." *Human Genetics* 130 (6): 749–57. https://doi.org/10.1007/s00439-011-1026-5.

Xiong, Fang, Chen Wu, Jiang Chang, Dianke Yu, Binghe Xu, Peng Yuan, Kan Zhai, Jian Xu, Wen Tan, and Dongxin Lin. 2011. "Genetic Variation in an MiRNA-1827 Binding Site in MYCL1 Alters Susceptibility to Small-Cell Lung Cancer." *Cancer Research* 71 (15): 5175–81. https://doi.org/10.1158/0008-5472.CAN-10-4407.

Yamakuchi, Munekazu, Marcella Ferlito, and Charles J Lowenstein. 2008. "MiR-34a Repression of SIRT1 Regulates Apoptosis." *Proceedings of the National Academy of Sciences of the United States of America* 105 (36): 13421–26. https://doi.org/10.1073/pnas.0801613105.

Yamamura, S., S. Saini, S. Majid, H. Hirata, K. Ueno, I. Chang, Y. Tanaka, A. Gupta, and R. Dahiya. 2012. "MicroRNA-34a Suppresses Malignant Transformation by Targeting c-Myc Transcriptional Complexes in Human Renal Cell Carcinoma." *Carcinogenesis* 33 (2): 294–300. https://doi.org/10.1093/carcin/bgr286.

Yao, Guang, Tae Jun Lee, Seiichi Mori, Joseph R. Nevins, and Lingchong You. 2008. "A Bistable Rb-E2F Switch Underlies the Restriction Point." *Nature Cell Biology* 10 (4): 476–82. https://doi.org/10.1038/ncb1711.

Zetterberg, A, and Olle Larsson. 1985. “Kinetic Analysis of Regulatory Events in G1 Leading to Proliferation or Quiescence of Swiss 3T3 Cells (GI Arrest/GO State/Epidermal Growth Factor/Platelet-Derived Growth Factor/Insulin).” *Cell Biology*. Vol. 82.

Zhang, Baohong, Xiaoping Pan, George P. Cobb, and Todd A. Anderson. 2007. “MicroRNAs as Oncogenes and Tumor Suppressors.” *Developmental Biology* 302 (1): 1–12. https://doi.org/10.1016/j.ydbio.2006.08.028.

Zhang, Cen, Juan Liu, Dandan Xu, Tianliang Zhang, Wenwei Hu, and Zhaohui Feng. 2020. “Gain-of-Function Mutant P53 in Cancer Progression and Therapy.” *Journal of Molecular Cell Biology* 12 (9): 674–87. https://doi.org/10.1093/JMCB/MJAA040.

Zhao, Jane, Paul Lammers, Chris J. Torrance, and Andreas G. Bader. 2013. “TP53-Independent Function of MiR-34a via HDAC1 and P21CIP1/WAF1.” *Molecular Therapy* 21 (9): 1678–86. https://doi.org/10.1038/MT.2013.148.

Zhong, Quan, Nicolas Simonis, Qian-Ru Li, Benoit Charloteaux, Fabien Heuze, Niels Klitgord, Stanley Tam, et al. 2009. “Edgetic Perturbation Models of Human Inherited Disorders.” *Molecular Systems Biology* 5 (January): 321. https://doi.org/10.1038/MSB.2009.80.

Zhu, Shiyou, Wei Li, Jingze Liu, Chen-Hao Chen, Qi Liao, Ping Xu, Han Xu, et al. 2016. “Genome-Scale Deletion Screening of Human Long Non-Coding RNAs Using a Paired-Guide RNA CRISPR-Cas9 Library.” *Nature Biotechnology* 34 (12): 1279–86. https://doi.org/10.1038/nbt.3715.

Zopf, C. J., Katie Quinn, Joshua Zeidman, and Narendra Maheshri. 2013. “Cell-Cycle Dependence of Transcription Dominates Noise in Gene Expression.” *PLOS Computational Biology* 9 (7): e1003161. https://doi.org/10.1371/JOURNAL.PCBI.1003161.

Zu, Yukun, Jinbao Ban, Zhenxiong Xia, Jianing Wang, Yixin Cai, Wei Ping, and Wei Sun. 2013. “Genetic Variation in a MiR-335 Binding Site in BIRC5 Alters Susceptibility to Lung Cancer in Chinese Han Populations.” *Biochemical and Biophysical Research Communications* 430 (2): 529–34. https://doi.org/10.1016/j.bbrc.2012.12.001.

BIOGRAPHICAL SKETCH

Chance Michael Nowak was born in Lafayette, Louisiana on March 20th, 1991. He graduated from Lafayette High School in 2009. He went on to receive his Bachelor of Science degree in Biological Sciences as well two minor degrees in Chemistry and Philosophy from Louisiana State University in 2013. In 2014 he worked as a Research Associate I at Louisiana State University before enrolling in the Molecular and Cell Biology Graduate Program the same year. He received his Master of Science degree in 2016. He then continued his doctoral research in systems and synthetic biology.

CURRICULUM VITAE

Personal Statement:

I am a hardworking and highly motivated doctoral student that has acquired an extensive depth of knowledge in the field of mammalian systems and synthetic biology through both wet lab work and in silico analysis that center on genome editing, gene delivery, and genetic circuit designs. Furthermore, I have strong track record of collaborations in many areas of scientific inquiry working alongside many scientists from diverse backgrounds for project completions, which often necessitated strong communication skills between individuals of disparate disciplines. I am seeking a scientist position in the biotechnology industry where I can utilize these skills for team management and project completions. My career goal is to assume a role that allows me to direct scientific research and execute team leadership in cutting-edge technologies for the purpose of developing genetic-based therapies that transforms patients' lives.

Education:

Bachelor of Science, Biological Sciences; Minor(s): Chemistry and Philosophy
December 2013, Louisiana State University, Baton Rouge, LA

Master of Science, Molecular and Cell Biology
September 2014-May 2016, University of Texas at Dallas

Doctor of Philosophy, Molecular and Cell Biology
June 2016-Present, University of Texas at Dallas
Expected graduation December 2021

Research Experience:

Undergraduate Research
Jan. 2013-Dec. 2013, Biological Sciences Department, Louisiana State University
Investigation of alternative functions of RNA Polymerase III in *S. cerevisiae*.

Research Associate I
Jan. 2014-Aug. 2014, Biological Sciences Department, Louisiana State University
Investigation of global defective RNA polymerase III complex assembly in *S. cerevisiae* and effects on the Pol II transcriptome.

Masters of Science
September 2014-May 2016, University of Texas at Dallas
Investigations into genome editing of cancer-relevant transcriptional regulatory motifs including microRNA binding sites and transcription factor binding sites.

Doctor of Philosophy, University of Texas at Dallas

Investigations into cell cycle control through mathematical modeling of DNA kinetics over time from synchronized cell populations as well genome editing of cell cycle control genes such as CDK4.

Research Interests:

Systems and Synthetic Biology
Biotechnology Research and Development
Genome Editing and Cell Engineering
CAR-T therapy
Transcriptional Gene Control
Epigenetic Gene Regulation
Chromosome Architecture and Chromatin Remodeling

Experimental Skills:

Flow Cytometry
Mammalian Cell Culture (HEK293T, HCT116, HeLa, MCF7, PBMC, etc.)
Viral production in mammalian cells
Genome editing (extensive knowledge of CRISPR-based systems, including base and prime editors)
NGS analysis (genome editing)
RNAseq analysis
Molecular cloning
Site-specific mutagenesis of plasmids and yeast
Yeast tetrad dissections
Analysis of mutant recombinants
DNA, RNA, and protein extractions
Northern and Western Blotting
cDNA synthesis and 5'RACE
Oligonucleotide design
Radiation safety certified

Publications:

Nowak, C.M., Bleris, L. Diverse edge editing outcomes of CDK4 3'UTR reveals selective growth advantages in polyclonal population (in preparation)

Nowak, C.M., Quarton, T., Nguyen, K., Bleris, L. Impact of Variability in Cell Cycle Periodicity on Cell Population Dynamics (under review)

Bellary, A., **Nowak, C.M.**, Bleris, L., Hernandez, S.L., Sirsi. Ultrasound Monitoring of a Targeted Non-Viral Nitric Oxide-Based Gene Therapy Improves Liposomal Doxorubicin Uptake in Neuroblastoma (submitted)

Ye, H., **Nowak, C.M.**, Liu, Y., Li, Y., Bleris, L., Qin, Z. Bimetallic Au-Ag Nanoshells as Ultrasensitive Colorimetric Sensors for Single-Molecule Detection of SARS-CoV-2 RNA. **Adv. Materials**, (under review)

Li, Y., **Nowak, C.M.**, U. Pham, Nguyen, K., Bleris, L. Cell Morphology-based Machine Learning Models for Human Cell State Classification. **npj *Systems Biology and Applications*, 2021**

Kang, T., Quarton,T., Ehrhardt, K., **Nowak, C.M.**, Singh, A., Li, Y., Bleris, L.. Robust filtering and noise suppression in intragenic miRNA-mediated host regulation. ***iScience*, 23(10), 2020**.

Quarton, T., Kang, T., Papakis, V., Nguyen, K., **Nowak, C.M.**, Li, Y. and L. Bleris Uncoupling gene expression noise along the central dogma using genome engineered human cell lines. ***Nucleic Acids Research*, 48(16), 2020**.

Hsieh MH, Choe JH, Gadhvi J, Kim YJ, Arguez MA, Palmer M, Gerold H, **Nowak C.M.**, Do H, Mazambani S, Knighton JK, Cha M, Goodwin J, Kang MK, Jeong JY, Lee SY, Faubert B, Xuan Z, Abel ED, Scafoglio C, Shackelford DB, Minna JD, Singh PK, Shulaev V, Bleris L, Hoyt K, Kim J, Inoue M, DeBarardinis RJ, Kim TH, Kim JW. p63 and SOX2 dictate glucose reliance and metabolic vulnerabilities in squamous cell carcinoma. ***Cell Reports*, 28(7), 2019**.

Li, Y., **Nowak, C.M.**, Withers, D., Pertsemlidis, A., L. Bleris. CRISPR-based editing reveals edge-specific effects in biological networks. ***The CRISPR Journal*, 2018**.

Lee, H., Benjamin, C.E., **Nowak, C.M.**, Tuong, L.H., Welch, R.P., Chen, Z., Dharmarwardana, M., Murray, K.W., Bleris, L., D'Arcy, S., Gassensmith, J.J. Regulating the Uptake of Viral Nanoparticles in Macrophage and Cancer Cells by via a pH Switch. ***Molecular Pharmaceutics*, 2018**.

Dharmarwardana, M., Martins, A.F., Chen, Z., Palacios, P.M., **Nowak, C.M.**, Welch, R.P., Li, S., Luzuriaga, M.A., Bleris, L., Pierce, B.S., Sherry, A.D., Gassensmith, J.J. Nitroxyl Modified Tobacco Mosaic Virus as a Metal-Free High-Relaxivity MRI and EPR Active Superoxide Sensor. ***Molecular Pharmaceutics*, 2018.**

Nowak, C.M., S. Lawson, M. Zerez, L. Bleris. Guide RNA engineering for versatile Cas9 functionality. ***Nucleic Acids Research*, 2016.**

Qing Wang, **Chance M. Nowak**, Asawari Korde, Dong-Ha Oh, Maheshi Dassanayake, and David Donze. Compromised RNA Polymerase III complex assembly leads to local alterations of intergenic RNA Polymerase II transcription in *Saccharomyces cerevisiae.* ***BMC Biology*** **2014**; 12:89. doi:10.1186/s12915-014-0089-x

Presentations:

2nd International Conference on CRISPR Technologies, presented by **Chance M. Nowak**

"CRISPR-Based Editing Reveals Edge-Specific Effects in Biological Networks" Yi Li, **Chance Nowak**, Daniel Withers Alexander Pertsemlidis, and Leonidas Bleris

Posters:

2016 Third International Mammalian Synthetic Biology Workshop, presented by **Chance M. Nowak**

"Exploiting the CRISPR/Cas9 PAM constraint for single-nucleotide resolution interventions" Li, Y., Mendiratta, S., Ehrhardt, K., Kashyap, N., White, M. A. and L. Bleris

2018 Fifth International Mammalian Synthetic Biology Workshop, presented by **Chance M. Nowak**

"CRISPR-Based Editing Reveals Edge-Specific Effects in Biological Networks" Yi Li, **Chance Nowak**, Daniel Withers Alexander Pertsemlidis, and Leonidas Bleris

2018 AIChE Annual Meeting, presented by **Chance M. Nowak**

"CRISPR-Based Editing Reveals Edge-Specific Effects in Biological Networks" Yi Li, **Chance Nowak**, Daniel Withers Alexander Pertsemlidis, and Leonidas Bleris